PETROLOGY AND GEOCHEMISTRY OF THE VOLCANIC HOST ROCKS TO THE WEST AND NORTH PITS OF THE SHERMAN MINE IRON FORMATION, TEMAGAMI, ONTARIO

PETROLOGY AND GEOCHEMISTRY OF THE VOLCANIC HOST ROCKS TO THE WEST AND NORTH PITS OF THE SHERMAN MINE IRON FORMATION, TEMAGAMI, ONTARIO

BY

TERESA DAWN HURLEY, B.Sc.
(McMaster University)

A Thesis
Submitted to the School of Graduate Studies
in Partial Fulfilment of the Requirements
for the Degree
Master of Science

McMaster University
December, 1985

MASTER OF SCIENCE (1985)
(Geology)

McMASTER UNIVERSIY
Hamilton, Ontario

TITLE: Petrology and Geochemistry of the Volcanic Host Rocks to the West and North Pits of the Sherman Mine Iron Formation, Temagami, Ontario

AUTHOR: Teresa Dawn Hurley, B.Sc. (McMaster University)

SUPERVISORS: Dr. Robert H. McNutt
Dr. James H. Crocket

NUMBER OF PAGES: xiii, 154

ABSTRACT

A detailed study was undertaken of the volcanic host rocks underlying the northern band of iron formation at the Sherman Mine, Temagami, Ontario. The main objective of the study was to characterize the volcanic activity which immediately preceeded the iron formation deposition. A 1.5 km volcanic section was characterized through detailed geological mapping and extensive lithogeochemical sampling.

Felsic pyroclastics are the immediate volcanics underlying the iron formation in the West Pit. The pyroclastics commonly host disseminated to massive, stratiform sulphide zones which carry anomalous Au, As and Sb contents. The section extending 1 to 1.5 km stratigraphically below the iron formation is dominated by calc-alkaline andesites with subordinate intercalated dacites, rhyolites, and calc-alkaline and tholeiitic basalts. A small eruptive center or focus of volcanism has been identified in the northeast corner of the section.

The volcanics are notably enriched in Cr and Zn and depleted in Cu and Ni. The dacites and rhyolites contain slightly elevated contents of Au. A pervasive depletion of Na is evident in all rock types, and Ca is generally depleted in the intermediate to mafic volcanics. It is suggested that these elements were leached from the rocks during hydrothermal seawater circulation. Various degrees of chloritization, carbonatization and silicification reflect hydrothermal alteration of the volcanic pile.

A similarity in the major element chemistry and rare earth element patterns exists between the volcanics underlying the iron formation and the volcanics of the Marda Complex, western Australia. A similar tectonic setting between the Marda Complex and the Temagami greenstone belt is inferred from this similarity. As such, the Temagami volcanics are considered analogous to continental margin calc-alkaline suites. Evidence of hydrothermal seawater circulation in the Temagami volcanics suggests some separation of volcanism from the continental margin, perhaps by a small ocean basin.

ACKNOWLEDGEMENTS

This study was financed in part through the Ontario Geological Survey Research Grants Program. I thank Mr. Bob Garrett of the Sherman Mine for access into the study area and permission to work on the mine property.

For the supervision of this thesis I express my appreciation and sympathy to Dr. Robert H. McNutt and Dr. James H. Crocket.

For their assistance in chemical analyses and neutron activation, I thank Ota Mudroch and Abdul Kabir respectively. To Jack Whorwood for his preparation of photographs and to Len Zwicker for his preparation of endless thin sections and terrific bookends, I am sincerely grateful.

I express my appreciation to Andy Fyon for sharing his time, wisdom and most of all his library.

I also wish to acknowledge the rare earth elements for occupying three months of my time and truly challenging my sanity. Finally, I must thank the Hamilton Hall games room, the Phoenix and the Olympic ice arena for occupying the rest of my time and restoring my sanity. Flash.

TABLE OF CONTENTS

Page

LIST OF FIGURES

LIST OF TABLES

LIST OF PLATES

CHAPTER 1

INTRODUCTION

1.1 LOCATION AND ACCESSIBILITY

The village of Temagami is located on Highway 11, 97 km north of North Bay and approximately 480 km north of Toronto (Fig. 1-1). Access to the Sherman Mine is via Highway 11 and west along the Milne-Sherman Road 1.5 km north of the village. Located within Strathy and Chambers Townships, the thesis area encompasses a 1.5 by 5.5 km section lying north of the West and North Pits of the Sherman Mine (Fig. 3-1). Access to the area is via the northern perimeter road on the mine property. Much of the thesis area lies on the property of the William Milne and Son Lumber Company.

1.2 PREVIOUS GEOLOGICAL MAPPING

Early geological mapping of the northeast Temagami area was carried out by A.E. Barlow for the Canadian Geological Survey (1899; 1907). Reports on the geology of Strathy Township by W.S. Savage (1935), and on the geology of the Northeastern Temagami area by W.W. Moorehouse (1942), were completed for the Ontario

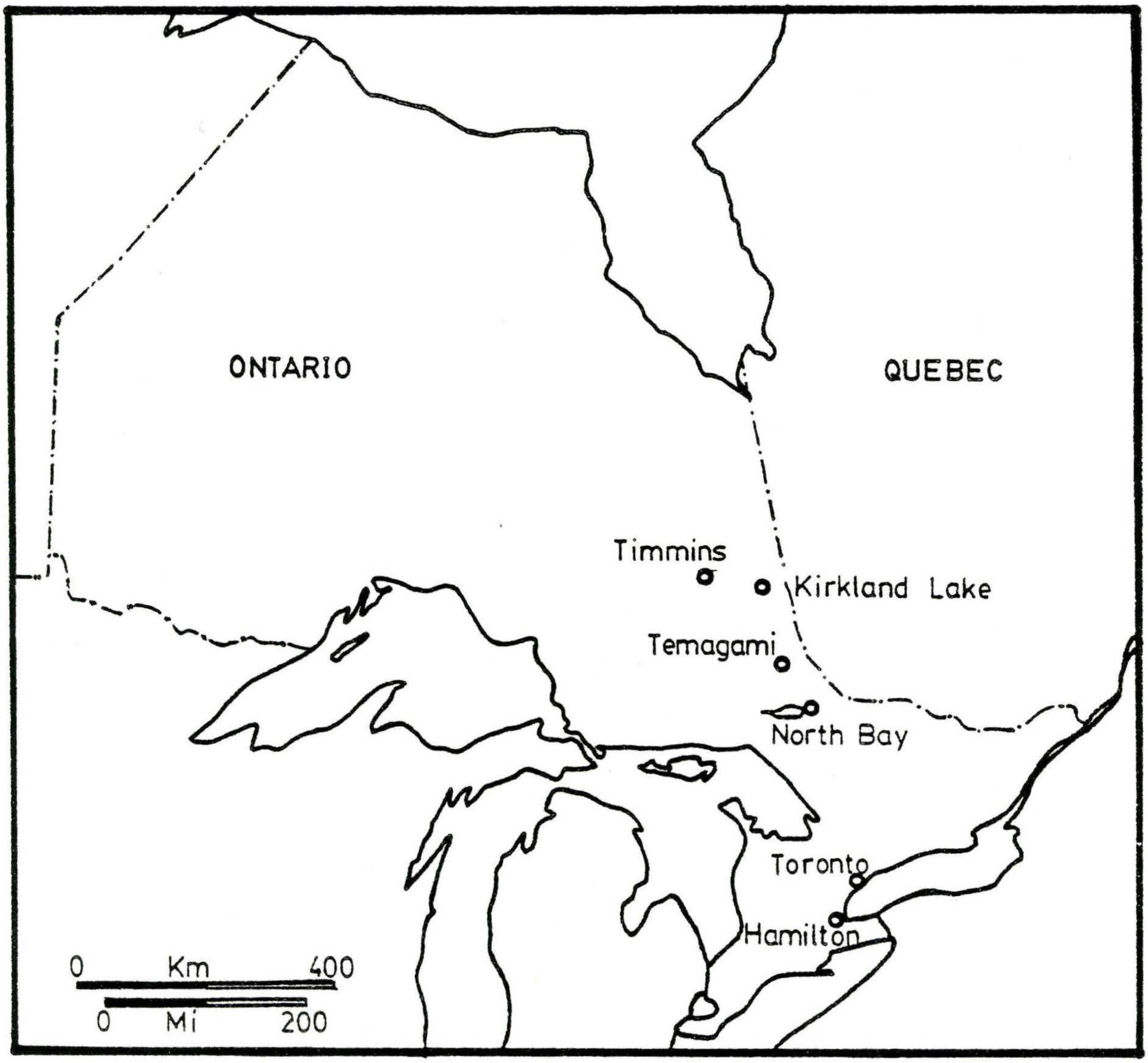

Figure 1-1. Location of Temagami, Ontario.

Department of Mines. In 1963, I.F. Downie submitted a company report for Keevil Consultants Limited on the geology and economic significance of the Doris Lake Group in Strathy Township.

More recent geological mapping of the Northeast Temagami area was completed by G. Bennett during the 1969, 1970 and part of the 1971, 1972 field seasons. An Ontario Geological Survey report on the results of this fieldwork was published in 1978 (Bennett, 1978).

1.3 HISTORICAL BACKGROUND

The Northeast Temagami area was investigated for its iron mining potential during the years 1898 to 1900 by H.P. Coleman (1900), W.G. Miller (1901) and D. O'Conner (Boyum and Hartviksen, 1970). An intensive examination of the iron ranges for the United States Steel Corporation was undertaken by M.H. Newman in 1903. German interests sought and obtained an option for the property in 1913. Although several diamond drill holes were sunk the program was abandoned abruptly in 1914 due to World War I (Boyum and Hartviksen, 1970).

By 1898 auriferous arsenopyrite and nickel-copper mineralization had been discovered north of Temagami (Coleman, 1900). Prospecting was stimulated by the development of the rich Cobalt silver camp, and, following the increase in the price of gold, active prospecting led to a number of encouraging discoveries in 1934-35. Four prospects in the Temagami area underwent under-

PLATE 1-1. Sherman Mine obelisk - Jasper-rich oxide facies banded iron formation.

PLATE 1-2. Main plant, Sherman Mine.


SHERMAN MINE
THIS MINE WAS DEDICATED
TO THE MEMORY OF
FRANK A. SHERMAN
1887-1967
A PIONEER OF
THE CANADIAN STEEL INDUSTRY
ON
SEPTEMBER 5TH. 1968
BY THE
HON. JOHN P. ROBARTS Q.C. LL.D
PRIME MINISTER OF ONTARIO


SHERMAN MINE

ground development, and one copper-nickel prospect, the Cuniptau, entered small-scale production (Moorehouse, 1942).

From 1959 to 1961, the Cleveland Cliffs Iron Company conducted geological mapping, sampling and testing of the iron formations. Plant designs were drawn up in 1964 and construction was in progress by 1965. Commencement of operations began in September, 1968.

The Sherman Mine is now a joint venture of Dominion Foundaries and Steel Limited (Dofasco, Hamilton), and the Tetapaga Mining Company, a wholly owned subsidiary of the Cleveland Cliffs Iron Company of Cleveland, Ohio. The operation and management of the mine is by Cliffs of Canada Limited. Manufactured iron ore pellets are sent to Dofasco, Hamilton for processing into steel.

1.4 OBJECTIVES AND THESIS

This thesis is concerned with the detailed characterization of the volcanics stratigraphically below the West and North Pits of the Sherman Mine iron formation (Figure 3-1). The host rocks are characterized through detailed field mapping, petrography and lithogeochemistry.

This study is part of the Ontario Geological Survey Geoscience Research Grant 132 (Crocket et al., 1983). The objective of the research is to establish whether Algoma-type iron formations and their contiguous volcanosedimentary piles are preferential concentrators of base and precious metals with a common genetic link to volcanism and volcanic evolution. The research is carried out by regional and detailed mapping of key sections, followed by isotopic, heavy metal and other compositional characterization of the rocks involved.

CHAPTER 2

METHODOLOGY

2.1 FIELD APPROACH

The intention of this study was, in part, to generate a geologic map updating the 1969-1972 regional mapping (1:15,840) of G. Bennett (1978). Continued operations at the Sherman Mine since 1972 have created various changes in outcrop exposure. For instance, much of the outcrop immediately adjacent to the pits is now covered by waste rock. In addition, the filling of Vermillion Lake with tailings has caused extensive flooding north of the lake. Lumbering operations by William Milne and Son have increased the outcrop exposure to the north of the mine property. Hence the outcrop exposure presently available in the thesis area is largely dissimilar to that which was available to G. Bennett.

The study area is 1.5 km by 5.5 km in area extending from the western edge of the West Pit to the eastern tip of Vermillion Lake (Fig. 3-1). Due to the lack of good outcrop exposure in the west, this area has been mapped on a reconnaissance scale using aerial photo control (1 cm to 156 m, 1 inch to 1320 feet; Figure 3-2). In the east, clear-cut lumbering has exposed sufficient outcrop to warrant more detailed mapping (Maps 1 to 5). This was carried out on grids established by pace and compass on a scale of 1 cm to 6 m, or 1 inch to 50 feet. In addition to the mapping, the fieldwork included an extensive lithogeochemical sampling program.

2.2 XRF ANALYSIS OF MAJOR AND TRACE ELEMENTS

A representative portion of each sample was crushed to -200 mesh using a ceramic lined pulverizer and tungsten carbide shatterbox. Metal contamination introduced by the tungsten carbide dish and puck may be crudely estimated from the trace element analysis of sample TDH 145 in Appendix A. Sample 145 is a quartz vein containing over 98 percent $SiO2$. The concentrations of most trace elements in this sample are at or near detection limits. An exception is noted for Co with a concentration of over 70 ppm. As a result, an evaluation of Co contents are not included in this report.

Fusion pellets were prepared following the procedure outlined by Hutchinson (1977). A 6:1 ratio of flux (1:1 mixture of lithium metaborate and lithium tetraborate) to rock powder was fused in a metal alloy crucible (97% platinum + 3% gold) and poured in a metal alloy pellet mold. The fusion pellets were analysed for the major elements Si, Al, total Fe, Mg, Ca, K, Ti, Mn and P.

Powder pellets were prepared following the procedure outlined by Marchand (1973). Approximately 3 grams of rock powder mixed with 2 drops of MOWIOL (polyvinyl alcohol) were pressed in an aluminum cup to 20 tons pressure. The powder pellets were analysed for the trace elements Cr, Co, Cu, Zn, V, Ni, S, Rb, Sr, Y, Zr, Nb and Ba. Sodium values were also determined on powder pellets. All analyses were carried out using a Philips Model 1450 AHP automatic sequential x-ray fluorescence spectrometer at McMaster University. Sulphur analyses of some samples were obtained by a Model WR-12 LECO sulphur determination (iodine titration), and the values are presented in parts per million. The results for 64 samples are listed in Appendix A.

Variance, standard deviation and coefficient of variation were used as estimates of the precision of the analyses. Precision estimates and the detection limits for the major oxide and trace element data are listed in Appendix B. With the exception of MgO, Na2O and K2O in sample 8, the oxides show a coefficient of variation of $\leq$5%. The coefficient of variation for all of the trace elements are $\leq$15% and most are $\leq$5%.

Accuracy of the XRF analysis is judged by comparing the determined values of standards with the recommended values of Abbey (1977). In Appendix B the comparison prepared by N. Blum (1986) indicates the accuracy for the major elements to be within 5%. Trace elements are generally accurate to within 9% with the exception of those elements with very low concentration, near the detection limits.

2.3 DETERMINATION OF VOLATILES

Loss on ignition (L.O.I.) was determined by heating approximately one gram of sample in an electric furnace at 1000 °C for one hour. The CO2 values were determined by fusing 300-400 mg in a Model WR-12 LECO automatic carbon determinator. Assuming SO2 to be insignificant, the total H2O was then estimated as L.O.I. - CO2.

2.4 ANALYSIS OF GOLD, ARSENIC AND ANTIMONY

Gold, arsenic and antimony were determined by epithermal instrumental neutron activation analysis using the McMaster Nuclear Reactor as a neutron source. Samples were packaged in batches of approximately twelve samples and two standards, and irradiated in a rotatable (two revolutions per minute) cadmium-shielded (transparent only to epithermal neutrons) RIFLS (Reactor Irradiation Facility--Large Samples) position where the approximate total thermal flux was 8x10exp12 neutron/cm2/sec. Samples of 500 to 1000 mg were packaged in 2/5 dram polyethylene flip top vials. Standards were prepared by weighing appropriate amounts of weakly acidic aqueous solutions of metals (Au, As and Sb) into plastic vials filled with volumes of silica powder sufficient to yield nearly equal volumes of standards and samples.

The schedule of irradiation, cooling, and counting times and the characteristics of analytical γ-rays are tabulated below.

Nuclide	Irradiation Time,hrs.	Cooling Time,hrs.	Counting Time,hrs.	Analytical γ-ray,KeV	T1/2 hrs.
Arsenic-76	1	50	0.5	559	26.3
Gold-197	1	72	1.0	412	64.7
Antimony-122	1	72	1.0	564	65.3

Gamma-ray spectra were taken on a Canberra Series 80 multichannel analyser (MCA) coupled to an intrinsic coaxial germanium detector (Aptec Egineering Ltd., Mississauga, Ontario). The detector characteristics were: active volume, 55 cm3; resolution 1.8 KeV (FWHM) at 1.33 MeV; relative efficiency 10% and peak to Compton ratio, 35/1. Spectra were taken in 4095 channels with the MCA calibrated at 0.16 KeV per channel. Under these conditions full peak width for Au, As and Sb were typically 22, 29 and 31 channels respectively.

The minimum detectable metal concentrations are dependent on sample bulk composition. For the rocks analysed in this study, they are approximately 2 ppb Au, 2 ppm As and 0.2 ppm Sb.

2.5 DETERMINATION OF RARE EARTH ELEMENTS

The rare earth elements (REE) were determined by neutron activation analysis using two irradiations. In the first irradiation the epithermal component of the neutron flux was used for determination of La and Sm. In the second irradiation the full thermal neutron flux was employed for determination of the remainder of the REE including Ce, Nd, Eu, Gd, Tb, Tm, Yb and Lu. The second irradiation was done on the sample material previously irradiated, after a decay period of approximately 14 days. The REE determined in the second irradiation were counted in two lots. The shorter lived elements were counted 7 to 10 days after the irradiation and the longer lived elements 50 to 60 days after irradiation. Batches of approximately 12 samples and 2 standards were irradiated. The usual sample weight taken was 500 to 1000 mg and 2/5 dram polyethylene flip top vials were used as sample containers.

The schedule of irradiation, cooling and counting times together with relevant nuclear data are summarized below.

First Irradiation (Epithermal);
Tir, 1h at 2 megawatts; Td, 3 to 5d; Tc, 2000s

Elements Determined	Reaction	Analytical γ-ray, KeV	Nuclide Half Life
La	139La(n,γ) 140La	1596	40.23h
Sm	152Sm(n,γ) 153Sm	103.2	46.7h

Second Irradiation (Thermal); Tir, 3.5h at 2 megawatts;
First Count after Td 7 to 10d; Tc, 4000s

Nd	146Nd(n,γ) 147Nd	91.1	10.99d
Tb	159Tb(n,γ) 160Tb	298.6	72.4d
Yb	174Yb(n,γ) 175Yb	282.5	4.19d
Lu	176Lu(n,γ) 177Lu	208.4	6.71d

Second Irradiation;
Second Count after Td 50 to 60d; Tc, 4000s

Elements Determined	Reaction	Analytical γ-ray, KeV	Nuclide Half Life
Ce	$^{140}Ce(n,\gamma)$ ^{141}Ce	145.4	32.5d
Eu	$^{151}Eu(n,\gamma)$ ^{152}Eu	121.8	13.4y
Gd	$^{152}Gd(n,\gamma)$ ^{153}Gd	103.2	241.6d
Tm	$^{169}Tm(n,\gamma)$ ^{170}Tm	84.3	129d

Tir	irradiation time
Td	decay time (end of irradiation to beginning of counting)
Tc	count time

y - years; h - hours; s - seconds
Source of γ-ray energies and nuclide half lives is : Chart of the Nuclides, 12th edition, 52p, 1977 by F.W. Walker, G.J. Kirovac and F.M. Rourke.

Rock powders used as standards were Open University AC(OURS). Chondrite normalization factors used are La=0.330, Ce=0.88, Nd=0.60, Sm=0.181, Eu=0.069, Gd=0.249, Tb=0.047, Tm=0.030, Yb=0.200 and Lu=0.034 (Haskin et al.,1968). The spectrometer and detector system (Canberra Series 80 MCA and Aptec intrinsic coaxial detector) were described in the previous section. For REE analysis spectra were taken in 4095 channels with the MCA calibrated at 0.40, 0.90 and 0.33 KeV per channel for the 1st, 2nd and 3rd count periods respectively. For the rocks analysed in this study which included no ultramafic compositions, REE were sufficiently high that no significant problems due to analytical sensitivity were encountered.

CHAPTER 3

GENERAL GEOLOGY

3.1 REGIONAL GEOLOGY AND METAMORPHISM

The regional geology of the northeast Temagami area is discussed by Bennett (1978), and his geological map of the area is shown with minor modifications in Figure 3-1. The greenstone belt at Temagami is Early Precambrian (Archean) in age. It trends northeast and is approximately 13 km (8 miles) wide and 29 km (18 miles) long. The volcanosedimentary complex is surrounded and intruded by Archean granitic batholiths, and overlain in the northwestern and southeastern areas by rocks of the Gowganda Formation, Huronian Supergroup. Small Archean mafic and ultramafic dykes intrude the volcanics, sediments and granitic stocks. The youngest rocks in the area are Late Precambrian northwest-trending diabase dykes (Bennett, 1978).

The main fold structure of the Temagami area is the northeast-trending Lake Tetapaga syncline (as shown in Figure 3-1). Its presence is inferred by top determinations of pillows in mafic volcanics north of the axis, and by graded bedding in sediments south of the axis. Three major fracture patterns trending north, northeast and northwest are present in the area. The

FIGURE 3-1. Location of the thesis area and regional geology of the Sherman Mine, modified after Bennett (1978).

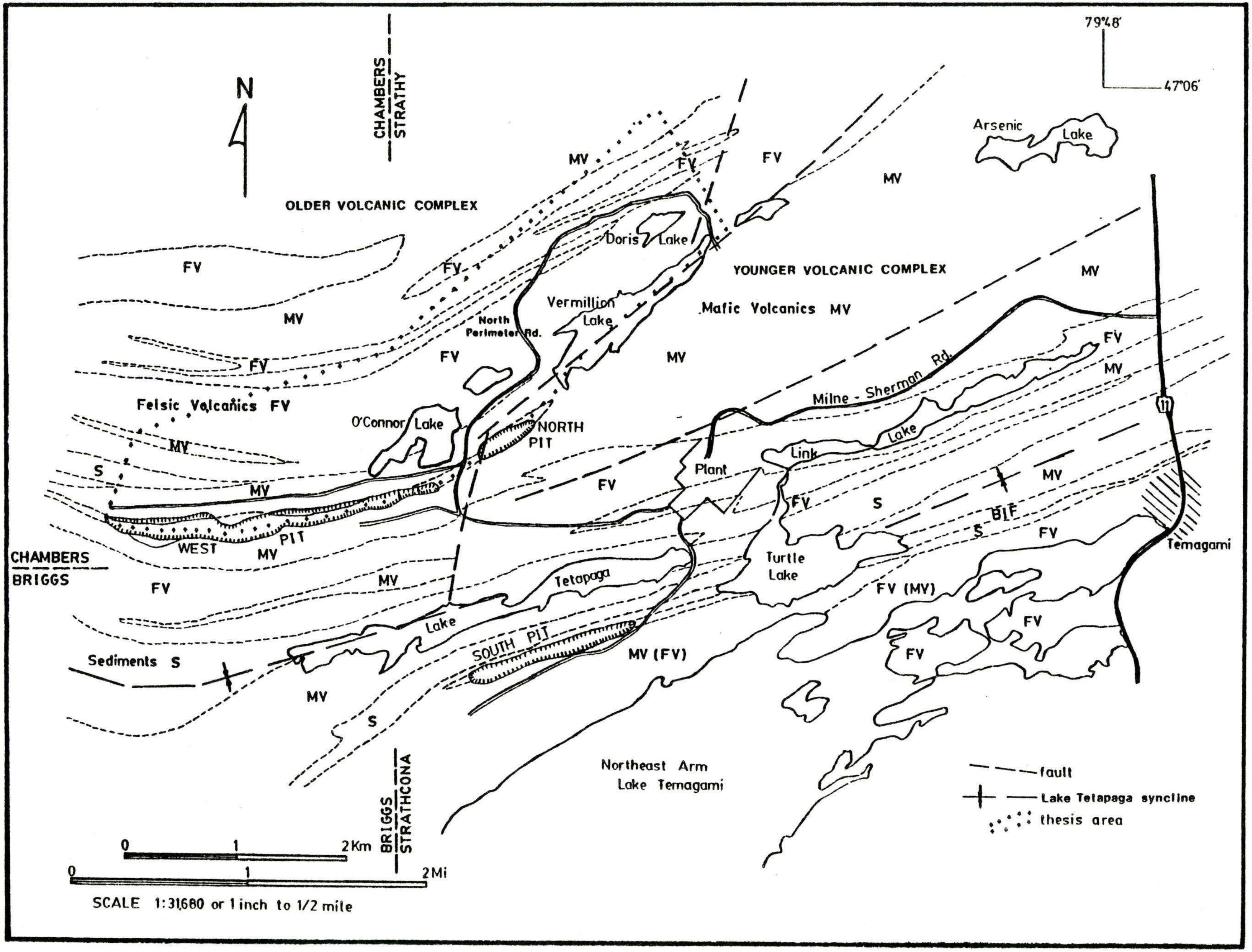
N
CHAMBERS
STRATHY
79°48′
47°06′
Arsenic Lake
OLDER VOLCANIC COMPLEX
YOUNGER VOLCANIC COMPLEX
Mafic Volcanics MV
Felsic Volcanics FV
Sediments S
MV
FV
S
Doris Lake
Vermillion Lake
North Perimeter Rd.
O'Connor Lake
NORTH PIT
WEST PIT
SOUTH PIT
Tetapaga Lake
Plant
Link Lake
Turtle Lake
Milne - Sherman Rd.
11
Temagami
BIF
FV (MV)
MV (FV)
Northeast Arm Lake Temagami
CHAMBERS
BRIGGS
BRIGGS
STRATHCONA
fault
Lake Tetapaga syncline
thesis area
0
1
2Km
0
1
2Mi
SCALE 1:31,680 or 1 inch to 1/2 mile

extensive northwest-trending faults are delineated by major topographic lineaments and by continuous diabase dykes. The northeast-trending faults and shear zones occur mostly along bedding planes. North-trending faults, as indicated by topographic lineaments, are numerous to the north and northeast of the thesis area, south of Kanichee Lake (Bennett, 1978).

The metavolcanics in the northeast Temagami area are altered to the quartz-albite-muscovite-chlorite subfacies of the greenschist facies of regional metamorphism (Bennett, 1978).

Two bands of Algoma-type iron formation form marker horizons in the greenstone belt (Figure 3-1). The northern band hosts the West and North Pits of the Sherman Mine. The average thickness of the northern band is 90 m with a maximum thickness of 180 m (Campbell, 1978). Felsic metavolcanics hosting the iron formation dip 80-85° south. The southern band hosts the South and East Pits and extends east of Turtle Lake crossing Highway 11. The southern band averages 55 m in thickness with a maximum of 85 m, and dips 75° to the north (Campbell, 1978).

The two bands of iron formation were interpreted by Bennett (1978) to represent stratigraphically equivalent marker horizons of the north and south limbs of the Lake Tetapaga syncline. Some features of the two iron bands and their immediate host rocks dispute this interpretation. The iron formation in the West Pit is underlain by felsic pyroclastics whereas the rocks that underly the South Pit iron formation are thinly bedded turbidite sediments (Fyon, pers. comm., 1984). A graphitic slate unit containing nodular pyrite is found in the footwall of the northern band of iron formation whereas in the southern band it is found in the hanging wall.

The marked asymmetry of the fold axis with respect to the northern and southern iron formation was noted by Bennett (1978). He suggested two possible causes. The first required faulting in which a wedge-shaped block of metavolcanics was either introduced into the metavolcanic pile just south of the northern limb of the syncline, or removed from the sequence just north of the southern band of iron formation. The second possibility was a lack of balance between depositional and erosional processes during accumulation of the volcanic pile. The latter was also maintained by Campbell (1978), who suggested that the inverse nature of the graphitic horizon in the Temagami iron formation was due to volcanic-sedimentary facies changes, whereby periods of volcanism, sedimentation and quiescence shifted throughout the basin with time.

Based on field mapping by A. Fyon (pers. comm., 1984 field season) in central Strathy Township, and by the author in the southern Chambers-Strathy Townships, the following is a suggested interpretation of the regional geology of the two bands of iron formation.

The northern band of iron formation lies at the top of an older volcanic complex (OVC; Figure 3-1) composed dominantly of calc-alkaline basalts, andesites, dacites and rhyolites, with felsic members becoming increasingly dominant toward the top of the cycle. The overlying younger volcanic complex (YVC) extends southwards from the northern band of iron formation. In the east it is separated from the OVC by a northeast-trending fault (Figure 3-1). Minor intercalations of iron formation with the basal members of the YVC occur northeast of Vermillion Lake. This implies that the deposition of iron in the east was disrupted by the onset of new volcanism. The tentative source for the volcanism in the YVC lies to the northeast (Fyon, pers. comm., 1984).

The basal members of the YVC are massive, pillowed and variolitic Fe-tholeiitic basalts, which are overlain by calc-alkaline basalts, andesites, rhyolite intrusives and pyroclastics. Overlying the volcanics are coarse turbidite conglomerates and thin bedded turbidite greywackes. South of the Lake Tetapaga syncline axis the iron formation lies within and near the top of a turbidite package, which in turn is overlain by Fe-tholeiitic basalts. North of the syncline axis the iron formation is absent from the sequence (Fyon, pers. comm., 1984).

Rather than representing stratigraphically equivalent marker horizons of north and south limbs of the Lake Tetapaga syncline, it is contended that the northern and southern bands of iron formation at Temagami are unrelated in time. The northern band lies at the top of an older volcanic complex, which is overlain by volcanics and turbidite sediments of a younger volcanic complex. The YVC is capped by the southern band of iron formation and overlain by mafic volcanics of a younger volcanic cycle.

3.2 MINERAL OCCURRENCES

Bennett (1978) reported a total of 130 mineral occurrences in the northeast Temagami area, including all visible concentrations of sulphide and arsenide minerals, and quartz veins known to contain significant values of gold or silver.

According to Bennett (1978) the highest concentration of mineral occurrences per unit area of rock type is found within the rhyolitic metavolcanics, followed by mafic intrusions, and finally by mafic metavolcanics. Eighty percent of the mineral occurrences within the metavolcanic assemblage are located within central Strathy Township. The highest frequency of mineral occurrences is located northeast of Vermillion Lake, just northeast of the thesis area.

The gold and silver deposits located northeast of Vermillion Lake are associated with pyritic ores (Moorehouse, 1942). Arsenic-bearing gold and silver showings such as the Big Dan and Arsenic Lake are hosted in north-trending chloritized shear zones in the mafic volcanics (Crocket et al., 1984).

Copper- and nickel-sulphide deposits are closely associated with the mafic to ultramafic intrusive rocks at Temagami (Bennett, 1978). The most significant deposit is located in central Strathy Township on the north edge of the Ajax Intrusion.

3.3 LOCAL GEOLOGY - OLDER VOLCANIC COMPLEX

Map 6a (Figure 3-2) is a layout of the geologic mapping completed in the thesis area. All mapping south and west of Map 1 was completed at a scale of 1 cm to 156 m , 1 inch to 1320 feet. Detailed field maps (1-5) of the area north of Vermillion Lake are located in the map pocket. Map 6b (Figure 3-3) is a simplified version of the geology across the entire section. The legend presented for maps 6a and 6b is the same for the field maps. A legend and symbols key is also printed on Map 5.

The volcanic section studied (Figure 3-1) represents the upper portion of a typical volcanic cycle as described in general terms by Goodwin (1977). Basal ultramafic flows are absent and mafic flows (basalts) are rare. This volcanic cycle is part of the youngest or stratigraphically uppermost units of the older volcanic complex discussed earlier. The volcanics strike between 50° and 72° and dip south at 80° to nearly vertical. The stratigraphic top, measured from graded pyroclastic units and flow tops, is to the south.

The most pronounced and regionally consistent foliation in the rocks is coincident with bedding. Small discontinuous shear zones are common and increase in frequency toward the northeast. The strike of the shear zones varies from 15° to 55°. They are usually accompanied by carbonate alteration and often by pyritization. Minor tight folding within a banded felsic intrusive (Plate 3-1) and within a mafic flow breccia (Plate 3-2) occurs in the north-central section of the thesis area (Map 3).

FIGURE 3-2. Geology of the volcanics immediately underlying the West and North Pits, and location of the detailed map areas north of Vermillion Lake.

LEGEND

LATE PRECAMBRIAN

MAFIC INTRUSIVE ROCKS

7a	Olivine diabase

EARLY PRECAMBRIAN (ARCHEAN)

FELSIC INTRUSIVE ROCKS

6a	Quartz-feldspar porphyry

INTERMEDIATE TO MAFIC INTRUSIVE ROCKS

5a	Diorite, quartz-diorite
5b	Lamprophyre

METASEDIMENTS

4a	Iron formation

FELSIC TO INTERMEDIATE METAVOLCANICS

INTRUSIVES

3	Unsubdivided
3a	Felsic intrusion - early
3b	Felsic intrusion - late
3c	Felsic intrusive breccia
3d	Intermediate intrusion containing fragments of underlying strata

FLOWS, PYROCLASTICS

2	Unsubdivided dacite
2a	Quartz-porphyritic rhyolite
2b	Phyric-bearing dacite
2c	Flow breccia, hyaloclastite
2d	Lithic tuff (<4mm)
2e	Crystal tuff (<4mm)
2f	Lapilli tuff (4-32mm)
2g	Tuff breccia (>32mm)

INTERMEDIATE TO MAFIC METAVOLCANICS

1	Unsubdivided andesite, basalt
1a	Feldspar-porphyritic andesite
1b	Phyric-bearing andesite, basalt
1c	Flow breccia, hyaloclastite
1d	Lithic tuff (<4mm)
1e	Crystal tuff (<4mm)
1f	Lapilli tuff (4-32mm)
1g	Tuff breccia (>32mm)
1h	Pyroclastic debris flow

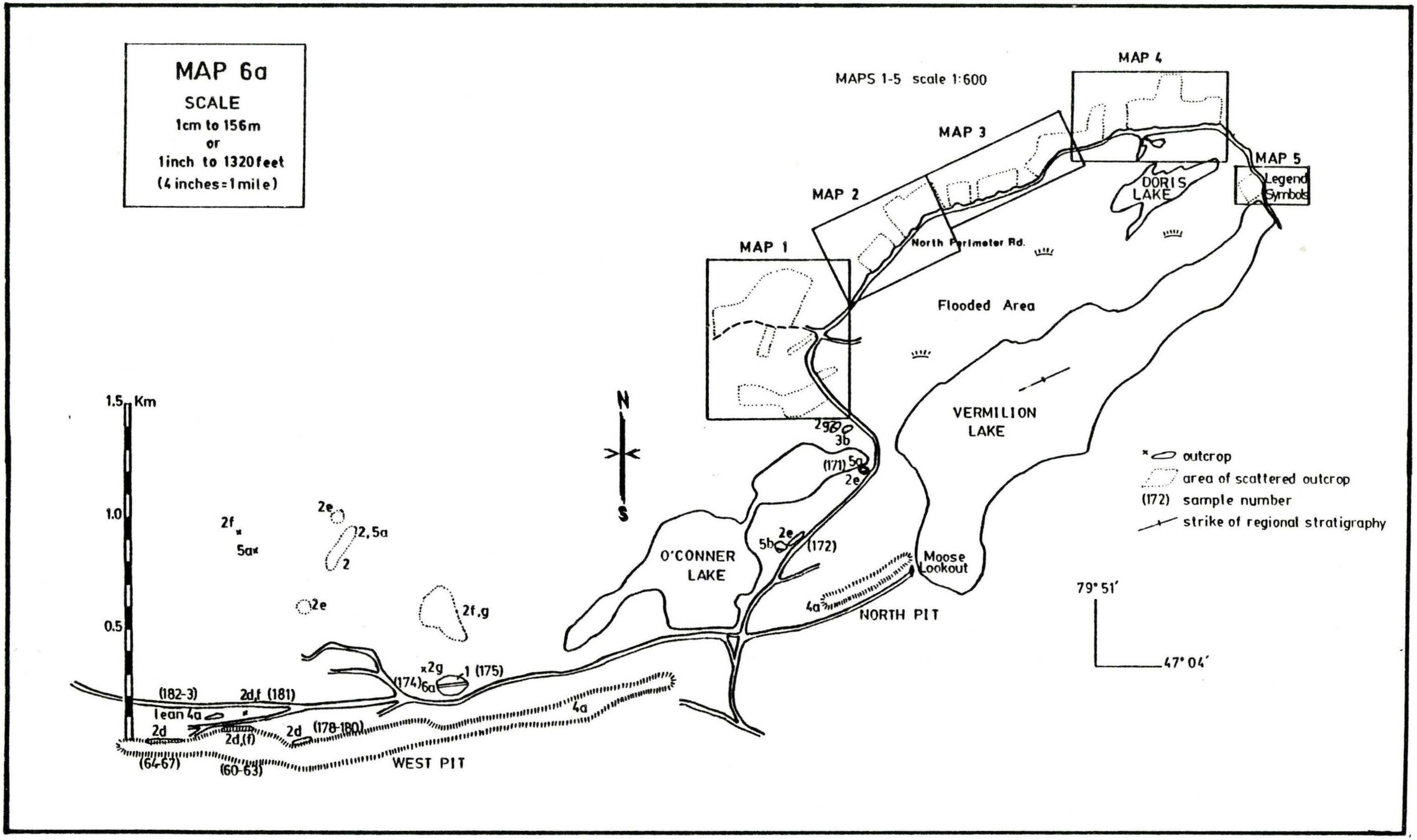
MAP 6a
SCALE
1cm to 156m
or
1inch to 1320feet
(4 inches=1mile)
MAPS 1-5 scale 1:600
MAP 1
MAP 2
MAP 3
MAP 4
MAP 5
Legend Symbols
North Perimeter Rd.
DORIS LAKE
Flooded Area
VERMILION LAKE
O'CONNER LAKE
Moose Lookout
NORTH PIT
WEST PIT
N
S
1.5 Km
1.0
0.5
outcrop
area of scattered outcrop
(172) sample number
strike of regional stratigraphy
79° 51′
47° 04′
2g
3b
(171) 5a
2e
2e
5b
(172)
4a
2e
2f
5a
2,5a
2
2e
2f,g
2g
1 (175)
(174) 6a
(182-3)
2d,f (181)
lean 4a
2d
2d,(f)
2d
(178-180)
4a
(64-67)
(60-63)

FIGURE 3-3. Simplified geology of the volcanics stratigraphically underlying the northern band of iron formation, Sherman Mine.

LEGEND

LATE PRECAMBRIAN

MAFIC INTRUSIVE ROCKS

7a	Olivine diabase

EARLY PRECAMBRIAN (ARCHEAN)

FELSIC INTRUSIVE ROCKS

6a	Quartz-feldspar porphyry

INTERMEDIATE TO MAFIC INTRUSIVE ROCKS

5a	Diorite, quartz-diorite
5b	Lamprophyre

METASEDIMENTS

4a	Iron formation

FELSIC TO INTERMEDIATE METAVOLCANICS

INTRUSIVES

3	Unsubdivided
3a	Felsic intrusion - early
3b	Felsic intrusion - late
3c	Felsic intrusive breccia
3d	Intermediate intrusion containing fragments of underlying strata

FLOWS, PYROCLASTICS

2	Unsubdivided dacite
2a	Quartz-porphyritic rhyolite
2b	Phyric-bearing dacite
2c	Flow breccia, hyaloclastite
2d	Lithic tuff (<4mm)
2e	Crystal tuff (<4mm)
2f	Lapilli tuff (4-32mm)
2g	Tuff breccia (>32mm)

INTERMEDIATE TO MAFIC METAVOLCANICS

1	Unsubdivided andesite, basalt
1a	Feldspar-porphyritic andesite
1b	Phyric-bearing andesite, basalt
1c	Flow breccia, hyaloclastite
1d	Lithic tuff (<4mm)
1e	Crystal tuff (<4mm)
1f	Lapilli tuff (4-32mm)
1g	Tuff breccia (>32mm)
1h	Pyroclastic debris flow

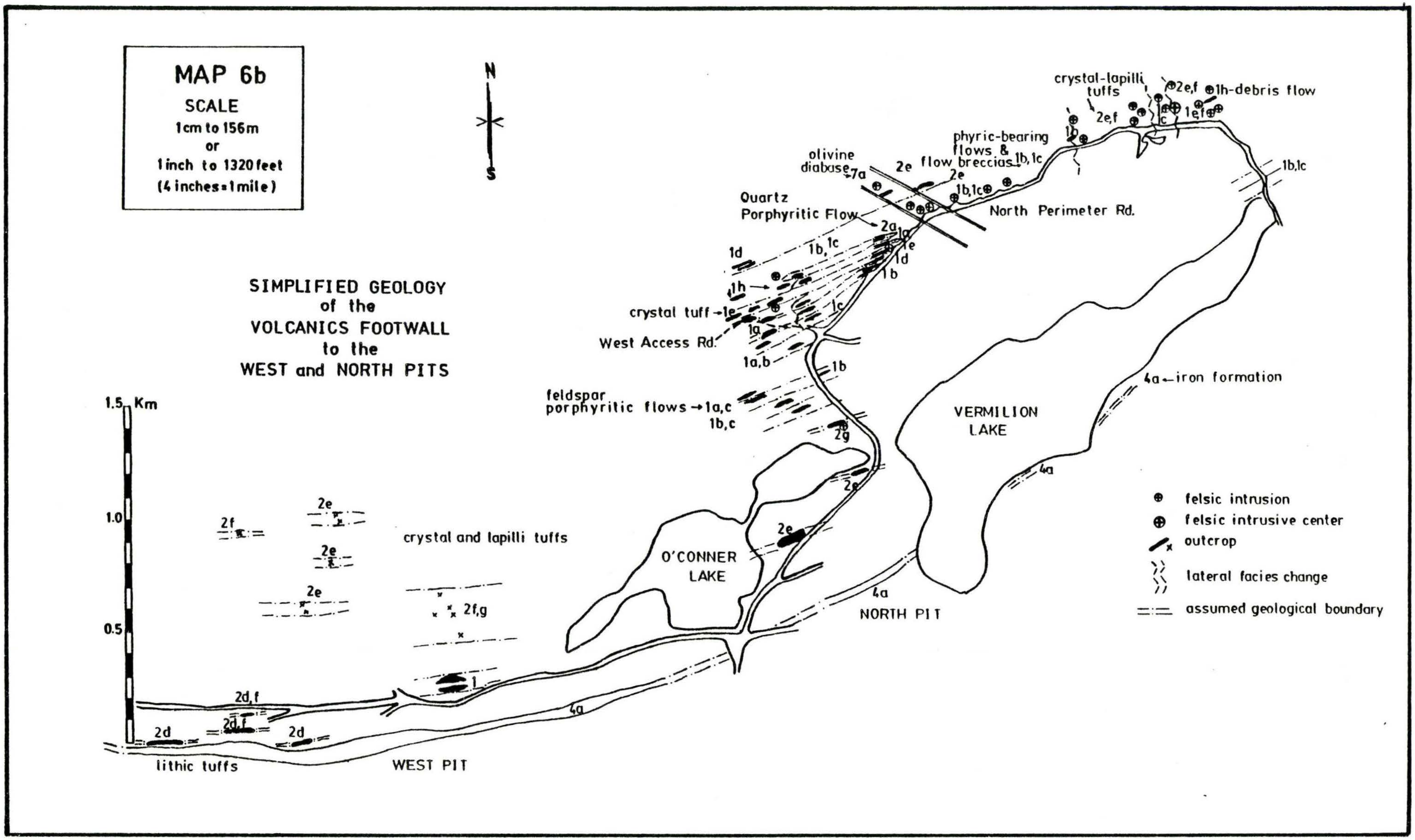

MAP 6b

SIMPLIFIED GEOLOGY of the VOLCANICS FOOTWALL to the WEST and NORTH PITS

PLATE 3-1. Minor folding in siliceous bands of the late felsic intrusive.

Pen magnet is 14 cm in length.

PLATE 3-2. Folded Fe-sulphide stains in a mafic flow breccia.

The fold axes are sub-parallel to the foliation and regional strike of the area. The immediate section (Map 3) is characterized by numerous small shear zones, pronounced carbonate alteration and rusty sulphide weathering. Localized silicification is apparent around gossan zones in the mafic to intermediate flows.

The 1 km stratigraphic section immediately underlying the West and North Pits (Figure 3-3) is dominated by felsic pyroclastics. An isolated mafic flow outcrops 250 m north of the West Pit. The rocks immediately adjacent to the West Pit are felsic lithic tuffs which grade into fine ash tuffs, cherts and graphitic sediments. The stratigraphic section extending 1 to 1.5 km stratigraphically below the iron formation is dominated by intermediate (andesite) flows and flow breccias. Intercalated with the andesites are mafic (basalt) flows and hyaloclastites, intermediate to mafic pyroclastics, and minor rhyolite flows and debris flows.

The northeast corner of the map area is dominated by a highly silicic, high level felsic intrusion which appears to be synvolcanic in nature and intruded in at least two consecutive episodes. A felsic intrusive center has been identified in this sector (Figure 3-3, Map 4). Intrusive breccias are also common in the area. Volcanic rock units in the north-central to northeast corner of the map area (Maps 3 and 4) are generally discontinuous, and abrupt lateral facies changes are apparent. The interpreted facies changes separate zones dominated by flows and flow breccias from zones dominated by pyroclastic rocks.

The presence of coarse intrusive breccias, lateral facies changes and a felsic intrusive center in the northeast corner implies a focus of volcanism in this area, possibly a small eruptive center (parasitic cone) on the flank of a larger volcano.

The volcanics and synvolcanic felsic intrusives are intruded by a swarm of Archean mafic intrusives. Two northwest-trending Late Precambrian diabase dykes outcrop in the north-central section of the map area.

3.4 INTERMEDIATE TO MAFIC METAVOLCANICS

Rocks classified as intermediate to mafic volcanics are greyish-green on fresh surfaces and range from blue-grey to blue-green on weathered surfaces. Carbonatized outcrops weather a typical light tan to buff colour. Most of the metavolcanics in this group are andesites in composition.

3.4.1 Flows, Flow Breccias, and Hyaloclastites

The most common intermediate to mafic flows in the area are fine- to medium-grained, phyric-bearing andesites and basalts. The flows are characterized by microscopic plagioclase crystals and dark chloritized phenocrysts. Flow banding is recognizable in many of the phyric flows. In thin section the banding is defined by the parallel arrangement of lath-shaped plagioclase crystals.

Feldspar-porphyritic andesites are fairly common and quite distinctive in the field. Their weathered surface is a typical blue-grey and spotted with white weathered stubby plagioclase crystals (Plate 3-3). The plagioclase crystals are poorly aligned (Plate 4-1) and flow banding is not obvious on the outcrop. The flows occasionally host darker fragments which are fine-grained equivalents of the matrix (Plate 3-3). Layering in the feldspar-porphyritic flows is sometimes characterized by a feldspar-rich and feldspar-poor zonation.

Due to limited outcrop exposure, the width and extent of the intermediate to mafic flows is not easily ascertained. Most flows appear to be thin (2 m or less) and discontinuous. It is not apparent that any flows in the area exceed 3 to 4 m in thickness. The longest distance over which individual flows can be traced is 1/2 km (Figure 3-3, Maps 1 and 2).

Flow breccias dominate in the north-central section of the thesis area (Maps 1 to 5). Many of the breccias form bases and tops to massive flows. The majority; however, are autoclastic flows in which the entire flow has been brecciated during flow movement. Autoclastic volcanic breccias are defined by Wright and Bowes (1963) as the fragmentation of lava during movement, or the explosive disruption of lavas by contained gases. Most of the flow breccias in the area contain monolithic subangular to subrounded fragments with an average size range of 5 to 25 cm. Other flow breccias contain blocky fragments up to 55 cm in diameter. Plate 3-4 is a moderately fine-grained breccia in

PLATE 3-3. Stubby white plagioclase phenocrysts and dark, fine-grained flow fragments in a feldspar porphyritic flow. Pencil sharpener is 2.5 cm in length.

PLATE 3-5. "Snake-skin" alteration texture in a mafic hyaloclastite. Pen magnet is 14 cm in length.

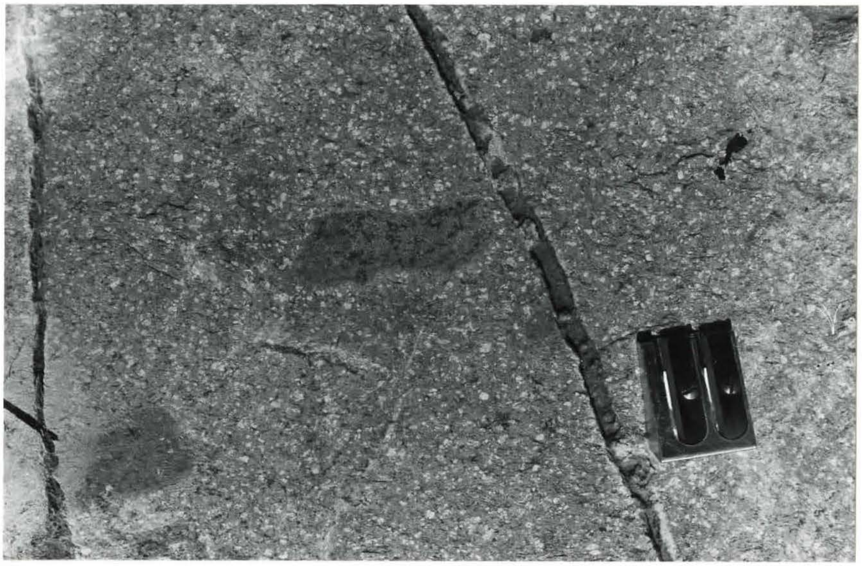

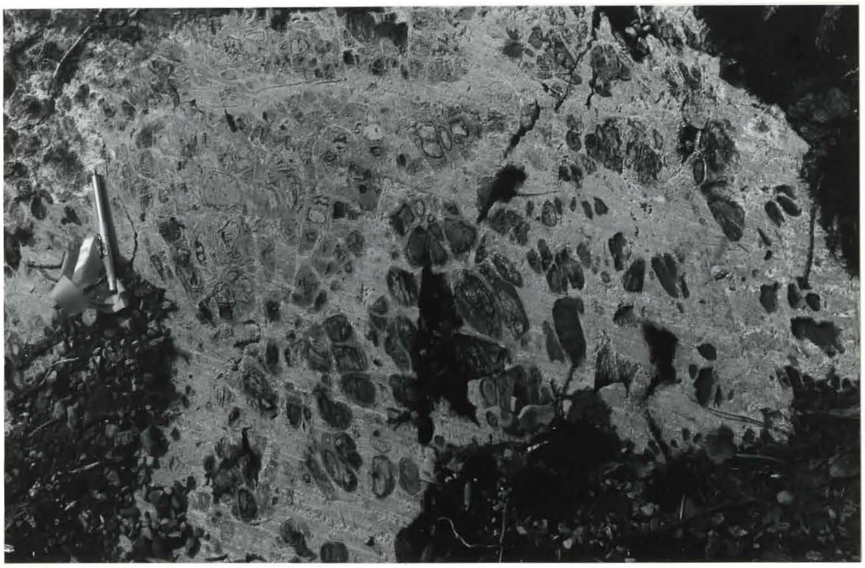

PLATE 3-4. Intermediate to mafic flow breccia. Jagged dark flow fragments are hosted in a granulated and sericitized matrix.

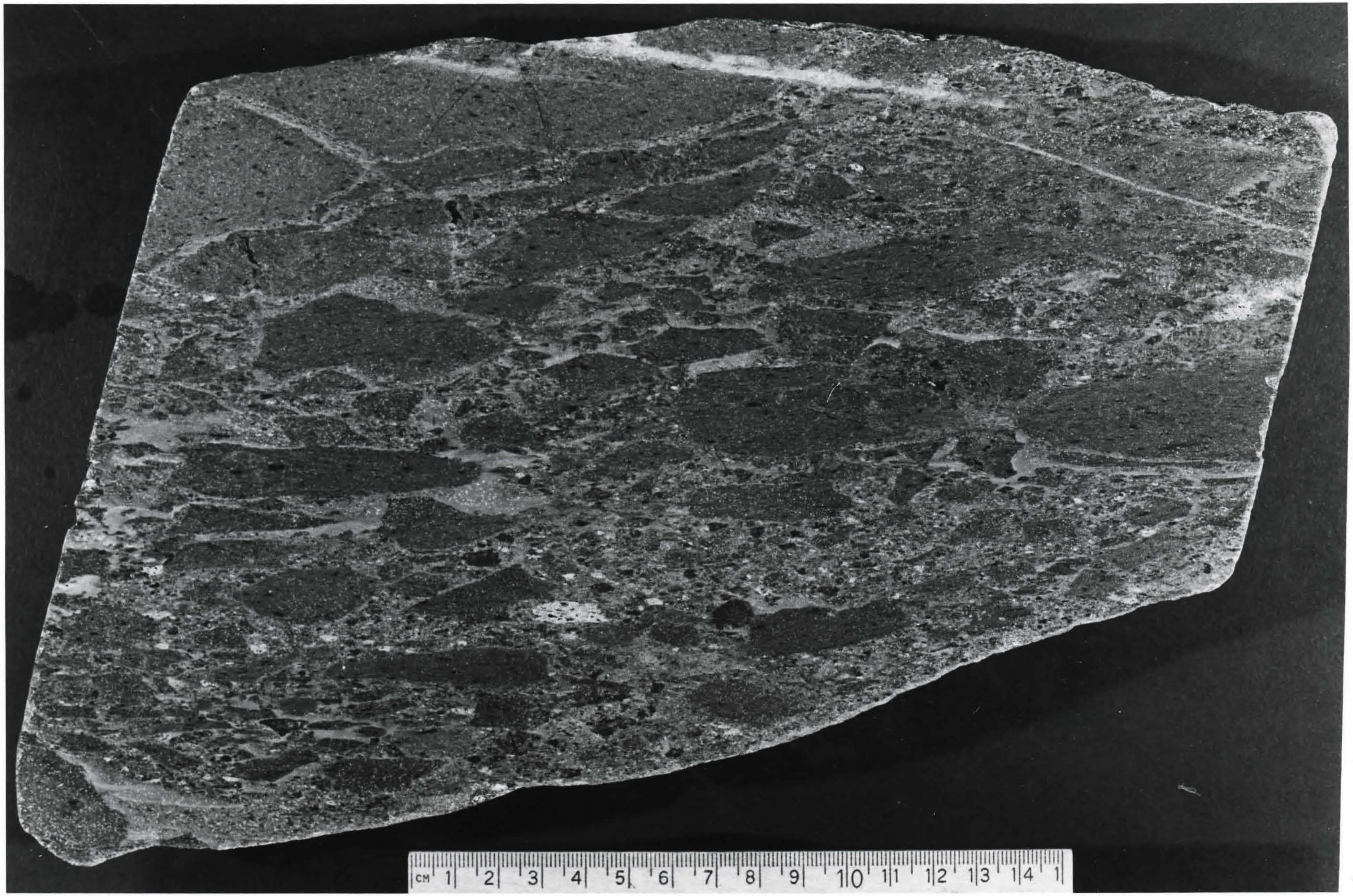
CM 1 2 3 4 5 6 7 8 9 10 11 12 13 14

which dark jagged flow fragments are hosted by a granulated and seriticized matrix.

Thin hyaloclastite breccias occur throughout the northern map area. They overlie massive flows and are recognized by a unique "snake-skin" texture (Plate 3-5) on the weathered surface. The subangular fragments range from less than 1 to 7 cm (average 1 to 2 cm) in diameter. In Plate 3-5 the matrix to the fragments is carbonatized and sericitized. Individual fragments are characterized by zonal alteration (Plate 4-2). Pichler (1965) defined hyaloclastites as fine- to coarse-grained volcaniclastic deposits formed by the quick chilling of fluid volcanic materials in contact with water. The fragmentation results from thermal strain within a differentially cooled solid (Carlisle, 1963). The hyaloclastites in Temagami are similar in character to those described by Dimroth (1977) in the Rouyn-Noranda area.

3.4.2 Pyroclastics

Pyroclastic rocks are produced by explosive or aerial ejection of material (tephra) from a volcanic vent (Fisher, 1966). The pyroclastic rocks in the thesis area are classified according to grain size and composition. The range in grain size for each class is:- tuff (<4 mm); lapilli tuff (4-32 mm); and tuff breccia (>32 mm). Pyroclastics described as "crystal" are composed dominantly of individual crystals and crystal fragments. Those described as "lithic" are composed dominantly of microcrystalline or phanerocrystalline rock fragments. Pyroclastics classified as crystal lapilli tuffs and crystal tuff breccias are composed of rock fragments hosted in a dominantly crystal tuff matrix.

The mafic to intermediate pyroclastics in the thesis area are crystal tuffs and lithic lapilli tuffs. The crystal tuffs are massive, ranging from 60 cm to 5 m wide with no internal variation. Mafic crystal tuffs located northeast of O'Conner Lake (Figure 3-3, Maps 1 and 2) can be traced along strike for 750 m. Disseminated pyrite and leucoxene crystals are visible in hand specimen. Abundant disseminated pyrite is found in a crystal tuff located in the northeast corner of the map area (TDH-34; Map 4). This rock is heavily carbonatized and quite vesicular on the weathered surface. It is an isolated volcanic unit located in a region dominated by felsic intrusives.

Lithic lapilli tuffs are found 200 m stratigraphically below the crystal tuffs (Map 1). The tuffs are poorly sorted with rock fragments ranging in size from 3 mm to 4 cm (average 7 mm). The average width of individual beds is 5 cm. A disseminated pyrite + magnetite zone was found near the contact with a mafic intrusive.

3.4.3 Pyroclastic Debris Flows

In the literature, pyroclastic debris flows (or laharic breccias) are defined as volcanic conglomerates produced by downslope flowage of volcanic debris off the side of a volcano (Fisher, 1960; Mullineaux and Crandell, 1962). Lahars may occur contemporaneously with major eruptions when large quantities of unconsolidated fragmental material are suddenly erupted on the flanks of a volcano, or long after eruptions when large volumes of volcanic debris become water saturated and unstable and collapse downslope as landslides of volcanic debris. Vent facies laharic breccias are interbedded with other pyroclastics and flows (Mullineaux and Crandell, 1962).

Possible pyroclastic debris flows in the thesis area are found as isolated units adjacent to flows and flow breccias (Maps 1 and 4). The debris fragments are essentially monolithic and subangular to subrounded in shape (Plate 3-6). Sorting is absent with fragments ranging in size from 1 cm to 1 m in diameter. Fragments may compose up to 90 percent of the flow. The matrix to the flow is a fine-grained chloritic "mud". Some of the fragments in the flows are partly to completely replaced by pyrite.

3.5 FELSIC TO INTERMEDIATE METAVOLCANICS

The rocks classified as felsic to intermediate volcanics are characterized by tan to white coloured weathered surfaces. Fresh surfaces range from light grey and light green in the dacites, to pale green and creamy white in the rhyolites. Although classified as dacite to rhyolite, some of the pyroclastic rocks mapped north of Vermillion Lake may well be andesites in composition.

PLATE 3-6. Pyroclastic debris flow. Subangular to subrounded rocks and boulders are hosted in a fine-grained chloritic matrix.

Pen magnet is 14 cm in length.

PLATE 3-7. Flow laminated base of a rhyolite ("moonrock").

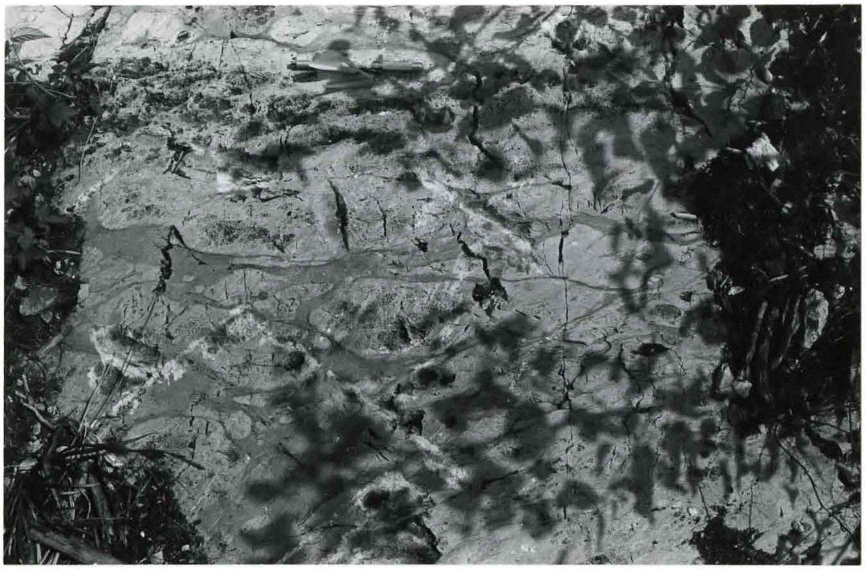

3.5.1 Flows

Felsic flows are rare in the section studied, and consist of one phyric-bearing dacite (Map 4) and one quartz-porphyritic rhyolite (Maps 1 and 2). The phyric-bearing dacite is fine-grained and massive in character. Small chlorite clots are disseminated throughout the flow and represent either infilled vesicles or a replacement of mafic minerals.

The quartz-porphyritic rhyolite outcrops in two locations, 1/2 km apart, along a stratigraphic horizon. In both locations the rhyolite flow is overlain by a feldspar-porphyritic andesite. The rhyolite flow was nicknamed "moonrock" for its distinctive white dome appearance in the field. Fresh surfaces of the rhyolite are pale green and translucent. Weathered surfaces are white with shades of violet and green.

The western outcrop of rhyolite has a flow-laminated base (Plate 3-7). The dark, contorted laminations are probably concentrations of sericite. Flow laminations in rhyolite flows from Rouyn-Noranda are defined by discontinuous streaks of chlorite and/or sericite which formed when vesicles were drawn out by shear flow (Dimroth and Rocheleau, 1979). Flow structure in the moonrock is also defined by an alternation of vesiculated and poorly-vesiculated lava (Plate 3-7). Similar flow structures are reported by Dimroth et al. (1979) for subaqueous rhyolites. The moonrock lacks the brecciated flow top that is typical of most subaqueous rhyolite flows.

3.5.2 Pyroclastics

The scheme used to classify the pyroclastics was outlined in section 3.4.2. The felsic to intermediate pyroclastics found north of Vermillion Lake are crystal lapilli tuffs, and lithic lapilli and lithic tuff breccias. The tuffs are largely dacite in composition, though some may be andesites. Lithic tuffs and lithic lapilli tuffs of dacite to rhyodacite composition underlie the West Pit. Crystal tuffs and lapilli tuffs are the dominant lithology for the first 700 m stratigraphically underlying the iron formation (Figure 3-3).

Coarse, stratified, crystal lapilli tuffs are found in the northeast (Map 4). Individual beds are poorly sorted and range from 1 to 50 cm (average 12 cm) in thickness (Plate 3-8). No grading is evident within the beds. Lapilli rock fragments are 1 to 3 cm in size, and occasional breccia-sized fragments (up to 5 cm) are also present. The beds are disrupted by minor northeast-trending offsets (Plate 3-8). The matrix of the pyroclastics was identified petrographically as a crystal tuff.

Lithic lapilli tuffs located in the northeast corner of Map 2 lack the well-defined stratification of the previous rocks. Angular lithic rock fragments are 5 mm to 3 cm (average 1.5 cm) in size and compose 30 percent of the rock. The rock fragments contain abundant chlorite spots, probably after mafic minerals, and are hosted by a medium-grained lithic matrix.

Lithic tuff breccias (Map 1) are poorly sorted with rock fragments varying from 1 to 60 cm in size. The frequency and

PLATE 3-8. Stratified crystal lapilli tuffs in the northeast section of the map area. Pen magnet is 14 cm in length.

PLATE 3-9. Felsic lithic tuffs underlying the iron formation, north wall of the West Pit.

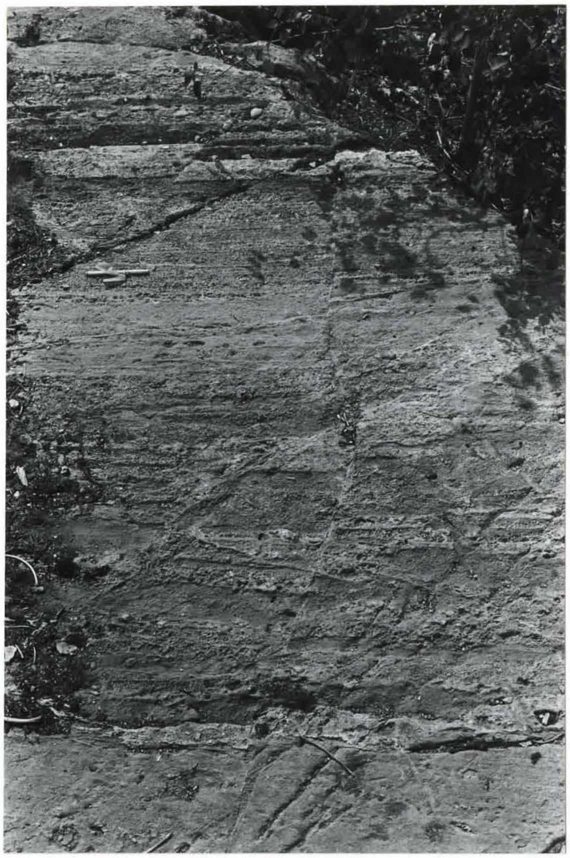

size range of rock fragments varies within some units and a crude stratification is developed. Elongated fragments are oriented parallel to the regional strike of the area.

Felsic crystal tuffs located east of O'Conner Lake (Figure 3-2) are composed of medium-grained quartz and feldspar crystals in an aphanitic felsic matrix. Bedding is well-defined in the tuffs ranging from 1 to 4 cm in thickness.

The felsic lithic tuffs located on the north wall of the West Pit are white weathering rocks (Plate 3-9). They are light grey on fresh surfaces and contain unsorted felsic lithic fragments and quartz crystals. Zones of massive to disseminated sulphide are frequent in the footwall rocks underlying the iron formation. The rusty zones in Plate 3-9; however, are largely due to iron-rich waters running down the walls of the pit. The massive sulphide zones occur in stratiform layers in the felsic tuffs. Sulphide mineralization is also localized along bedding-parallel shear zones. Most of the tuffs contain finely disseminated pyrite. Lithic lapilli fragments may be partly to entirely replaced by sulphide.

3.5.3 Intrusives

At least two episodes of synvolcanic high level felsic intrusion have occurred in the area. The intrusives are highly silicic (74-82 weight percent SiO_2) and have white to pale pink and pale green weathered surfaces. Fresh surfaces are light coloured and translucent. A center of felsic intrusion occurs in the northeast corner of the map area, (Figure 3-3, Map 4). Small intrusive units have been identified as far as 2 km away from this center.

There are two main stages of felsic intrusion. The early felsic intrusion (EFI) cuts all of the volcanic units (Plate 3-10). It is generally massive in character but sometimes exhibits a distinctive blocky alteration pattern as illustrated in Plate 3-11. This patter is interpreted as a fracture system developed by contraction on cooling. The fractures have been emphasized by alteration. The $SiO2$ content of the EFI ranges from 74 to 76 weight percent. The later felsic intrusive (LFI) ranges in $SiO2$ content from 79 to 82 weight percent. Quartz phenocrysts are typical of both intrusives and most abundant in the LFI.

Plate 3-12 shows the EFI intruded by a tongue of LFI. The LFI unit is banded near the contact with the EFI and fragmental in the interior. The fragmental texture may be due to fracturing on cooling or perhaps autobrecciation. In most cases the intrusion tongues are banded throughout rather than just at their margins. Clasts of the EFI are sometimes included in the later intrusion (Plate 3-12). The orientation of the intrusives is quite random near the felsic center, but felsic sills are found further west in the north-central map area.

The felsic intrusive center contains five oblong-shaped and concentrically banded ring structures located within a massive dome of highly siliceous LFI. Plate 3-13 is a photograph of one ring structure. It is approximately 1.5 m in width and 3 m

PLATE 3-10. A stratified pyroclastic unit cut by a massive, early felsic intrusion (EFI; left).

Pen magnet is 14 cm in length.

PLATE 3-11. Cooling fracture pattern in the early felsic intrusion (EFI).

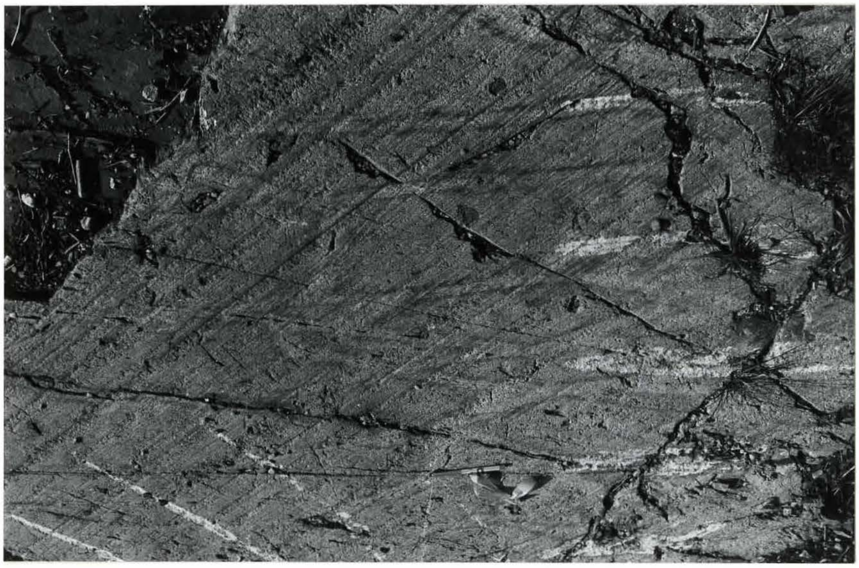

PLATE 3-12. Tongue of the late felsic intrusion (LFI) in the massive, early felsic intrusion (EFI). The tongue is banded near the contact and fragmental in the interior. A fragment of the EFI is included in the LFI (as indicated). Pen magnet (highlighted) is 14 cm in length.

PLATE 3-13. Concentrically banded ring structure in the late felsic intrusive rock, hammer located at center.

PLATE 3-14. Junction of two concentrically banded ring structures (close-up of lower left corner of Plate 3-13). Banding in the right unit is displaced by the abuttment of the left structure. Pen magnet is 14 cm in length.

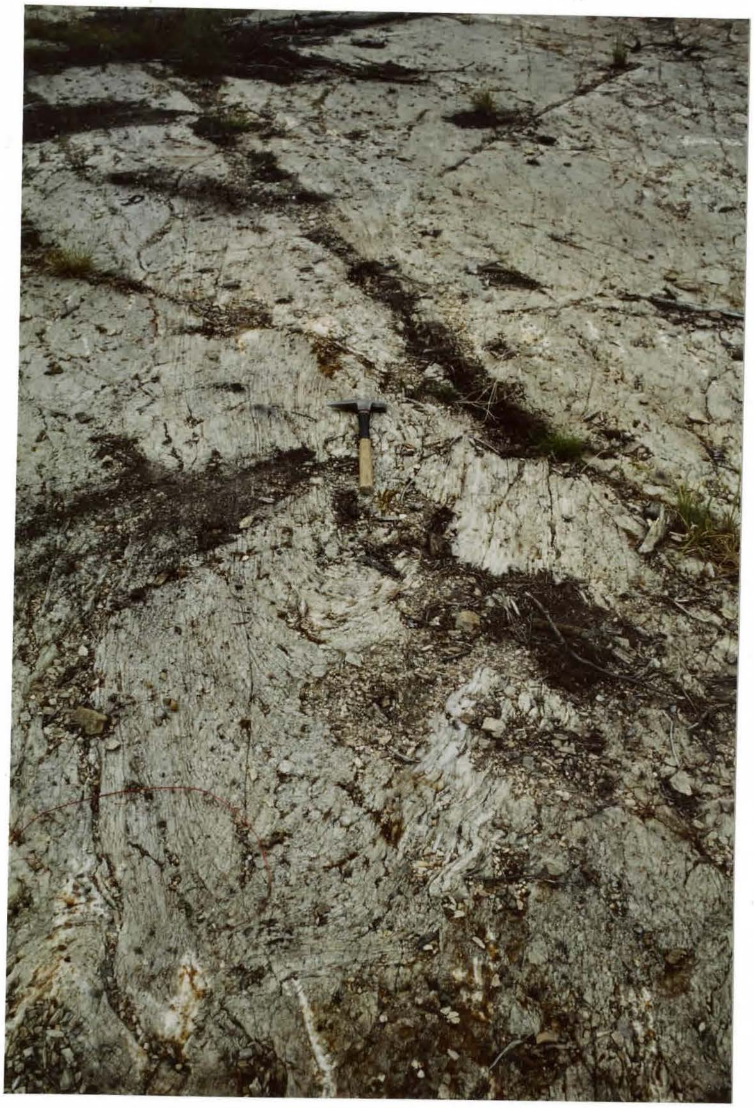

long. The banding in this structure is defined by thick quartz-rich bands and thin sericite-rich layers. The ring structures are connected to each other in a way analogous to a string of sausages. The junction of two ring structures is seen in the lower left-corner of Plate 3-13. In Plate 3-14 (close-up), the banding is confined within each structure. The banding in the right has been displaced by the abuttment of the left structure. It is proposed that each of the five ring structures represents the extrusive expression of felsic magmatic material through small volcanic conduits or "pipes". The concentric banding around each conduit, and the banded nature of the LFI is perhaps due to the highly viscous nature of the siliceous magma.

There is a possibility that the ring structures are not magmatic in origin, but rather, represent doubly plunging folds. However, there is no evidence of folding outside the ring structures in the massive LFI or in the immediate volcanics. It seems unlikely that such structural deformation would be exclusively confined to the small area of the ring structures alone.

3.5.4 Intrusive Breccias

Intrusive breccias are formed by the fragmentation and mobilization of consolidated rock by magma or gases. They are common in volcanic vents and are distinguished by their crosscutting relationships according to Wright and Bowes (1963). Two kinds of volcanic breccia are found in the northeast section of the map area (Map 4).

One type is a felsic intrusive breccia containing coarse, angular fragments of the felsic intrusive rocks, along with occasional fragments of a dark chloritic rock (Plate 3-15). The matrix is composed of finer grained unsorted fragments of the same material. Narrow dykes of the breccia crosscut the felsic intrusives and adjacent volcanic rocks (Plate 3-16). The dark chloritic fragments are derived from the pyroclastic rocks in the immediate area (Plate 3-10).

The second kind of intrusive breccia is of intermediate composition containing fragments of underlying strata. The intrusions are heterolithic in character containing fragments of most of the volcanic rock types in tha area (Plate 3-17). The matrix in the breccias is fine-grained and siliceous. Narrow dykes containing subangular to rounded pebble-sized fragments crosscut the volcanics and felsic intrusives, but do not intrude the mafic dykes in the area.

3.6 QUARTZ-FELDSPAR PORPHYRY

A small sill of quartz-feldspar porphyry, 1 to 2.5 m thick, is located in a mafic flow found 250 m north of the West Pit (Figure 3-2). The porphyry is medium-grained with phenocrysts of feldspar and quartz. Fresh and weathered surfaces are white to pale pink in colour. Considerable carbonate veining is found within the mafic flow and the felsic porphyry.

PLATE 3-15. Felsic intrusive breccia containing light fragments of felsic intrusive rock and darker fragments of pyroclastic rock. The breccia cuts the late felsic intrusive (lower right). Pen magnet is 14 cm in length.

PLATE 3-16. Narrow dyke of felsic intrusive breccia cutting a light coloured felsic intrusive unit and a brown coloured pyroclastic rock. Sulphide mineralization is concentrated along the contact. The dyke is offset by a small north-trending fault.

PLATE 3-17. Intermediate intrusion containing fragments of underlying strata. The intrusion cuts the late felsic intrusive (upper right) and is intruded by the mafic diorite dyke (left).

Pen magnet (highlighted below) is 14 cm in length.

PLATE 3-18. Narrow dykes of mafic intrusive (diorite) in the late felsic intrusive rock.

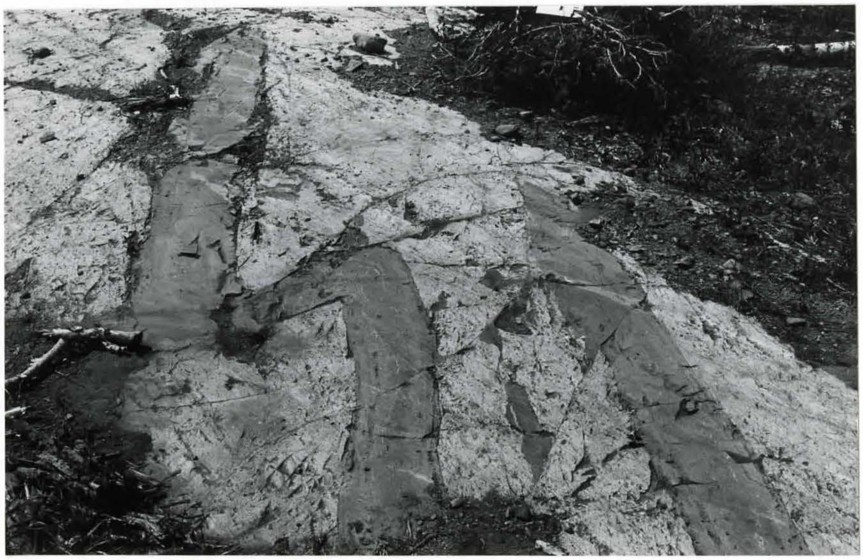

3.7 INTERMEDIATE TO MAFIC INTRUSIVE ROCKS

3.7.1 Diorites, Quartz-Diorites

The mafic dykes and sills are classified petrographically as diorites and quartz-diorites. Weathered surfaces vary in colour from dark blue-grey in the most unaltered intrusives, to dark green where heavily chloritized, to light green where epidote occurs as the dominant alteration mineral. Fresh surfaces are grey to dark green. The highest density of mafic intrusive rocks is in the northeast (Map 4). The dykes are randomly oriented and crosscut all of the volcanic lithologies and synvolcanic intrusives and breccias (Plate 3-18).

3.7.2 Lamprophyre

Two occurrences of lamprophyre were noted in the thesis area. Narrow black dykes, 15 and 22 cm wide, occur together in the northwest corner of Map 1. The dykes strike 115° and are kink-folded about an axis parallel to the regional foliation. The second occurrence of lamprophyre is in the crystal tuffs located 300 m northwest of the North Pit (Figure 3-2). The dykes are dark brown, 2.5 m thick, and strike 100°.

3.8 LATE PRECAMBRIAN OLIVINE DIABASE

Two northwest-trending diabase dykes are located north of Vermillion Lake (Figure 3-3, Maps 2 and 3). The dykes are coarse-grained and 65 to 70 m in thickness. Weathered surfaces are brown, and fresh surfaces have a typical salt and pepper texture with light plagioclase crystals and dark pyroxenes.

CHAPTER 4

PETROGRAPHY

4.1 INTERMEDIATE TO MAFIC METAVOLCANICS

4.1.1 Flows

Fine-grained phyric andesites and feldspar porphyritic andesites make up the intermediate to mafic flows of the area. Based on silica content some of the phyric andesites may be more properly classified as phyric-bearing basaltic andesites (49%<SiO2<52%) and phyric basalts (SiO2<49%).

The phyric andesites exhibit a flow banding defined by the parallel arrangement of plagioclase laths. A fine-grained matrix of untwinned plagioclase, sericite, quartz and chlorite composes 40 to 90 percent of the rock. The sericite occurs as an alteration mineral after feldspar. Phenocrysts of sanidine may be present and chlorite occurs commonly as an alteration of mafic phenocrysts. Chlorite pseudomorphs of hornblende exhibit the typical basal section of amphibole.

Samples that contain less than 52 percent SiO2 have palagonite in their matrix. The palagonite is an alteration product from the devitrification of volcanic glass. Leucoxene usually occurs as an accessory mineral but may constitute 8-10 modal percent (visual estimate). It represents the alteration of ilmenite or titaniferous magnetite. Other accessory minerals present are rutile, iron oxides, pyrite and epidote. Epidote occurs as an alteration mineral after plagioclase.

Calcite is present as vug fillings and as interstitial crystals throughout the matrix of the flows ranging from 5 to 35 modal percent. Quartz occurs fairly commonly as a vug and vein filling. It is also present in the form of fresh-looking quartz "eyes" and as blocky fillings in some of the replaced amphibole crystals.

The secondary nature of the quartz is an indication of silicification in the rock. Silicification may result from the local redistribution of SiO2 in the rock; for example, when silica is released during chloritization. In the case of local redistribution, SiO2 values should show limited variation (Gelinas et al., 1982). Silica introduced by hydrothermal metasomatism alters the overall chemistry of the rock. Geochemical evidence of silicification in the intermediate to mafic volcanics will be discussed in Chapter 5.

The feldspar porphyritic andesites contain euhedral to subhedral phenocrysts of plagioclase and sanidine in a fine-grained matrix of feldspar, sericite and quartz (Plate 4-1). The plagioclase is andesine to oligoclase in composition (determined by the Michel-Levy method). Secondary embayed quartz "eyes" are present and chlorite occurs as flattened parallel

PLATE 4-1. Feldspar porphyritic andesite with poorly aligned plagioclase phenocrysts and a foliation defined by sericite. Field of view is 1.2 cm. (Sample TDH 15; crossed polars).

PLATE 4-2. Zonal alteration texture in a hyaloclastite (flow breccia). Light areas reflect plagioclase and sericite. Dark coloured areas are enriched in chlorite and Fe-Ti oxides. Field of view is 3.5 cm. (Sample TDH 127; crossed polars).

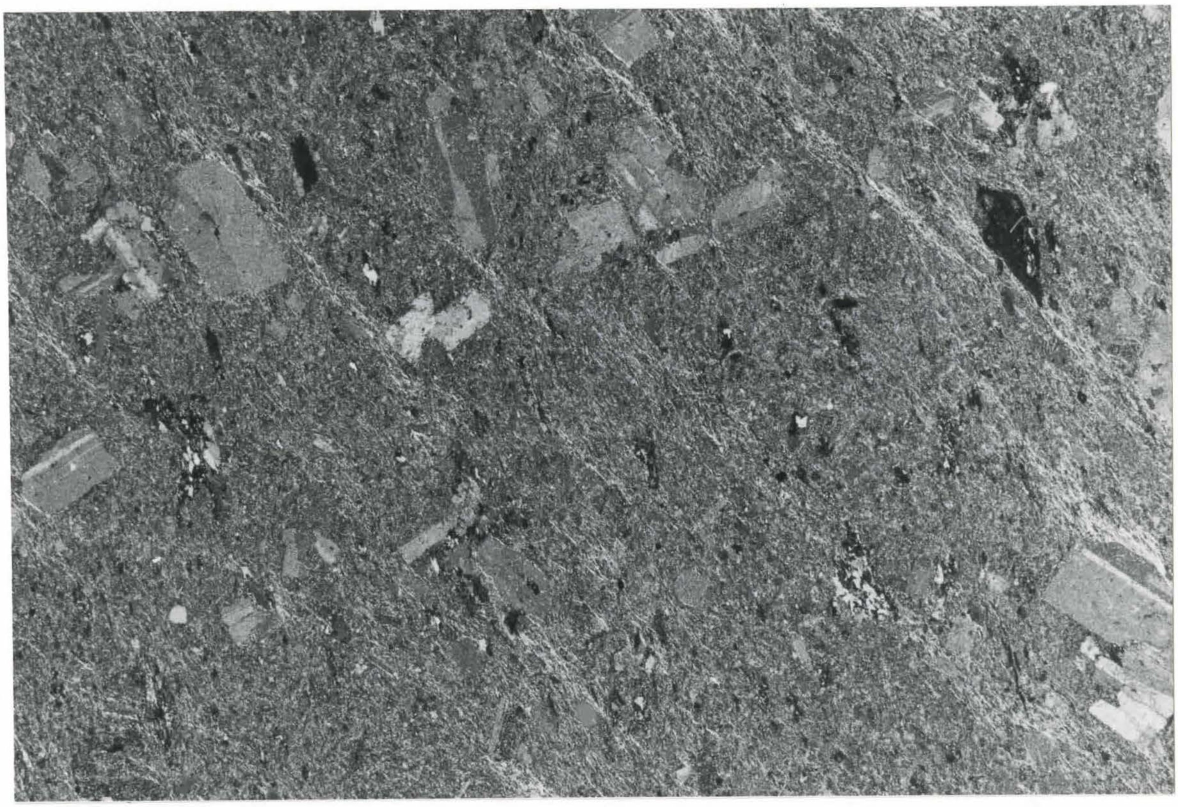

wisps in the matrix. Accessory minerals include leucoxene (maximum 2 modal percent) and epidote. Carbonate alteration is minor or absent in these flows.

4.1.2 Flow Breccias

The flow breccias exhibit a wide variation in texture and mineralogy. Fragments vary from jagged and closely spaced, indicating minimal movement (Plate 3-4), to subrounded and more widely spaced where flowage appears to have continued after initial brecciation. Mafic flow breccias consist of chloritized jig-saw fitting fragments set in a finely granulated matrix of feldspar (± quartz), chlorite and sericite. Flow breccias more intermediate in composition differ by the presence of feldspar in the fragments. The feldspar is accompanied by varying amounts of epidote, sericite, chlorite and carbonate. These fragments are set in a microcrystalline, sericitized matrix of feldspar and quartz. Flow breccias more felsic in composition are characterized by jagged fragments rich in quartz and feldspar set in a fine-grained matrix of equivalent composition. In these breccias there is less of a distinction between the alteration of the fragments and the matrix. Both exhibit a fairly pervasive alteration to epidote, sericite, chlorite and calcite.

4.1.3 Hyaloclastites

A unique alteration texture is noted in the mafic hyaloclastites. As fragmentation forms by thermal strain during cooling rather than by flow movement (Carlisle, 1963), there is essentially no matrix in these rocks. Individual fragments are clearly defined by their alteration zoning (Plate 4-2). Fragment cores show the least alteration and are composed of feldspar, chlorite and sericite. The cores are rimmed by a thin chlorite-rich zone which also contains some feldspar and sericite. Surrounding the chlorite layer is a bleached sericitic margin containing minor feldspar. The sericitic margins are essentially continuous between fragments. Leucoxene is abundant in the chlorite rim, and carbonate occurs as a pervasive alteration.

Dimroth and Lichtblau (1979) describe a similar metamorphic alteration of Archean hyaloclastites from the Noranda area. They conclude that the present mineralogy is indicative of a load metamorphism. The original products of seafloor metamorphism, palagonite, zeolites and smectites, are replaced by chlorite, carbonate and silica. The hyaloclastite granules (Noranda) consist of a concentrically banded rim of chlorite and Fe-Ti oxides (after palagonite), surrounding a core of chloritized sideromelane. Further alteration is by carbonatization and silicification. These hyaloclastite granules represent rapidly chilled glass fragments devoid of quench microlites. Hence the mineralogy after seawater alteration reflects the devitrification and replacement of volcanic glass (Dimroth and Lichblau, 1979).

In the Temagami hyaloclastites, less rapid chilling has allowed the crystallization of plagioclase.

4.1.4. Pyroclastics

The intermediate to mafic pyroclastics are crystal and lithic tuffs with SiO2 contents ranging from 44 to 50 percent. Two varieties of crystal tuff are present. One is a crystal tuff unit located in the northeast corner of the map area (TDH 34; Map 4) isolated by surrounding felsic intrusives. It is characterized by fragmented crystals of sanidine (~ 4 modal percent), quartz (~ 5 modal percent), and grains of chlorite (~ 35 modal percent) dispersed throughout a fine groundmass composed of the same minerals. Accessory minerals present are leucoxene (~ 2 modal percent), pyrite (~5 modal percent) and epidote. Minor quartz "eyes" and quartz overgrowths are also present. Approximately 40 modal percent calcite is distributed evenly throughout the rock. Sample TDH 34 plots as a calc-alkaline basalt on a Jensen cation plot (Figure 5-2).

The second variey of crystal tuff (eg. TDH 13; Map 1) is characterized by fragmented crystals of quartz, sanidine and leucoxene (5-10 modal percent) scattered throughout a fine-grained chloritic matrix. Accessory minerals include epidote and pyrite. The carbonate content in these tuffs ranges from 5 to 25 modal percent. Sample TDH 13 plots as an Fe-tholeiite on a Jensen cation plot (Figure 5-2).

Rock fragments in the lithic tuffs vary in size and shape and make up 25 to 80 modal percent of the rock. They are set in a groundmass of plagioclase, quartz and alkali-feldspar, with or without sericite alteration. The fragments exhibit a more intense alteration with varying proportions of sericite, chlorite and calcite. Further alteration in these tuffs is evident by the presence of epidote, embayed quartz "eyes" and quartz-carbonate veining. In some lithic tuffs bedding is evident by a change in chlorite content and grain size. The beds are internally laminated with fine ash layers, feldspar crystals and aligned rock fragments. Carbonate alteration is most extensive in the coarse layers reflecting a higher original porosity.

4.2 FELSIC TO INTERMEDIATE METAVOLCANICS

4.2.1 Quartz-Porphyritic Flow

The quartz-porphyritic flow ("moonrock") is as distinctive in thin section as it is in the field. Phenocrysts of quartz and feldspar are hosted by a mirocrystalline matrix of untwinned plagioclase and quartz.

The quatrz phenocrysts have the hexagonal dipyramidal habit characteristic of their original high-temperature (β-quartz) form. The phenocrysts are often embayed indicating that some degree of resorption has taken place. Such resorption may result from a change in load pressure. At high pressure quartz is in the liquidus phase, and early crystallized quartz phenocrysts are in equilibrium with the melt. As the magma rises to a low pressure environment, the quartz phenocrysts are no longer in equilibrium with the melt and resorption results (Green and Ringwood, 1968). The feldspar phenocrysts present are euhedral, high-temperature sanidines (optic angle >40°).

The matrix to this flow is microcrystalline to microspherulitic. The spherulites are composed of an intergrowth of quartz and feldspar. Small flakes of biotite and sericite are scattered throughout the matrix forming a network around the quartz and feldspar. Other alteration minerals present are epidote and calcite. Silica remobilization and possible addition is evident by anhedral quartz overgrowths around the euhedral quartz phenocrysts. Minor leucoxene occurs as an accessory mineral.

4.2.2 Pyroclastics

Felsic crystal tuffs occur in coarsely stratified deposits in the northeast section of the map area. In thin section there is a rough sorting into fine and coarse layers consisting of quartz, sanidine and plagioclase crystals. Epidote and minor chlorite are present as alteration minerals. These tuffs are intensely carbonatized containing up to 50 modal percent calcite. There is no silicification apparent in these rocks.

Felsic lithic tuffs are the dominant lithology immediately underlying the iron formation of the West Pit. Ranging in composition from dacite to rhyolite these tuffs lack any centimetre scale bedding. Angular to subrounded phenocrysts of quartz, minor sanidine, and various felsic rock fragments are set in a fine-grained granular groundmass of quartz, feldspar and fine sericite (Plate 4-3). Crystals and fragments make up more than 60 modal percent of the rock. The felsic rock fragments exhibit a varying proportion of microcrystalline quartz, feldspar and chlorite alteration. Their lack of sericite distinguishes them from the compositionally similar but pervasively sericitized matrix. Accessory minerals present are leucoxene (<1 modal percent), pyrite (up to 5 modal percent) and epidote. Devitrification of original glass in the tuffs is noted by the presence of small irregularly shaped spherulites of quartz and feldspar. Secondary quartz and calcite occur as minor cavity fillings.

Alteration is greater in the footwall tuffs at the western edge of the West Pit. These tuffs contain up to 20 modal percent chlorite as rock fragments and as interstitial flakes throughout the groundmass of microcrystalline quartz and feldspar.

4.2.3 Intrusives

As indicated in the section on local geology, two stages of felsic intrusion are apparent in the northeast section of the field area. Petrographically there is little difference between the early and late intrusions. Both contain occasional high-temperature quartz phenocrysts set in a matrix of microcrystalline quartz and feldspar. The quartz phenocrysts exhibit quartz overgrowths suggesting silica remobilization and possibly silica addition to the rock. Quartz also occurs as vein and vug fillings. Small flakes of sericite occur throughout the matrix approaching 15 modal percent in the late intrusives. Carbonate alteration is present in the early intrusive but virtually absent

PLATE 4-3. Felsic lithic tuff from the north wall of the West Pit, with quartz crystals and lithic fragments (f) outlined by sericite. Field of view is 1.2 cm. (Sample TDH 60; crossed polars).

PLATE 4-4. Quartz-feldspar porphyry with euhedral phenocrysts of orthoclase and twinned andesine, and subhedral phenocrysts of mosaic quartz. Field of view is 1.2 cm. (Sample TDH 174; crossed polars).

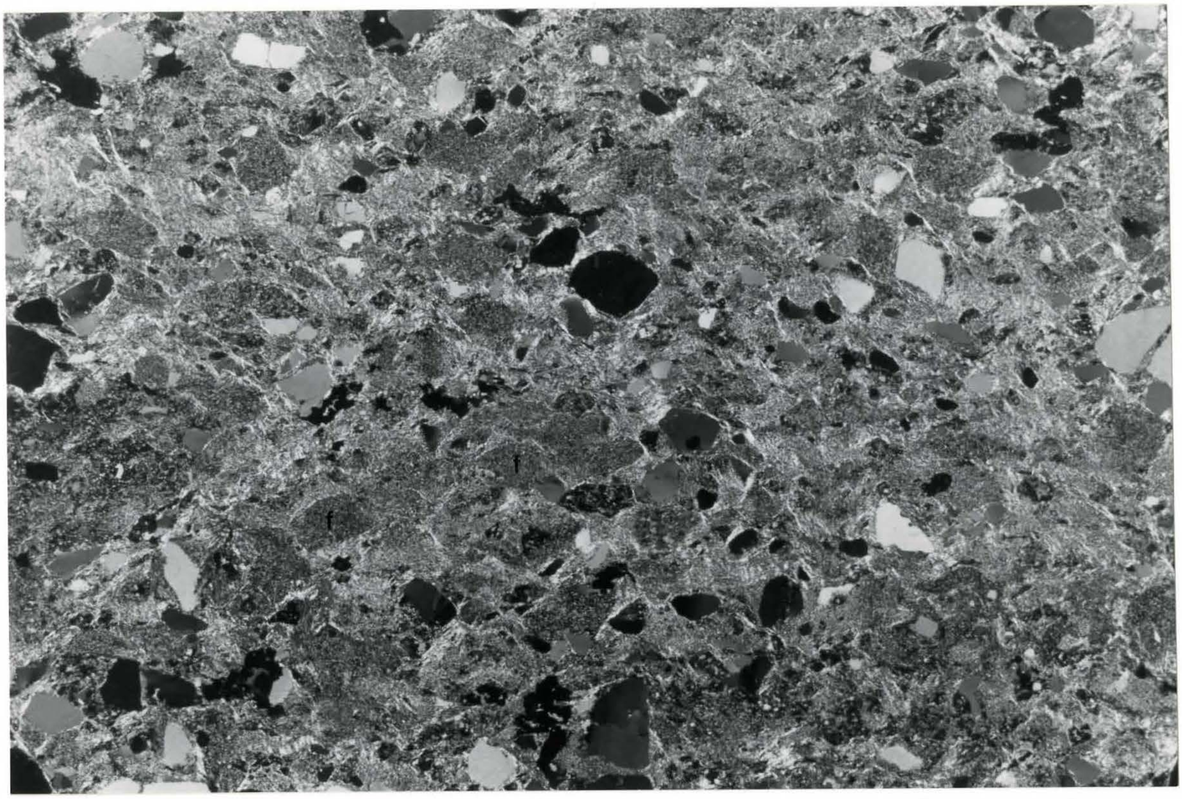
f
f

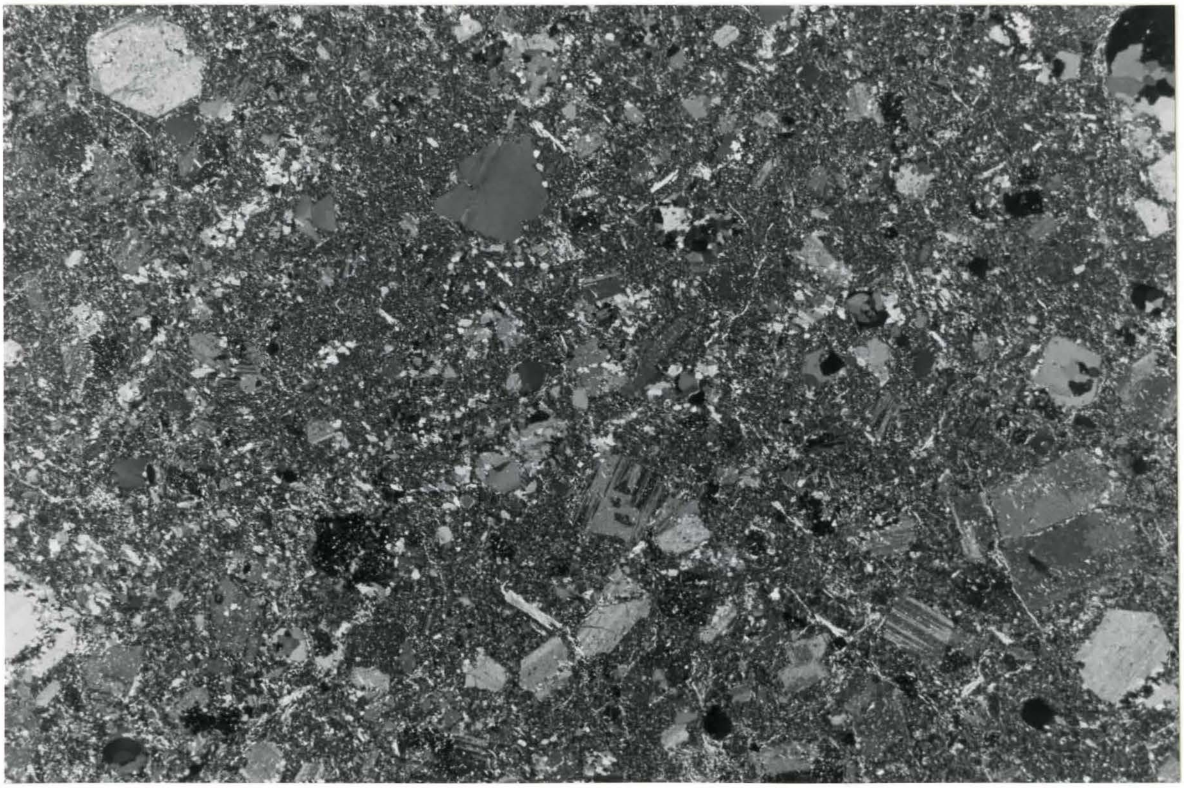

in the more siliceous late intrusive. Accessory minerals include epidote, leucoxene, apatite and pyrite. The pyrite forms small subhedral crystals in the matrix and large euhedral cubes along quartz-carbonate veins.

In some of the late felsic intrusives a compositional banding is evident as thin sericite-rich zones separating quartz-rich bands. The sericite shows parallel alignment and is often accompanied by disseminated pyrite and goethite veinlets.

4.2.4 Intrusive Breccias

The mineralogy of the intrusive breccias is most similar to that of the felsic intrusives. They are composed of felsic fragments (up to 90 modal percent) set in a fine-grained matrix of quartz, feldspar and sericite. The felsic fragments are differentiated by their grain size and sericite content. Some fragments contain euhedral quartz phenocrysts hosted by microcrystalline quartz and feldspar. Others are quartz-poor and sericite-rich, or simply blocks of coarse mosaic quartz. A second source rock is evident by the presence of fragments rich in chlorite. These fragments are derived from the pyroclastic rocks in the immediate area. Accessory minerals in the breccias are epidote, leucoxene, apatite and pyrite. Chlorite and mosaic quartz fill euhedral vugs which may represent dissolved pyrite cubes. Up to 15 modal percent carbonate occurs as a fine-grained pervasive alteration.

4.3 Quartz-Feldspar Porphyry

The small sill of quartz-feldspar porphyry found north of the West Pit represents the only hypabyssal felsic intrusive within the map area. Euhedral phenocrysts of andesine, orthoclase, chlorite after amphibole, and suhedral phenocrysts of mosaic quartz are hosted by a fine-grained crystalline matrix of quartz, feldspar and sericite (Plate 4-4). The chlorite crystals are intergrown with the andesine. Approximate modal abundances of the constituents are:- Phenocrysts (60%) - andesine (40%), orthoclase (10%), quartz (5%), chlorite or amphibole (5%); and matrix (40%). Carbonate alteration occurs interstitially throughout the matrix.

4.4 INTERMEDIATE TO MAFIC INTRUSIVE ROCKS

4.4.1 Diorite, Quartz-Diorite

The Archean mafic dykes and sills are altered diorites and quartz diorites (Plate 4-5). In the most unaltered samples, modal abundances of the minerals are:- andesine (30-40%), chlorite (25-40%), quartz ± alkali-feldspar (5-15%), and leucoxene (5-15%). The leucoxene is very euhedral and often exhibits the typical skeletal structure of ilmenite. Myrmekitic texture is present in some samples representing the symplectic intergrowth of quartz and plagioclase from microcline (Nockolds et al., 1978). Much of the chlorite is present as euhedral pseudomorphs

PLATE 4-5. Quartz-diorite with translucent leucoxene crystals (l) and anhedral quartz (q) in a matrix of sericite, plagioclase and dark coloured chlorite. Light coloured carbonate is disseminated throughout. Field of view is 1.2 cm. (Sample TDH 31; crossed polars).

PLATE 4-6. Olivine diabase with small augite crystals (a) and fractured olivine crystals (o) interstitial to coarse andesine crystals. Field of view is 1.2 cm. (Sample TDH 160; crossed polars).

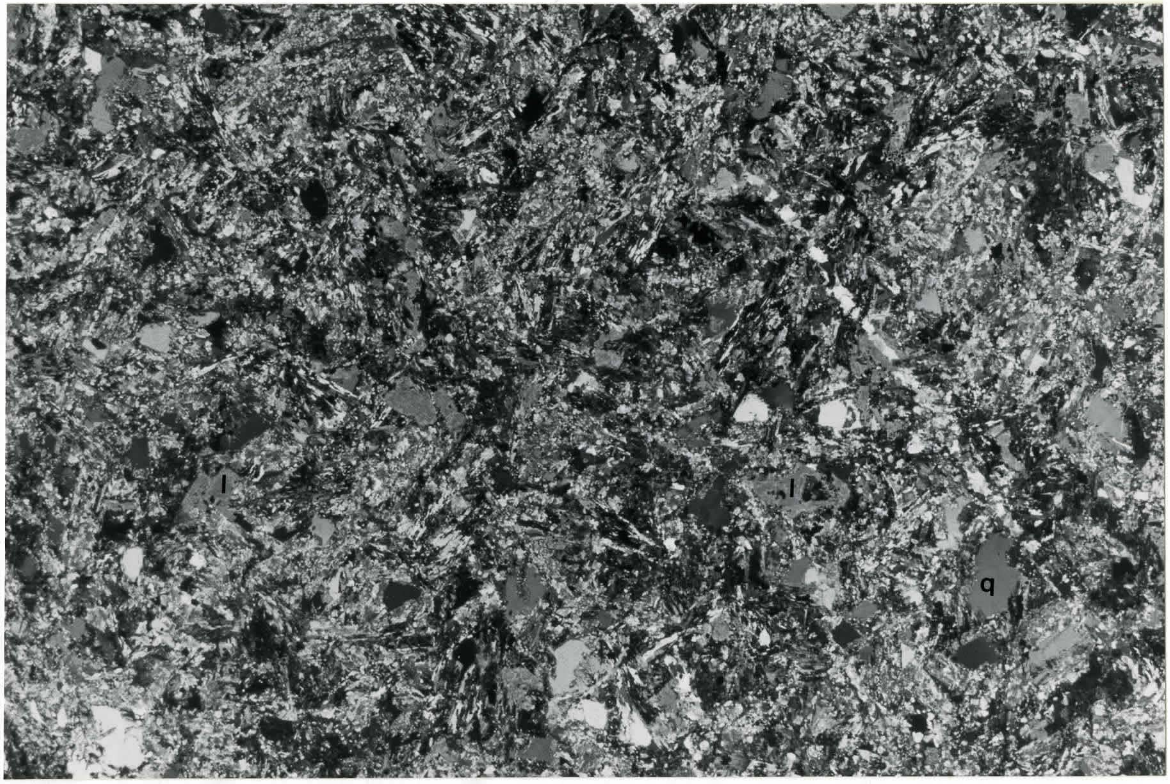
l
l
q


a
o
a
o

of amphibole and plagioclase. In many of the diorites the plagioclase has altered to epidote and sericite. Diorites lacking any primary plagioclase may contain up to 20 modal percent epidote, and a light green weathered surface is noted on the outcrop. Accessory minerals include apatite, magnetite, hematite and pyrite. Carbonate alteration varies from 1 to 20 modal percent and occurs as finely disseminated to veinlet calcite.

4.4.2 Olivine Diabase

The olivine diabase is coarse-grained and exhibits the characteristic diabasic texture of anhedral augite interstitial to plagioclase (Plate 4-6). The approximate modal composition of the rock is andesine (45%), augite (30%), olivine (10%), iron oxides (10%), and 5% accessory quartz, apatite and pyrite. The andesine crystals may be zoned containing more calcium-rich cores. The iron oxides contain alteration rims of a highly birefringent iron-rich biotite.

4.5 ORE PETROGRAPHY

Zones of sulphide mineralization are generally small and discontinuous, and occur for the most part along narrow shear zones. Iron sulphide patches are also found in some flow breccias, debris flows, and less commonly in pyroclastric rocks. These patches represent partly to completely replaced rock fragments, and show little evidence of structural control. In the north central section of the map area where deformation appears to be highest, iron stained fragments in a flow breccia are affected by small-scale folding (Plate 3-2), indicating that the sulphide replacement took place prior to the folding event. The amount of disseminated sulphide mineralization does not appear to be related to any specific lithology or horizon. The majority of volcanics in the area contain from trace amounts up to 2 modal percent pyrite. In rocks with notably higher concentrations, polished sections were made to examine the nature of the mineralization.

4.5.1 Felsic Intrusives and Intrusive Breccias

Small and isolated patches of pyrite mineralization are found in the late intrusive rocks. Most of the pyrite is recrystallized and occurs throughout the matrix in concentrations of 2 to 7 modal percent. Pyrite is also concentrated along secondary quartz-carbonate veins and occasionally forms small, nearly pure pyrite veinlets. Disseminated pyrite is most abundant within the sericite-rich alteration layers. A common replacement of the pyrite by a hematite-rich goethite is seen along crystal borders and in fractures. In some sections the pyrite has presumably been dissolved away leaving only the goethite rim. In other sections pyrite cubes have apparently dissolved and the resulting space has been filled with quartz. Thin limonite veining is common throughout the matrix.

A fairly prominent zone of sulphide mineralization was noted at the contact of a felsic intrusive breccia with a crystal tuff (TDH 151; Map 4). In the breccia unit large euhedral pyrite cubes are found within the coarse fragments. Some crystals contain minor inclusions of chalcopyrite and magnetite. Five to ten modal percent subhedral and cataclastic pyrite is scattered in the matrix. The contrast in the nature of the pyrite suggests that the mineralization took place prior to fragmentation of the rock. Oxidation to goethite along borders is present in both types of pyrite.

4.5.2 Flows and Flow Breccias

Within the flows pyrite occurs in subhedral to euhedral crystals disseminated in the matrix and concentrated in quartz-carbonate veins. Within the flow breccias a similar mineralization is apparent but also accompanied by the concentration of pyrite in partially replaced volcanic fragments. Oxidation to goethite is common in the breccias but rare to absent in the flows. This reflects a difference in the original porosity of the rock.

4.5.3 Pyroclastics

In the mafic crystal tuffs 1 to 5 modal percent pyrite of anhedral to subhedral habit is randomly distributed throughout the matrix. In contrast, highly euhedral pyrite is noted in the mafic crystal tuff located in the northeast section of the map area (TDH 34; Map 4). This euhedral habit may reflect a thermal recrystallization of the pyrite. The tuff is an isolated volcanic unit located in a region dominated by felsic intrusives.

Pyrite in the felsic to intermediate tuffs is subhedral to euhedral and has grown over the crystals, fragments and matrix. Concentrations range from trace in the fine-grained tuffs to as much as 10 modal percent in some of the coarse tuff breccias. In the coarse units there is some indication of layering into pyrite-rich and pyrite-poor layers. The felsic lithic tuffs along the edge of the West Pit contain up to 5 modal percent pyrite. The pyrite is subhedral and fragmented, and unlike the previous examples exhibits ragged contacts with the matrix. No secondary recrystallization is apparent and only minor goethite alteration is present.

4.5.4 Immediate Footwall Rocks to the West Pit

The transition of volcanics to oxide facies iron formation in the West Pit is marked by the gradational change from coarse felsic tuffs to fine ash tuffs, cherts and graphitic sediments. The coarse felsic tuffs as just described contain finely disseminated pyrite. The fine ash tuffs host massive and stratiform sulphide zones intermixed with quartz-rich sediments. In polished section, fine euhedral pyrite crystals with minor inclusions of chalcopyrite are interlayered with the silicate material (TDH 178). The graphitic sediment contains up to 40 modal percent pyrite in the form of fine euhedral crystals and irregular masses with relict colloform texture (TDH 182). Elsewhere in the West Pit, spectacular nodular and colloform pyrite textures are characteristic of this graphitic horizon.

CHAPTER 5

GEOCHEMISTRY

5.1 LITERATURE REVIEW ON THE EFFECTS OF ALTERATION AND METAMORPHISM

Before placing any degree of certainty on a chemical rock classification of Archean volcanics it is neccessary to evaluate the effect of alteration. At the very least, H2O and CO2 are introduced during metasomatic reactions, so the total volatiles in a rock represent a minimum measurement of the alteration intensity. Total volatile contents in the thesis area volcanics range from 5 to 14 weight percent in the basalts, 3 to 15 weight percent in the andesites, and 2 to 7 weight percent in the dacites and rhyolites. The relative mobility of major and trace elements during seafloor hydrothermal alteration through to regional greenschist facies metamorphism is discussed below.

5.1.1 Mobility of the Major Elements

The following mineralogical and chemical changes during hydrothermal alteration of oceanic basalts were noted by Humphris and Thompson (1978). Chlorite-rich assemblages gained significant quantities of Mg and lost Ca during chlorite formation. In contrast, alteration to epidote-rich assemblages resulted in little change in Mg and Ca contents. Silica was generally leached from the rocks and locally redistributed within the basaltic pile. Sodium content was variable between samples, and from core to rim within individual pillows; however, no consistant trend was evident. Some mobility of aluminum and titanium was evident but overall concentrations of these elements were relatively unaffected.

The following discussion on the mobility of major elements from the Rouyn-Noranda district has been taken from Gelinas et al., (1982). Relative mobilities were established by using variation coefficients to measure chemical heterogeneities introduced by alteration. The elements Ti, Al and P are considered relatively immobile. Silica is immobile; however, silicification may result from the local redistribution of SiO_2 released during chloritization. The elements Mg, Fe(II) and Na are moderately mobile, while Ca is mobile and Fe(III), K, S, H_2O+ and CO_2 are highly mobile.

Gelinas et al. (1982) subdivided the metavolcanics into three alteration types of which Type II: chlorite-epidote, and Type III: chlorite + sericite, are found in the volcanics within the thesis area. In these alteration types calcic plagioclase is totally albitized resulting from the substitution of Na+Si for Ca+Al. The loss of Ca from pillow interiors generated an excess of Al with respect to the combined molecular proportions of Na, K and Ca, and normative corundum appears in CIPW norm calculations.

Further Ca loss is generated through the substitution of Mg and Fe from the hydrothermal fluid for Ca in ferromagnesium minerals, and is indicated by the presence of chlorite. In the Type III chlorite ± sericite alteration, the absence of epidote implies a high degree of Ca loss. The amount of Ca remaining in the rock is entirely accounted for by the presence of calcite. Sericite is a product of K metasomatism and may be accompanied by a loss of Na2O (Gelinas et al., 1982).

The following discussion on the mobility of major elements during silicification of the Amulet Rhyolite is taken from Gibson et al. (1983). The Amulet Rhyolite Formation at Noranda, Quebec is composed of mottled (epidote-quartz) altered andesites and silicified (58 to 70 percent SiO2) andesites. Constant volume calculations of the mottled andesites indicate that Si and Ca were added to the rock during alteration, whereas Al, Fe, Mg and Ti were removed. Silicification is characterized by a systematic decrease in Al, Fe, Mg and Ti with increasing silica content, suggesting a uniform exchange of the elements for Si during alteration. In contrast Na, K and Ca remain relatively constant. A similar dilution effect on the major elements is noted by Dostal and Strong (1983) for the silicification of basalts in Saint John, New Brunswick.

MacGeehan (1978) discusses the effect of progressive chloritization of the Garon Lake Rhyolite, Mattagami, Quebec, noting that a uniform decrease in SiO2 content (75 to 47 percent) is accompanied by a decrease in Na and K and a uniform enrichment of Fe, Mg, Ti, Al and P. MacGeehan suggests that a silica-saturated hydrothermal fluid leached these elements from the underlying basalt, and precipitated them at various discharge points to form chlorite alteration patches in the overlying rhyolite.

The significance of carbonatization on the major element chemistry has been discussed by various authors. Studies on tholeiites from the Barberton belt indicate a decrease in Si, Al, Mg, Ca and K accompanied by an increase in Fe, Ti and H_2O during carbonatization (Condie, 1981). Fyon (1980) reported a depletion of Si, Mg and Ti, and an enrichment of K, P and CO_2 with increasing carbonatization in metavolcanics from the Timmins district. According to Fyon (1980) the major elements Al, Fe, Ca and Mn underwent depletion during initial hydration but were subsequently enriched during carbonatization. Except for Ca, element concentrations did not exceed those of the parent rock.

In summary, the following changes in major element chemistry may be expected from progressive seafloor hydrothermal alteration through to regional metamorphism.

In hydrothermally altered oceanic basalts, Mg is enriched and Ca is depleted. Silica is mobile during alteration but redistribution is local. Aluminum and Ti show some mobility but overall concentrations are relatively constant.

In Archean volcanics of greenschist facies metamorphic grade, Ti, Al and P are probably immobile, whereas all other major elements are mobile to some degree. Silica is released during chloritization.

Intense silicification and chloritization in Archean volcanics affects all major elements, but Al/Ti ratios should remain constant. Aluminum and Ti are not immobile during carbonatization.

A major implication of the preceeding discussion is that any geochemical classification scheme which utilizes major element concentrations will prove to be meaningless for highly altered rocks.

5.1.2 Mobility of the Trace Elements

The following discussion on the mobility of trace elements during hydrothermal alteration of oceanic basalts is taken from Humphris and Thompson (1978). Strontium is leached from the basalts and is taken up in epidote-rich assemblages. Barium, Co, Cr and Ni show only slight variation in the altered basalts. The chromium content of the basalts varies widely due to the effect of fractional crystallization, and, although some analyses of oceanic basalts indicate a variability in the Cr contents of fresh and altered basalts, no consistent trends are observed. Copper is leached from the basalts but may be locally precipitated in sulphide veins. Manganese is mobilized during hydrothermal alteration and may be redistributed in the altered basalts. Concentrations of V, Y and Zr do not appear to be affected by secondary processes (Humphris and Thompson, 1978).

The enrichment of Co and Ni in chloritic zones of greenstone rocks has been reported by Floyd (1976). Rubidium, Sr and Ba in metavolcanics from the Rouyn-Noranda are known to be mobile at all levels of alteration (Ludden et al., 1982).

The relative immobility of the high field strength elements (Zr, Y, Ti), V and Nb, is well established in the literature (Condie, 1976; Floyd and Winchester, 1978; Ludden et al., 1982) and these elements are often used to identify and discriminate between altered volcanic rocks. Ludden et al. (1982) found that ratios of Zr, Y and Ti remain unchanged in highly altered zones. However, in a study of the Ascot Formation, SE Quebec, Hynes (1980) reported that both absolute and relative amounts of Zr, Y and Ti were affected by carbonatization, and attributed their mobility to high CO2 levels in a metamorphic fluid phase. Two alteration trends have been defined by Hynes for the carbonatization of metabasalts in the Ascot Formation. Low carbonate rocks were severely depleted in Ti, Y and Zr whereas high carbonate rocks were depleted in Y and Zr and enriched in Ti. According to Hynes there is a close relationship between the metamorphic assemblage and the relative enrichment or depletion of trace elements. Extrapolation of alteration trends enables the primary or pre-alteration concentrations of these trace elements to be estimated with some accuracy.

The rare earth elements (REE) are also noted for their isochemical behaviour during low grade metamorphism (Menzies et al., 1979; Ludden et al., 1982). The REE are enriched during epidotization (Hellman et al., 1979; Ludden et al., 1982) and diluted during mild carbonatization (Hellman et al., 1979). A dilution effect of the REE is also noted during the silicification of basalts in New Brunswick (Dostal and Strong, 1983). Where alteration is extreme, the REE are leached and redistributed by carbonate-rich and K-rich metasomatic fluids (Ludden et al., 1982). Kerrich and Fryer (1979) reported that carbonate-rich hydrothermal solutions are capable of mobilizing the heavy REE relative to the light REE. This modification has been noted for all metasomatized Archean mafic rocks associated with gold deposits (Kerrich et al., 1981).

In summary, the high field strength elements (Zr, Y, Ti), V, Nb and the REE are relatively immobile during low grade metamorphism. The use of these elements to identify and discriminate altered volcanic rocks, and to define magma origin, is acceptable up to levels of intense carbonatization (or high CO2 levels in the fluid phase during metamorphism) where all elements must be considered mobile.

5.2 CHEMICAL ROCK CLASSIFICATIONS

The whole rock analysis of each sample was normalized to 100 percent and run through a CIPW normative calculation program. The volatiles H2O and CO2 are not included in this calculation on the assumption that these volatiles were added during alteration of the rock, and are of no interest in respect to original magmatic composition (Irvine and Baragar, 1971). The

CIPW norm (in weight percent) was used to compliment petrographic observations, and to aid in determining the nature of alteration in the rocks. Normative calculations must be viewed with caution due to the mobility of the alkali and alkaline earth elements.

Iron, magnesium and alkalies were plotted on an AFM diagram. Aluminum, total iron + titanium and magnesium for each sample was plotted on a Jensen diagram. Immobile trace elements were used in variation diagrams to verify or dispute the classification of the rocks by the AFM and the Jensen plot.

5.2.1 AFM Plot

The AFM plot is designed to subdivide the subalkaline rocks into calc-alkaline and tholeiitic series. As this classification relies on the immobility of the alkalies (Na, K), it is rather limited in dealing with chemically altered rocks.

In Figure 5-1, an AFM diagram, 54 percent of the volcanics (including felsic intrusives) fall in the calc-alkaline field, 34 percent in the tholeiitic field, and 12 percent (6 samples) plot above the general trend for both subalkaline and alkaline rocks (as defined by Irvine and Baragar, 1971). Two of the 6 samples are silicified (70-74% SiO_2) and exhibit strong MgO depletion. The other 4 samples are altered dacites, enriched in Fe from chloritization and depleted in alkalies. The majority of volcanics are depleted in Na_2O (below 2 weight percent) and this has caused a shift towards the iron-magnesium tie-line. It is evident from a Y-T-C plot (see Figure 5-3 for definition) that

FIGURE 5-1. AFM diagram for the classification of the thesis area volcanics and intrusives. The tholeiitic - calc-alkaline field boundary is after Irvine and Baragar (1971).

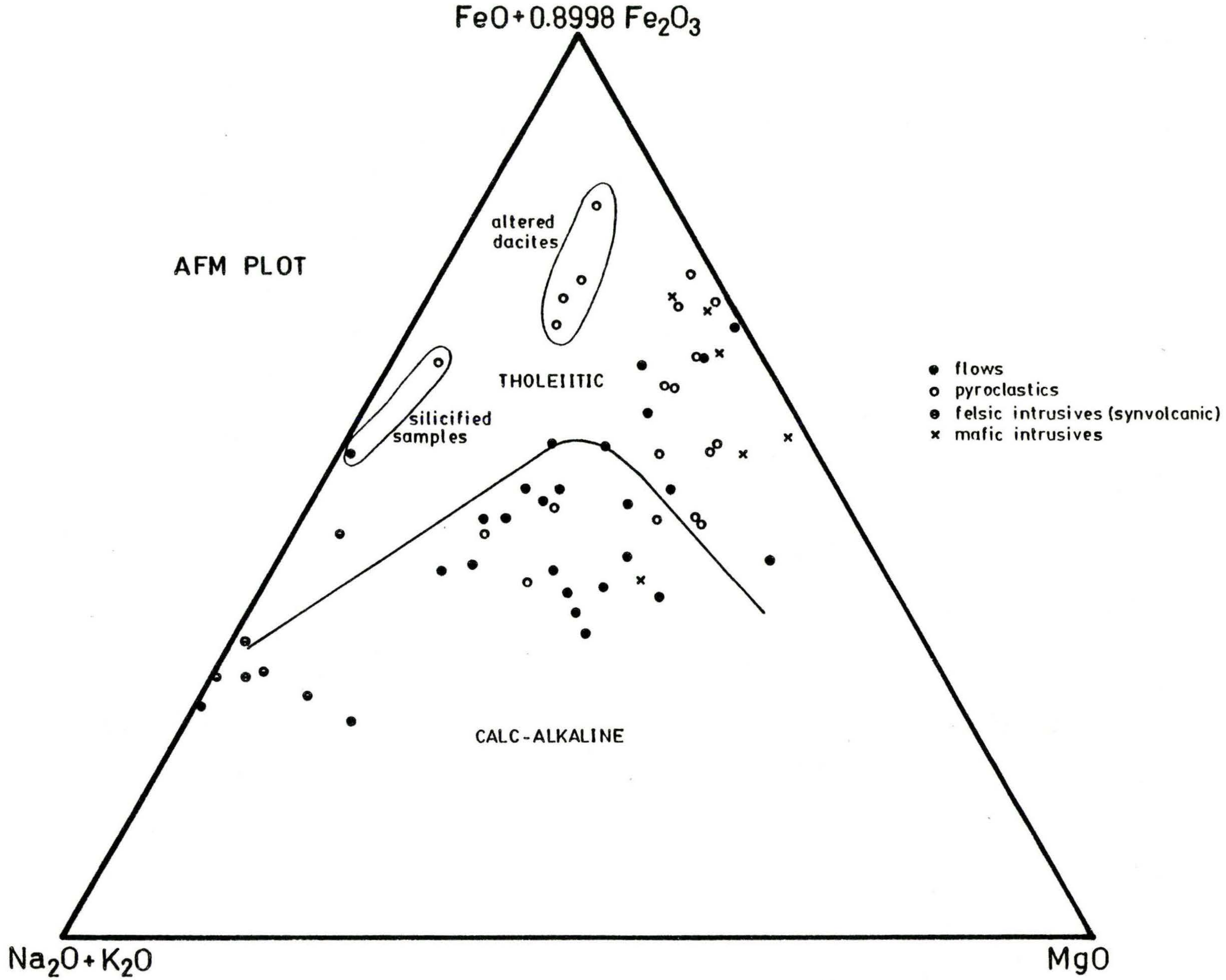
FeO+0.8998 Fe$_2$O$_3$
AFM PLOT
altered dacites
silicified samples
THOLEIITIC
CALC-ALKALINE
● flows
○ pyroclastics
⊙ felsic intrusives (synvolcanic)
× mafic intrusives
Na$_2$O+K$_2$O
MgO

approximately 15 percent of the samples lying in the tholeiitic field are of calc-alkaline affinity.

5.2.2 Jensen Cation Plot

In the ternary plot proposed by Jensen (1976) molecular proportions of Al_2O_3, $FeO + Fe_2O_3 + TiO_2$ and MgO are used so that the alkalies are replaced by Al_2O_3 in comparison with standard AFM plots. These elements were chosen because of their relative stability during metamorphism of volcanic rocks, and for the constancy of their ratios during alteration and metamorphism. This classification scheme becomes unusable when alteration becomes intense enough to selectively change the content of one element relative to another.

In Figure 5-2, a Jensen cation plot, 70 percent of the volcanics (including the synvolcanic felsic intrusives) fall in the calc-alkaline field, and 20 percent are classified as high-Fe or high-Mg tholeiites. Twelve percent or 6 samples plot as tholeiitic rhyolites and dacites. These are the same 6 samples which plotted above the general trend of the volcanics in the AFM diagram (Figure 5-1). Trace element discrimination diagrams (Figures 5-3, 5-4 and 5-7) and petrographic observations indicate that the two tholeiitic rhyolites (according to the Jensen diagram) are a silicified calc-alkaline andesite (TDH-154) and a silicified calc-alkaline dacite (TDH-123), while the 4 tholeiitic dacites (according to the Jensen diagram) are chloritized calc-alkaline dacites (TDH 64-67).

FIGURE 5-2. Jensen cation plot for the classification of the Temagami volcanics and intrusives.

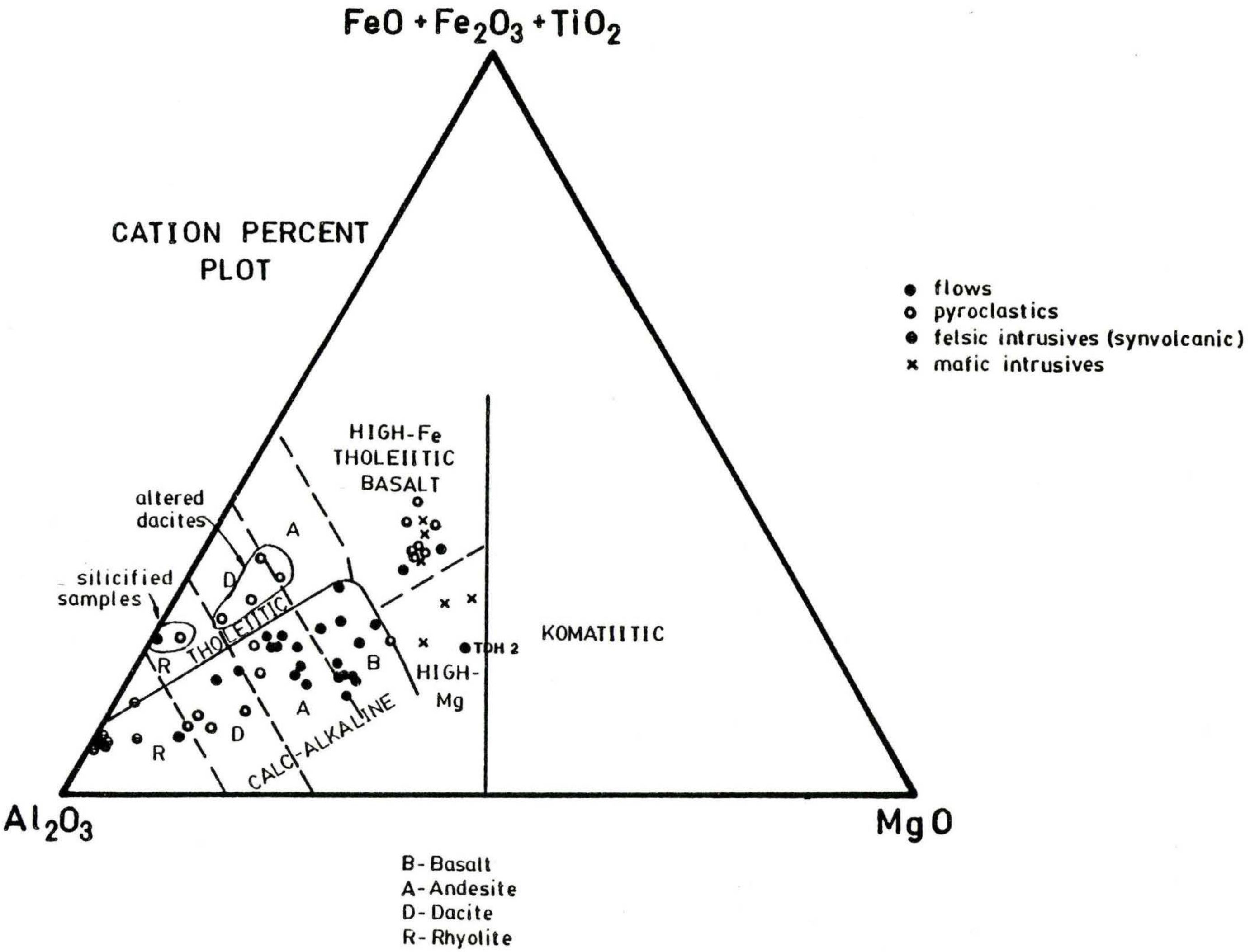

FeO + Fe_2O_3 + TiO_2
CATION PERCENT PLOT
● flows
○ pyroclastics
● felsic intrusives (synvolcanic)
× mafic intrusives
HIGH-Fe THOLEIITIC BASALT
altered dacites
silicified samples
A
D
R
THOLEIITIC
B
HIGH-Mg
TDH 2
KOMATIITIC
CALC-ALKALINE
A
D
R
Al_2O_3
MgO
B - Basalt
A - Andesite
D - Dacite
R - Rhyolite

A highly carbonatized and chloritized sample (TDH 2) plots on the Jensen diagram as a Mg-tholeiite. In most of the trace element variation diagrams (eg. Figures 5-4 and 5-7) TDH 2 consistently groups with the calc-alkaline andesites. This sample will be further discussed in section 5.2.3.

All but 4 of the samples classified as calc-alkaline basalts on the Jensen diagram (Figure 5-2) consistently group with andesites on trace element diagrams (Figures 5-4 and 5-7). Petrographically these samples are phyric and feldspar-porphyritic andesites. Three of the basalts (Jensen classification) contain less than 53 percent SiO_2 and consistently plot between the andesite field and the basalt field in Figures 5-4 and 5-7. They are similar in thin section to the phyric andesites and have been classified on the trace element diagrams as basaltic andesites (TDH-34, 120 and 138). One of the basalts (Jensen classification; TDH 100) consistently groups with the tholeiitic basalts on the trace element diagrams (Figures 5-3, 5-4 and 5-7).

The erroneous classification of these samples on the Jensen diagram can be attributed to their intense alteration (chloritization, silicification and carbonatization). Taking into account the misclassification of the highly altered samples, the volcanics of the thesis area may be subdivided into 80 percent calc-alkaline (rhyolite to basalt) and 20 percent Fe-tholeiite (basalt only).

5.2.3 Immobile Trace Element Variation Diagrams

5.2.3.1 Y-T-C Plot

The trace elements Y+Zr, TiO2 and Cr have fractionation patterns that parallel those of the alkalies, FeO and MgO respectively. They usually display characteristic patterns within different units, whether altered or unaltered (Davies et al., 1979). These elements form the apices of the ternary Y-T-C plot (Figure 5-3). In such a plot, felsic members of a volcanic series usually show a progressive enrichment of Y and Zr. The TiO2 content is enriched in tholeiitic rocks and decreases in the calk-alkaline series while chromium follows magnesium during magmatic differentiation. The Y-T-C plot subdivides the thesis area volcanics into 75 percent calc-alkaline, 18 percent tholeiite and 7 percent magnesian (Figure 5-3).

Of the three samples which plot in the Archean magnesian field (Figure 5-3), the most Cr-rich rock is TDH 2 which plotted in the Mg-tholeiitic field of the Jensen diagram (Figure 5-2). It contains a very high Cr content (1045ppm) for its whole rock chemistry (Figure 5-4). Secondary Cr and Ni enrichment has been noted by Fyon (1980) in chloritized rocks from the Timmins area. Because this sample plots with the andesites in other trace element diagrams (Figures 5-4 and 5-7) it is suggested that TDH 2 is a chromium-enriched, altered andesite. The remaining two samples in the Archean magnesian field (TDH 102 and 103; Figure 5-3) are also enriched in chromium containing 790 and 550 ppm

FIGURE 5-3. Y-T-C plot for the classification of the Temagami volcanics and intrusives. Boundaries for the Archean tholeiitic and magnesian fields are inferred after Davies et al. (1979; Figure 5, p.309).

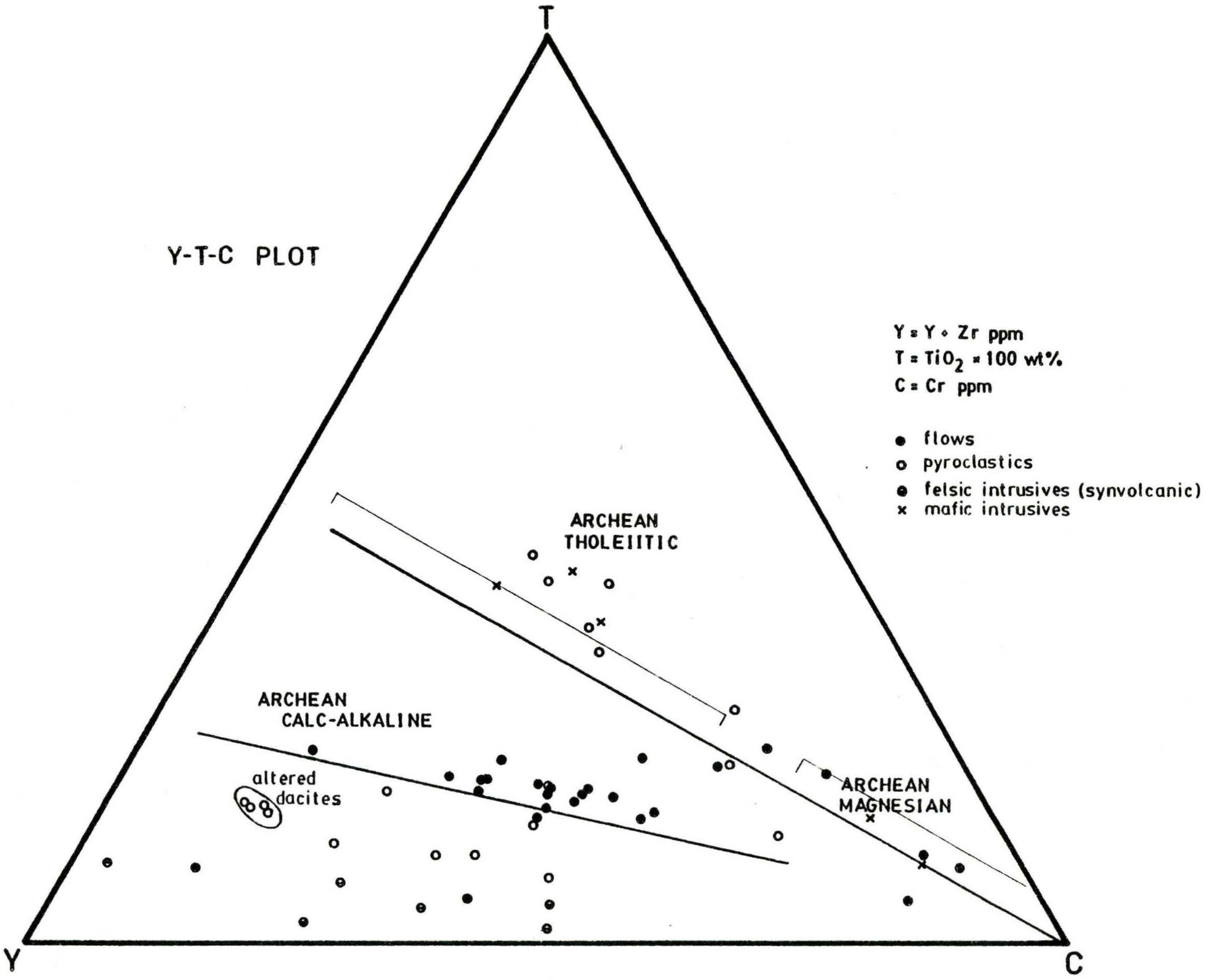
Y-T-C PLOT
T
Y
C
Y = Y + Zr ppm
T = TiO$_2$ × 100 wt%
C = Cr ppm
● flows
○ pyroclastics
● felsic intrusives (synvolcanic)
× mafic intrusives
ARCHEAN THOLEIITIC
ARCHEAN CALC-ALKALINE
ARCHEAN MAGNESIAN
altered dacites

respectively (Figure 5-4). The presence of fuchsite (Cr-rich mica) veining in the area from which these samples were collected suggests that this Cr enrichment may be a local remobilization. On the Jensen plot they are classified as Fe-tholeiites and calk-alkaline basalts. In other trace element diagrams they consistently group with the basalts.

5.2.3.2 TiO2 vs. Zr, V and Cr

The binary plots in Figure 5-4 illustrate the distinct geochemical character of the various volcanic rock types in the area. There are 4 samples which consistantly plot away from the fields for the majority of samples. These are the highly altered calc-alkaline dacites which plot in the tholeiitic field on the Jensen diagram and within the calk-alkaline field on the Y-T-C plot.

As a group the rhyolites, dacites and andesites each have fairly constant Ti/Zr ratios. The basalts vary in Ti over a restricted range in Zr. The rhyolites and rhyodacites have Zr contents which are approximately 100 ppm lower than expected for siliceous volcanics; however, their Zr/TiO2 ratios are typical of high silica rocks (comparison made with average values from Winchester and Floyd, 1977).

A plot of TiO2 versus V indicates a progressive decrease in both elements (constant TiO2/V ratio) with increasing magma differentiation. This plot effectively separates the mafic through felsic volcanics and intrusives regardless of silica con-

FIGURE 5-4. TiO_2 versus Zr, V and Cr for the Temagami volcanics and intrusives.

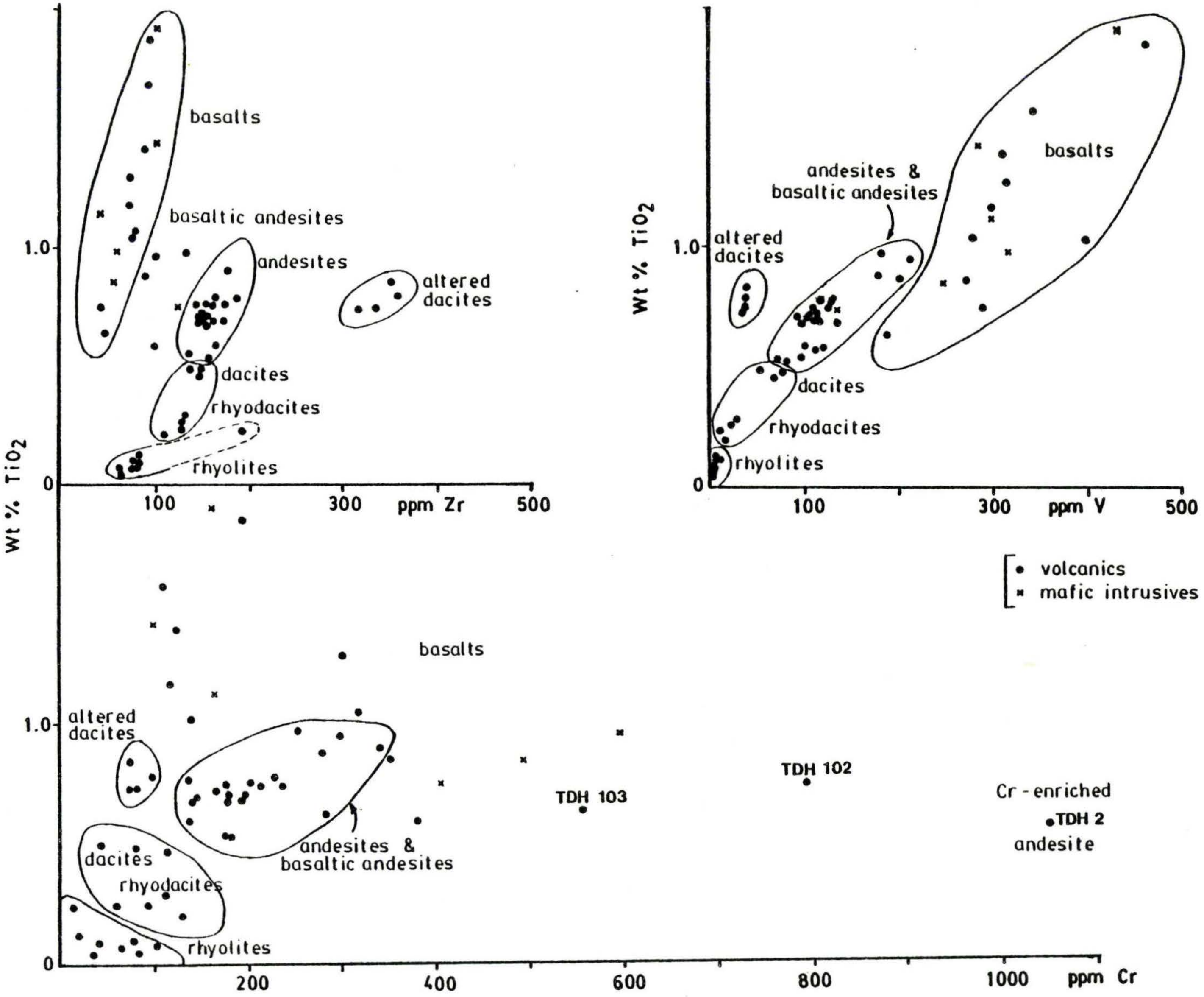
Wt % TiO2
1.0
0
100
300
ppm Zr
500
basalts
basaltic andesites
andesites
altered dacites
dacites
rhyodacites
rhyolites
Wt % TiO2
1.0
0
100
300
ppm V
500
basalts
andesites &
basaltic andesites
altered dacites
dacites
rhyodacites
rhyolites
● volcanics
× mafic intrusives
1.0
0
200
400
600
800
1000
ppm Cr
basalts
altered dacites
dacites
rhyodacites
rhyolites
andesites &
basaltic andesites
TDH 103
TDH 102
Cr - enriched
TDH 2
andesite

tent, hence silicified andesites and dacites (up to 74 percent SiO2) plot within their respective fields.

In the TiO2 versus Cr diagram, the wide scatter of samples suggests that Cr is generally fairly mobile in response to alteration and/or metamorphism.

5.2.3.3 SiO2 vs. Zr/TiO2 and Nb/Y

The progressive differentiation of basic magma can be roughly measured in a plot of Zr/TiO2 against SiO2 (Winchester and Floyd, 1977). Figure 5-5 shows an increasing Zr/TiO2 ratio with increasing SiO2 content; that is, from mafic to felsic rocks. The increasing Zr/TiO2 ratio reflects an overall decreasing TiO2 content in the non-basaltic differentiated rocks. The samples which lie above this trend are highly silicified (TDH 4, 123 and 154).

A plot of SiO2 versus Nb/Y is a useful indicator of alkalinity (Winchester and Floyd, 1977). Unlike the Zr/TiO2 ratio, Nb/Y does not change substantially with increasing SiO2 content in the differentiated intermediate to felsic rocks of the thesis area (Figure 5-6). The suggested value of Nb/Y to subdivide subalkaline and alkaline magma suites is 0.67 (Figure 5-6) but this value increases for the most siliceous rocks (Winchester and Floyd, 1977). In Figure 5-6, this division line crosses through the andesite and dacite field of the thesis area volcanics. If these rocks were mildly alkaline they would display other geochemical traits of alkaline rocks; however, the average P2O5 and

FIGURE 5-5. SiO2 versus Zr/TiO2 for the Temagami volcanics and intrusives.

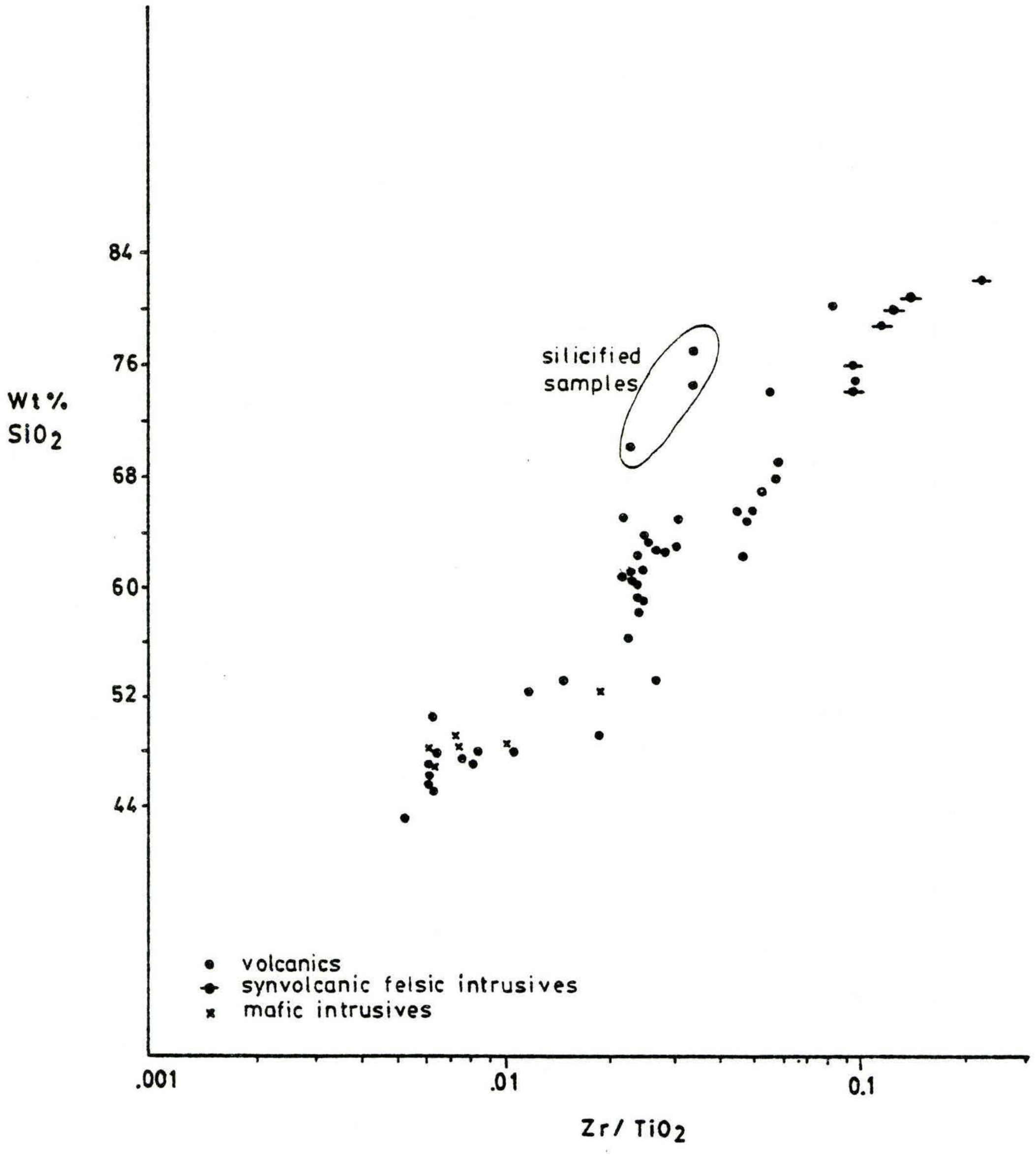

Wt %
SiO2
84
76
68
60
52
44
silicified
samples
● volcanics
synvolcanic felsic intrusives
× mafic intrusives
.001
.01
0.1
Zr / TiO2

FIGURE 5-6. SiO2 versus Nb/Y for the Temagami volcanics and intrusives.

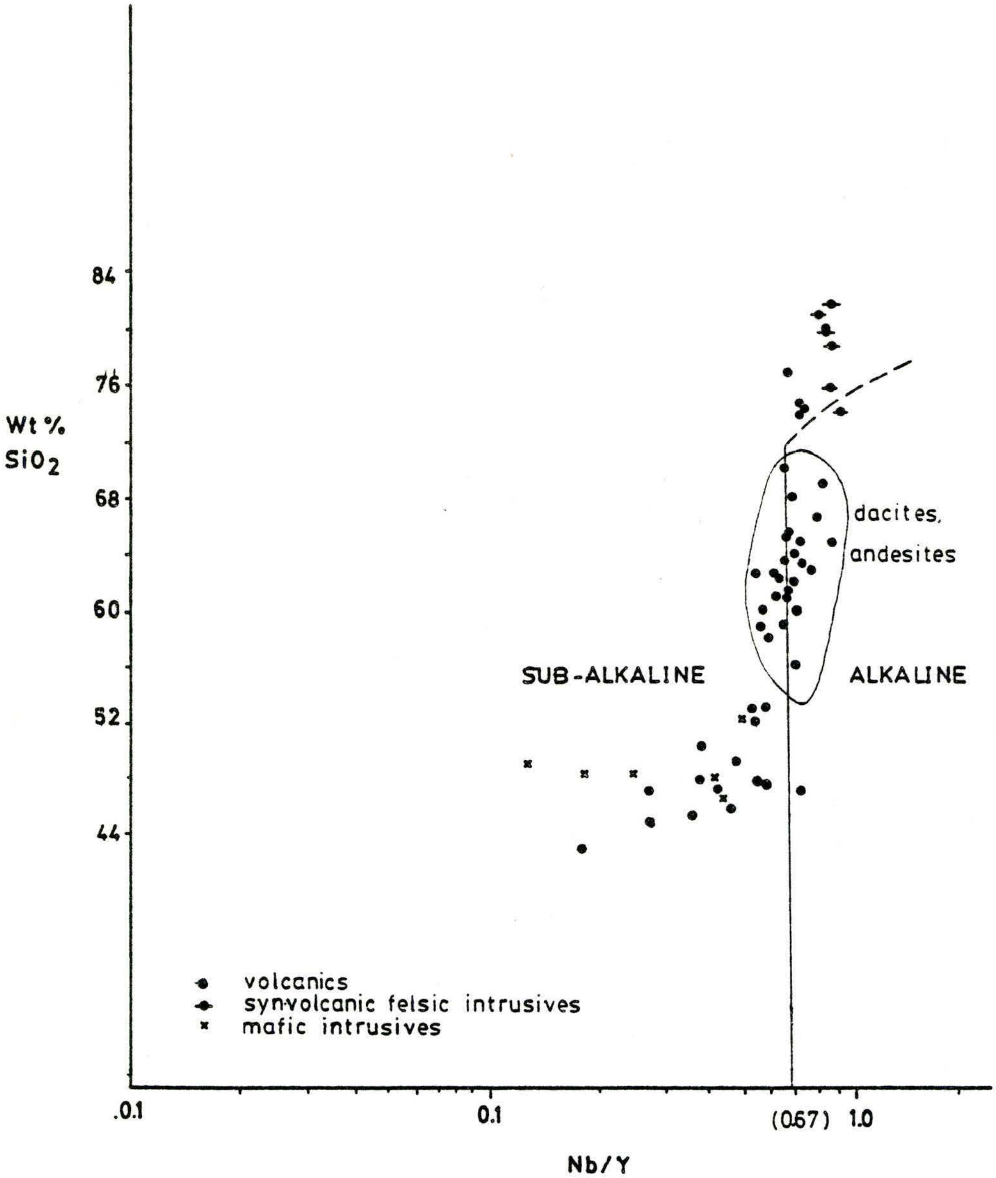
Wt %
SiO2
84
76
68
60
52
44
.0.1
0.1
(0.67)
1.0
Nb/Y
SUB-ALKALINE
ALKALINE
dacites,
andesites
volcanics
synvolcanic felsic intrusives
mafic intrusives

FIGURE 5-7. Zr/TiO2 versus Nb/Y for the Temagami volcanics and intrusives.

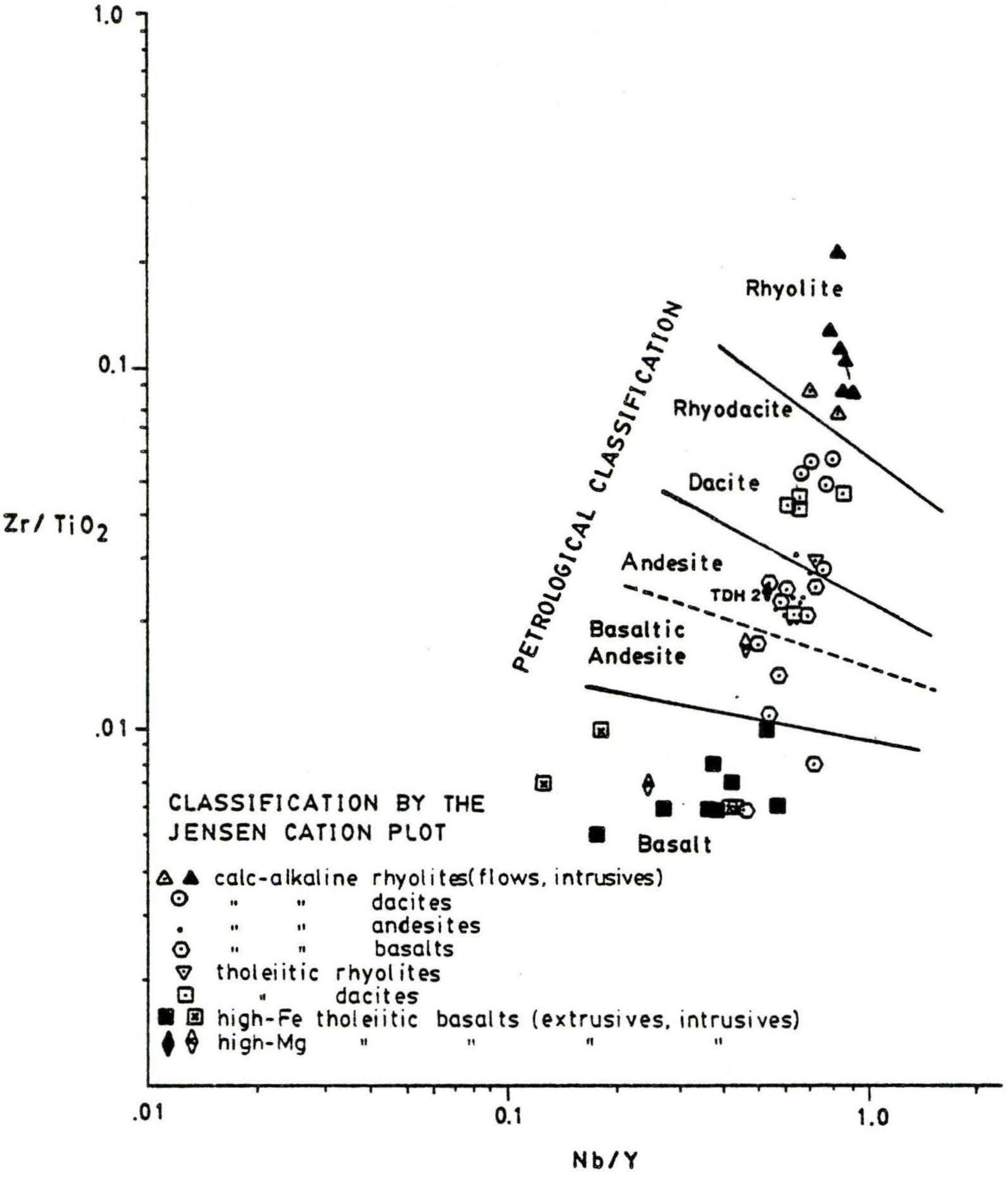
1.0
0.1
.01
Zr/TiO$_2$
.01
0.1
1.0
Nb/Y
PETROLOGICAL CLASSIFICATION
Rhyolite
Rhyodacite
Dacite
Andesite
TDH 2
Basaltic Andesite
Basalt
CLASSIFICATION BY THE JENSEN CATION PLOT
△ ▲ calc-alkaline rhyolites(flows, intrusives)
⊙ " " dacites
• " " andesites
⊙ " " basalts
▽ tholeiitic rhyolites
⊡ " dacites
■ ⊠ high-Fe tholeiitic basalts (extrusives, intrusives)
◆ ◇ high-Mg " " " "

Zr contents of these rocks are typical of subalkaline andesites and dacites reported by Winchester and Floyd (1977). The ratio of Nb/Y in the thesis area volcanics may have been slightly elevated by alteration.

5.2.3.4 Zr/TiO2 vs. Nb/Y

In Figure 5-7, the separation of samples by Zr/TiO2 versus Nb/Y closely parallels petrographic observations. The symbols on this diagram represent the classification of the samples on the Jensen cation plot.

In the following discussion regarding the whole rock and trace element chemistry of the volcanics, the subdivision of tholeiitic and calk-alkaline series is based on both the Jensen diagram and the Y-T-C plot. When the two plots disagree, the classification from the Y-T-C plot is chosen as correct. The subdivision of basalt through rhyolite is based on the Zr/TiO2 versus Nb/Y plot, and on petrographic observations.

5.3 MAJOR ELEMENT CHEMISTRY

The major and trace element data for all samples are listed in Appendix A. In Table 5-1, the average whole rock composition of each rock type is compared with other Archean examples (Abitibi belt, Eastern Goldfields Region, Marda Complex) and with modern island arc volcanics.

TABLE 5-1. Comparison of the average compositions of the Temagami volcanics with other Archean examples and modern island arc volcanics.

Tholeiitic Basalt

	ARCHEAN		MODERN
	Temagami (n=10)	Eastern (n=1)	Island Arc #1
SiO_2	46.16	51.3	51.57
Al_2O_3	14.09	14.8	15.91
Fe_2O_3	15.82	10.7	9.78
MgO	5.85	6.7	6.73
CaO	7.30	10.8	11.74
Na_2O	1.08	2.7	2.41
K_2O	.46	.18	.44
TiO_2	1.12	.96	.80
MnO	.19	.21	.17
P_2O_5	.13	.12	.11
CO_2	4.43	0.1	--
H_2O	4.04	1.1	.45

Calc-Alkaline Basalt

	ARCHEAN		MODERN
	Temagami (n=3)	Abitibi	Island Arc #2
SiO_2	51.30	50.2	53.3
Al_2O_3	14.08	16.8	19.0
Fe_2O_3	8.30	9.1	9.46
MgO	4.81	5.8	4.12
CaO	8.68	8.2	9.0
Na_2O	1.96	3.0	3.7
K_2O	1.04	0.5	.46
TiO_2	.83	1.0	.89
MnO	.17	.18	0.2
P_2O_5	.24	.13	0.1
CO_2	7.64	.56	--
H_2O	2.68	3.56	.40

Calc-Alkaline Andesite

	ARCHEAN		MODERN
	Temagami (n=18)	Marda (n=15)	Island Arc #3
SiO_2	60.88	60.8	59.64
Al_2O_3	14.50	14.7	17.38
Fe_2O_3	6.92	7.0	5.26
MgO	3.73	3.5	3.95
CaO	3.53	5.5	5.92
Na_2O	2.36	3.6	4.40
K_2O	1.52	1.7	2.04
TiO_2	.69	.77	.76
MnO	.09	.11	.09
P_2O_5	.19	.23	.28
CO_2	3.72	0.2	--
H_2O	2.84	1.8	1.08

Calc-Alkaline Dacite

	ARCHEAN		MODERN
	Temagami (n=11)	Marda (n=2)	Island Arc #4
SiO_2	67.94	70.75	66.8
Al_2O_3	14.46	13.94	18.24
Fe_2O_3	5.90	3.72	2.27
MgO	1.61	.71	1.50
CaO	1.64	1.36	3.17
Na_2O	.60	4.59	4.97
K_2O	.95	2.99	1.92
TiO_2	.50	.50	.23
MnO	.14	.07	.06
P_2O_5	.11	.11	.09
CO_2	.61	.19	--
H_2O	2.65	1.19	.26

Calc-Alkaline Rhyolite

	ARCHEAN		ARCHEAN		MODERN
	Temagami		Marda Complex		Island Arc
	E,(n=2)	I,(n=6)	E,(n=14)	I,(n=6)	#5
SiO_2	77.36	78.62	75.3	78.2	70.7
Al_2O_3	12.50	12.73	12.6	11.3	13.4
Fe_2O_3	.85	.97	2.0	0.8	3.7
MgO	.64	.22	0.2	0.3	0.0
CaO	1.16	1.17	0.3	1.1	2.8
Na_2O	2.14	1.30	3.9	3.7	4.9
K_2O	2.43	2.23	4.1	2.6	2.0
TiO_2	.10	.10	.23	0.1	0.3
MnO	.07	.05	.08	.03	0.3
P_2O_5	.03	.04	.02	.06	0.0
CO_2	1.75	1.12	0.2	0.5	--
H_2O	1.62	1.61	0.8	0.8	2.4

Temagami - Average compositions of the thesis area volcanics.
Abitibi - Average composition of calc-alkaline basalts from the Abitibi belt (Goodwin, 1979).
Eastern - Average composition of tholeiitic basalts from the Eastern Goldfields Region (Hallberg, 1972).
Marda - Average compositions of the calc-alkaline andesites to rhyolites from the Marda Complex (Hallberg et al., 1976).
Island Arc - Typical major element abundances in representative rocks from:-
#1 Typical island arc tholeiitic basalt from Jakes and White (1971).
#2 Calc-alkaline basalt, St. Kitts, West Indies, from Baker (1968b).
#3 Typical island arc calc-alkaline andesite from Jakes and White (1971).
#4 Typical island arc calc-alkaline dacite from Jakes and White (1971).
#5 Rhyolite, St. Lucia, West Indies from Tomblin (1975).

"I" = intrusives
"E" = extrusives
"n" = number of samples

5.3.1 Comparison with Modern Island Arc Volcanics

The island arc data are compiled from Baker (1968b), Jakes and White (1971), and Tomblin (1975). Consistent with comparisons reported by Condie (1976; 1981) for Archean volcanics and possible modern analogs, average compositions of the Temagami volcanics are lower in Al2O3 and usually higher in total Fe (here reported as Fe2O3; Table 5-1). Lower Fe2O3 averages occur in the calc-alkaline basalts and rhyolites. Condie also reports higher MgO contents in Archean volcanics; however, at Temagami this is true only in the calc-alkaline basalts, dacites and rhyolites. Compared to the modern volcanics, silica averages in the Temagami volcanics are higher in the calc-alkaline dacites and rhyolites and lower in the tholeiitic basalts. Calcium averages are lower in all of the Temagami volcanics, and this reflects a loss of CaO during carbonate alteration. Sodium contents are also low by 1 to 3 percent. The titanium averages for Temagami are slightly higher in the tholeiitic basalts and calc-alkaline dacites compared to modern examples. An enrichment in transition metals (Ti, Cr, Fe, Co, Ni, Cu and Zn) in Archean volcanics compared to modern counterparts is noted by Condie (1976). His explanation for this enrichment is that the Archean upper mantle was undepleted in transition metals relative to the present mantle.

5.3.2 Comparison with other Archean Volcanics

The major element chemistry of the Temagami volcanics is compared with other Archean examples in order to ascertain overall similarities with other well studied Archean terrains. The purpose of this comparison is to clearly define the local (outcrop scale) and regional (thesis area scale) alterations which have affected the chemistry of the Temagami volcanics.

The tholeiitic basalts are compared with those from the Eastern Goldfields Region of the Yilgarn block, western Australia. The calc-alkaline andesites through rhyolites are compared with those from the Marda Complex, Yilgarn block, western Australia. Calc-alkaline volcanics are uncommon in the Yilgarn block (Hallberg et al., 1976), and partly for this reason Condie (1976) suggests that the greenstone belts of western Australia belong to a different tectonic setting from those of North America. These examples were nevertheless chosen for comparison due to their overall similarity to some Canadian greenstone belts (Hallberg, 1972; Hallberg et al., 1976), and for the availability of the compiled data.

The Eastern Goldfields volcanics are 2650 to 2750 m.y. in age and have undergone a low-grade regional metamorphism (Hallberg, 1972). Carbonate and chlorite alteration in the tholeiites is restricted to amygdule and secondary vein fillings. The volcanic belts are composed principally of mafic flows and rare acid volcanic sequences. The Marda Complex volcanics are slightly younger at 2635 m.y. and consist of a sequence of andesites, dacites and rhyolites. Metamorphism is at lower greenschist facies and local shearing, silicification and carbonatization is common (Hallberg et al., 1976).

5.3.2.1 Tholeiitic Basalts

The tholeiitic basalts of the thesis area do not correlate well with the Goldfields volcanics; however, much of the difference can be explained by alteration. Carbonate alteration in the mafic flows and tuffs has caused depletion of SiO_2, Al_2O_3, MgO, and CaO, and enrichment of Fe_2O_3 (total iron) and TiO_2. The contents of MnO and P_2O_5 are unaffected. Chlorite alteration in the Temagami volcanics has caused depletion of SiO_2 and Na_2O, and enrichment of Fe_2O_3 and TiO_2. In contrast to carbonatization, chlorite alteration may also increase MgO and Al_2O_3. The low K_2O average of the Goldfields basalts is typical of Australian tholeiites and is suggested by Condie (1976) to reflect a different upper mantle composition. Low K_2O values; however, are not typical of the Marda Complex.

5.3.2.2 Calc-Alkaline Basalts

The calc-alkaline basalts are compared with the volcanics from the Abitibi belt (Goodwin, 1979). There is a fair agreement in the major elements except for Al_2O_3 and Na_2O. The Temagami basalts are affected by carbonatization and may be chloritized or silicified (section 4.1.1). The Al_2O_3 content varies from 12.2 percent in a highly carbonatized basalt (TDH 34) to 15.8 percent in a chloritized basalt (TDH 120). As there are only three samples in this group the low aluminum content may not be statistically significant. The approximate sodium depletion in the calc-alkaline basalts is one percent.

5.3.2.3 Calc-Alkaline Andesites

A good correlation exists in the major element chemistry of the Temagami intermediate to felsic volcanics with that of the Marda Complex, and this reflects the similar alteration and metamorphic history of the two areas. In averaging the major element compositions of the andesites, a highly silicified sample (TDH-154) was omitted. The criteria for classifying TDH 154 as a silicified andesite is based on the its trace element chemistry and high SiO_2 content (70 weight percent). In Figure 5-5, TDH 154 lies above the trend of magma differentiation in the Temagami volcanics. In Figure 5-7 it plots within the andesite field. If the typical range in SiO_2 for andesites is 53 to 62 percent (from Jakes and White, 1971) the minimum SiO_2 addition in this sample is 8 percent.

Due to carbonate alteration, the calc-alkaline andesites of the thesis area are depleted in CaO compared to the Marda volcanics (Table 5-1) . Sodium is also depleted by more than one weight percent. However, except for CaO, Na_2O and volatiles (CO_2 and H_2O), the chemistry of the Temagami calc-alkaline andesites is remarkably similar to that of the Marda andesities.

Carbonate and chlorite occur as minor alteration minerals in the Temagami rocks and some of the andesites are silicified (Section 4.1.1). The distribution of silicification on a mapping scale seems erratic. In Figures 5-8 and 5-9 the major oxides for 18 Temagami andesites are plotted against their SiO_2 contents in order to study the effect of silicification on the major element chemistry. Aluminum and P remain nearly constant with increasing silica. Titanium, Fe, Mg and Ca decrease while Na and K increase. The best correlations with silica are shown by Fe and Mg with correlation coefficients (r values, Figures 5-8 and 5-9) of 0.57 and 0.39 respectively. Weaker correlations are shown by Ca, K, Ti and Na where correlation coefficients decrease from 0.29 to 0.13. The overall scatter of points in each diagram is a result of the varying degrees of chlorite and carbonate alteration in the andesites. MacGeehan (1978) and Gibson et al. (1983) report more systematic changes in Al, Fe, Mg and Ti with increasing silica content in basalts and andesites respectively. Gibson suggests that Al, Fe, Mg and Ti are uniformly exchanged with Si during alteration, whereas Na, K and Ca remain relatively constant during progressive silicification.

5.3.2.4 Calc-Alkaline Dacites

The calc-alkaline dacites are compared with porphyritic dacites from the Marda Complex (Table 5-1). Chlorite alteration in the 11 samples that were analysed may account for the enriched Fe and Mg and depleted Na and K in the Temagami dacites. Manganese in the 11 dacites is quite variable suggesting a high mobility of the element during alteration.

Two of the dacites analysed (TDH 4 and 123) are silicified with 77 and 74 weight percent SiO_2 respectively. In Figure 5-5 these samples lie above the general trend of magma differentiation in the Temagami volcanics. In Figure 5-7 both samples plot

FIGURE 5-8. Binary plots of the major oxides versus SiO2 for the Temagami calc-alkaline andesites.

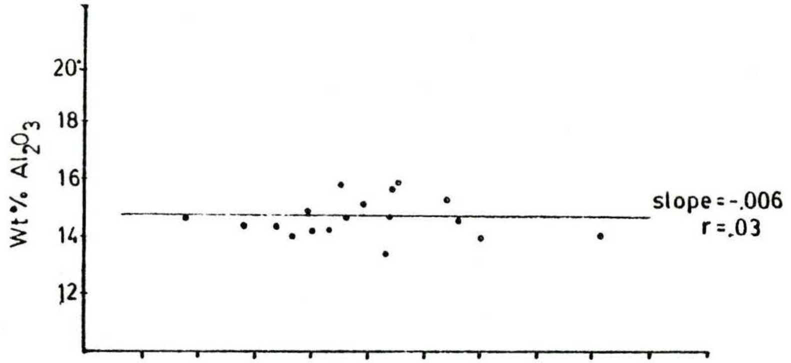
Wt% Al_2O_3
20
18
16
14
12
slope = -.006
r = .03

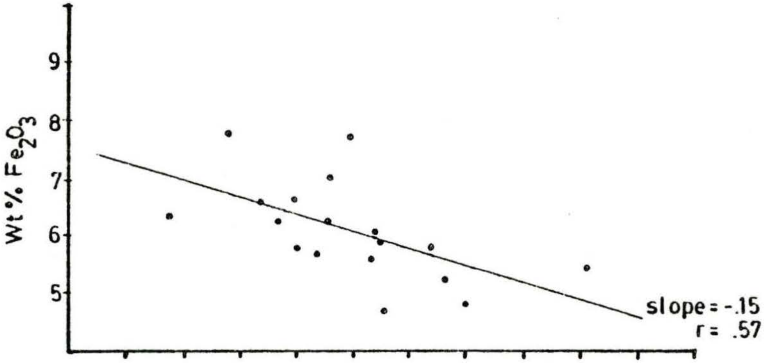
Wt% Fe_2O_3
9
8
7
6
5
slope = -.15
r = .57

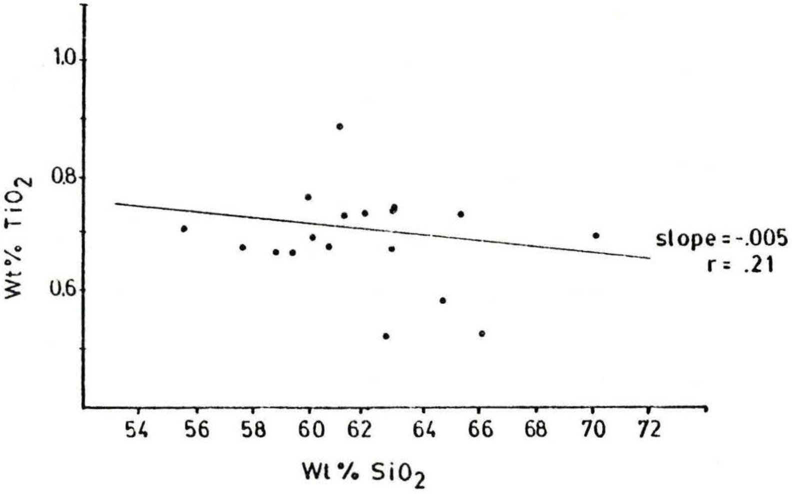
Wt% TiO_2
1.0
0.8
0.6
slope = -.005
r = .21
54
56
58
60
62
64
66
68
70
72
Wt% SiO_2

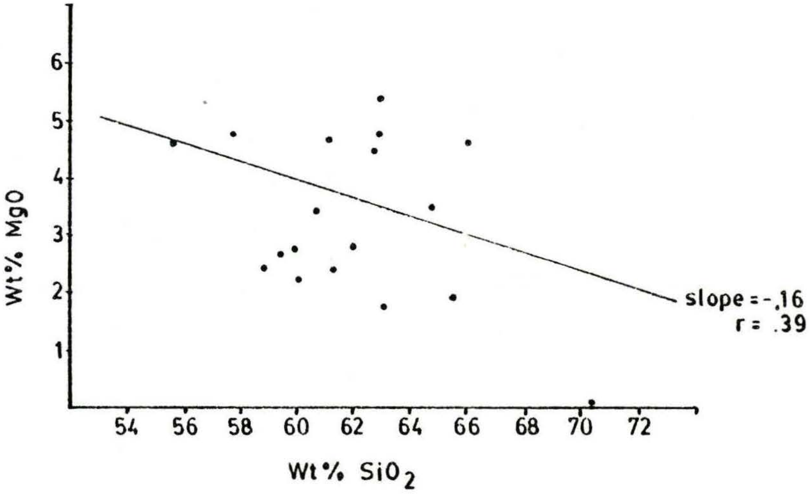
Wt% MgO
6
5
4
3
2
1
slope = -.16
r = .39
54
56
58
60
62
64
66
68
70
72
Wt% SiO_2

FIGURE 5-9. Binary plots of the major oxides versus SiO2 for the Temagami calc-alkaline andesites.

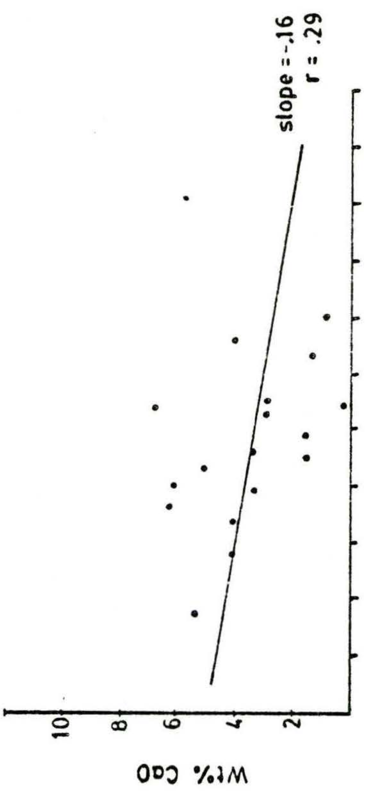
slope = -.16
r = .29
Wt% CaO
10
8
6
4
2

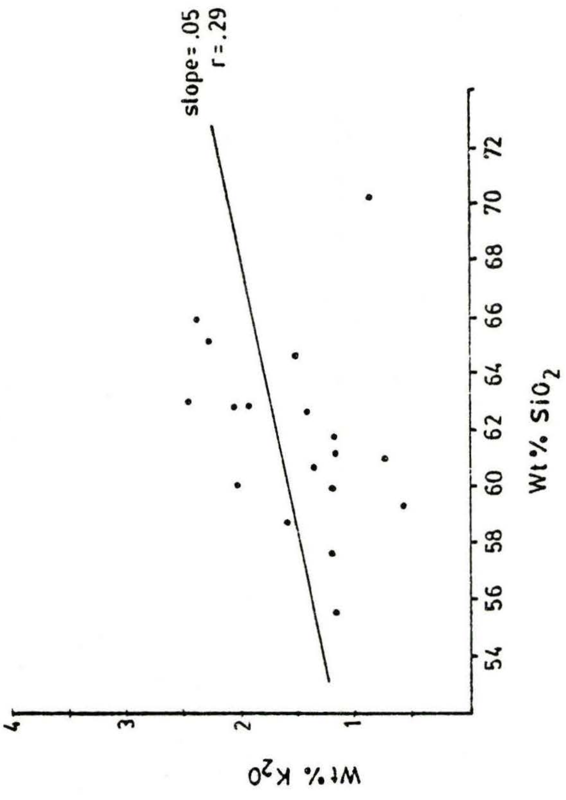
slope = .05
r = .29
Wt% K$_2$O
4
3
2
1
54
56
58
60
62
64
66
68
70
72
Wt% SiO$_2$

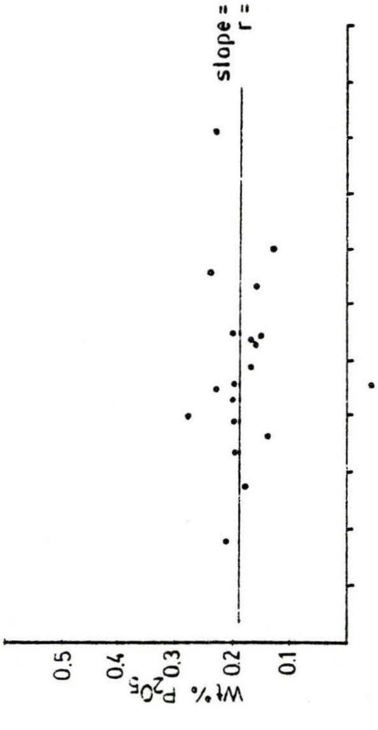
slope = -.0005
r = .05
Wt% P$_2$O$_5$
0.5
0.4
0.3
0.2
0.1

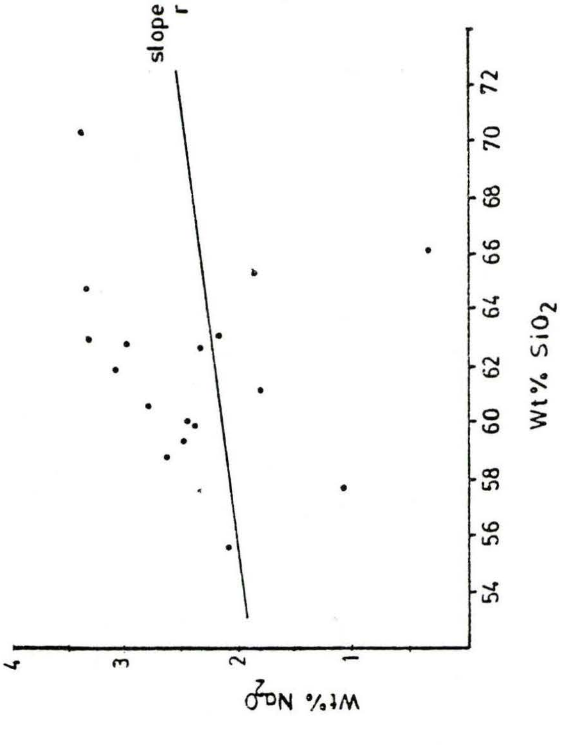
slope = .03
r = .13
Wt% Na$_2$O
4
3
2
1
54
56
58
60
62
64
66
68
70
72
Wt% SiO$_2$

within the dacite field. If the typical range in SiO2 contents for dacites is 62 to 70 weight percent (from Jakes and White, 1971) the minimum SiO2 addition to these samples is 4 to 7 percent. Silicification in the dacites has caused a depletion in Al2O3, MgO and CaO with values as low as 11, 0.34 and 0.16 weight percent respectively.

5.3.2.5 Calc-Alkaline Rhyolites

In Table 5-1, the calc-alkaline rhyolites of the thesis area are subdivided into flows and synvolcanic intrusives. Except for the slightly higher Fe2O3 and lower MgO contents, the intrusives are chemically similar to the flows. In the field, the appearance of the flows and intrusives is quite dissimilar. As mentioned in the section on local geology, the rhyolite flow ("moonrock") can be traced as a conformable unit for at least 1/2 kilometer. The felsic intrusives rarely form stratiform units with the other volcanics. The calc-alkaline rhyolites of the thesis area are compared with the rhyolite ignimbrites and flows of the Marda Complex, and also with the rhyolite porphyry dykes which intrude all units in the Marda Complex. Hallberg et al. (1976) considers the dykes to be associated with later faulting and folding, and unrelated to the complex. Nevertheless these dykes are apparently igneous in origin and may represent a primary silica-rich magma.

With the exception of aluminum and phosphorous, the Temagami rhyolites do not compare well with the Marda extrusives. A higher SiO_2 average in Temagami is accompanied by higher MgO and lower Fe_2O_3 and TiO_2 averages. The Na_2O average is also low by more than one percent. The chemistry of the rhyolites compares more closely with the rhyolite dykes of the Marda Complex. Again the Temagami rocks are relatively depleted in sodium. Unfortunately little detail is given on the Marda dykes, and it is unknown whether or not they are silicified. Hallberg et al. (1976) mentions that the dykes tend to occur along secondary faults. As such they may be affected by later silica-rich fluids.

It is necessary at this point to determine whether the rhyolites at Temagami are primary high-silica rocks, or silicified rhyolites. In thin section the rhyolites contain sericite and minor carbonate and chlorite alteration. Quartz overgrowths around euhedral quartz phenocrysts are also present. In Figure 5-5, the majority of rhyolites fall along what is interpreted as a trend for progressive differentiation of a basic magma. Samples of dacite and andesite which fall off this trend are known to be silicified, with approximate SiO_2 additions of 4 to 8 percent (sections 5.2.3.3 and 5.2.3.4). The Zr/TiO_2 ratios appear to be unaffected by this addition. The Zr/TiO_2 ratios of the rhyolites in the thesis area increase with increasing SiO_2 content but do not deviate from the common trend defined by all rock types, suggesting that these rocks are indeed progressive differentiates rather than progressively silicified rhyolites. There are two rhyolite samples (TDH 124 and 158) which plot away from the trend. Their SiO_2 contents of 80 and 82 weight percent do suggest some silicification. It is apparent; however, that the rhyolite flows and intrusives at Temagami are from primary felsic magmas, and that silicification in these rocks involves no more than the addition of 2 to 3 weight percent SiO2.

5.3.3 Summary

Comparison of the thesis area rocks with other Archean examples and modern island arc volcanics has delineated certain features characteristic of the Temagami volcanics. A pervasive depletion in Na2O is evident for all rock types. Calcium averages are lower in the intermediate to mafic volcanics and this may be attributed to higher carbonate alteration in these rocks. Silicification has occurred in some rocks, but no large-scale pervasive silica alteration in any particular rock type or along any stratigraphic horizon is apparent. In silicified samples, Al and P remain constant, Ti may be slightly depleted and Fe is moderately depleted. Magnesium is depleted in two silicified samples (TDH 123, 154), but its behaviour in other samples is modified by chlorite alteration. No consistent trend in potassium is exhibited by these volcanics.

The observed alteration of plagioclase to sericite in thin section (Section 4.1.1) is reflected in normative corundum values in CIPW normative calculations. The normative corundum indicates that the molecular proportion of Al2O3 exceeds the combined proportion of Na2O, K2O and CaO. This implies that CaO and Na2O have been leached from the rock. The depletion of Na2O and CaO in alteration zones that underlie or occasionally overlie massive sulphide deposits is well documented, and this depletion is not confined to the immediate footwall rocks, but occurs on a regional scale (Sopuck et al., 1980; Franklin et al., 1981). The implication that the Temagami volcanics may have been subject to alteration by "ore-forming" solutions will be discussed in section 5.4.3.

5.4 TRACE ELEMENT CHEMISTRY

5.4.1 K/Rb Ratios

The K/Rb ratios for all volcanics and synvolcanic intrusives are plotted in Figure 5-10. The arithmetic mean K/Rb ratio for the Temagami volcanics is 356. Most of the samples plot near the main trend for igneous rocks according to Shaw (1968). The mobility of the alkalies during alteration accounts for the scatter of samples across the main trend. Condie (1976) reports that ratios such as K/Rb may change as a function of degree of alteration and low-grade metamorphism.

The average ratios for Archean tholeiites, andesites and siliceous volcanics (from Condie, 1976) are also reported in Figure 5-10 . The mean ratio for the thesis area volcanics is close to the 350 average for Archean tholeiites, and it also falls within the range for undepleted siliceous Archean volcanics. There is no suggestion of high K/Rb rocks indicative of oceanic tholeiites in the Temagami area. This suggests that the

FIGURE 5-10. K/Rb plot for the Temagami volcanics and synvolcanic intrusives.

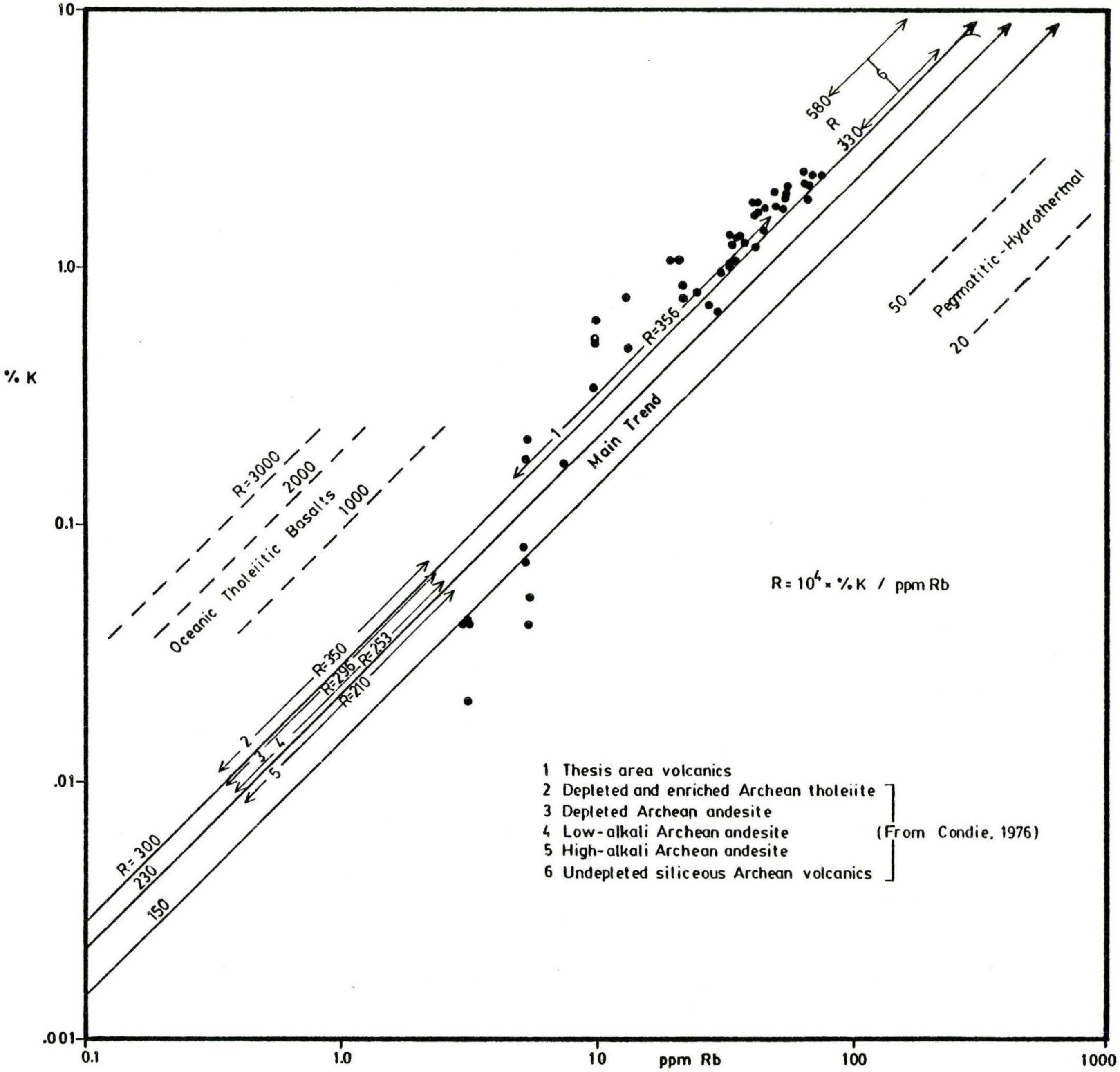
%K
10
1.0
0.1
.01
.001
0.1
1.0
10
100
1000
ppm Rb
R = 10^4 × %K / ppm Rb
580
R
330
6
R=356
1
Main Trend
50
Pegmatitic-Hydrothermal
20
R=3000
2000
Oceanic Tholeiitic Basalts
1000
R=350
R=296
R=253
R=210
2
3
4
5
R= 300
230
150
1 Thesis area volcanics
2 Depleted and enriched Archean tholeiite
3 Depleted Archean andesite
4 Low-alkali Archean andesite
5 High-alkali Archean andesite
6 Undepleted siliceous Archean volcanics
(From Condie, 1976)

mega-tectonic environment is not a seafloor mid-ocean ridge spreading environment, and probably not a rift-like setting.

5.4.2 Rare Earth Elements

The rare earth element (REE) data for 22 samples are listed in Appendix A, and chondrite-normalized REE patterns are presented in Figures 5-11 through 5-18. The increase in abundance from Yb to Lu in all samples may be due to a bias in the analytical method, but does not affect the overall interpretation of the REE patterns.

5.4.2.1 Mafic Intrusive Rocks

The REE patterns in Figure 5-11 are for the Archean mafic dykes (diorites) of the thesis area. Samples TDH 14 and 29 plot compositionally as Mg-tholeiites on both the Jensen cation plot and the Y-T-C trace element plot. Their relatively flat REE patterns are typical of the type TH 1 Archean tholeiite (formerly depleted, DAT) discussed by Condie (1981), and except for the high Lu contents lie within the TH 1 envelope of variation. According to Condie (1976) an overall similarity is apparent between DAT and modern rise and arc tholeiites.

Sample TDH 12b is a diorite which plots as an Fe-tholeiite on the Jensen diagram (Figure 5-2). It differs from the other two intrusives by showing a greater REE enrichment and exhibiting a negative Eu anomaly. Condie (1981) noted that Abitibi tholeiites differ from the TH 1 tholeiite group by having higher overall REE abundances, Eu anomalies, and a somewhat different major and trace element chemistry. The REE pattern for TDH 12b is similar to the pattern for the average Abitibi tholeiite presented by Condie except for a higher REE enrichment.

5.4.2.2 Mafic Pyroclastics

The REE patterns for four mafic pyroclastics are shown in Figure 5-12. All of the tuffs plot compositionally as Fe-tholeiites. The relatively flat pattern for TDH 30 is again fairly typical for an Archean tholeiite and closely matches the patterns for samples 14 and 29 in Figure 5-11. Sample TDH 16 has a REE pattern similar to that of TDH 12b, and also contains higher than average overall REE abundances for a type TH 1 Archean andesite. Higher abundances are typical of type TH 2 tholeiites; however, these rocks are also characterized by light rare earth (LREE) enrichment and a sloping REE pattern.

Samples TDH 12a and 13 exhibit rather unique patterns. TDH 12a is characterized by a flat LREE pattern (up to Sm) followed by an abrupt decrease in abundance of Eu and Tb, with an increase in abundance of the heavy rare earth elements (HREE). TDH 13 is characterized by a relatively flat pattern of the LREE, a negative Eu anomaly, followed by an abrupt and continuous decrease in the HREE. Samples 12a and 13 are similar in their major and trace element chemistry, and both are affected by carbonate alteration. The CO2 contents are 8 and 6 percent respectively.

Figure 5-11.
CHONDRITE-NORMALIZED RARE EARTH ELEMENTS PATTERNS

ARCHEAN MAFIC INTRUSIVES

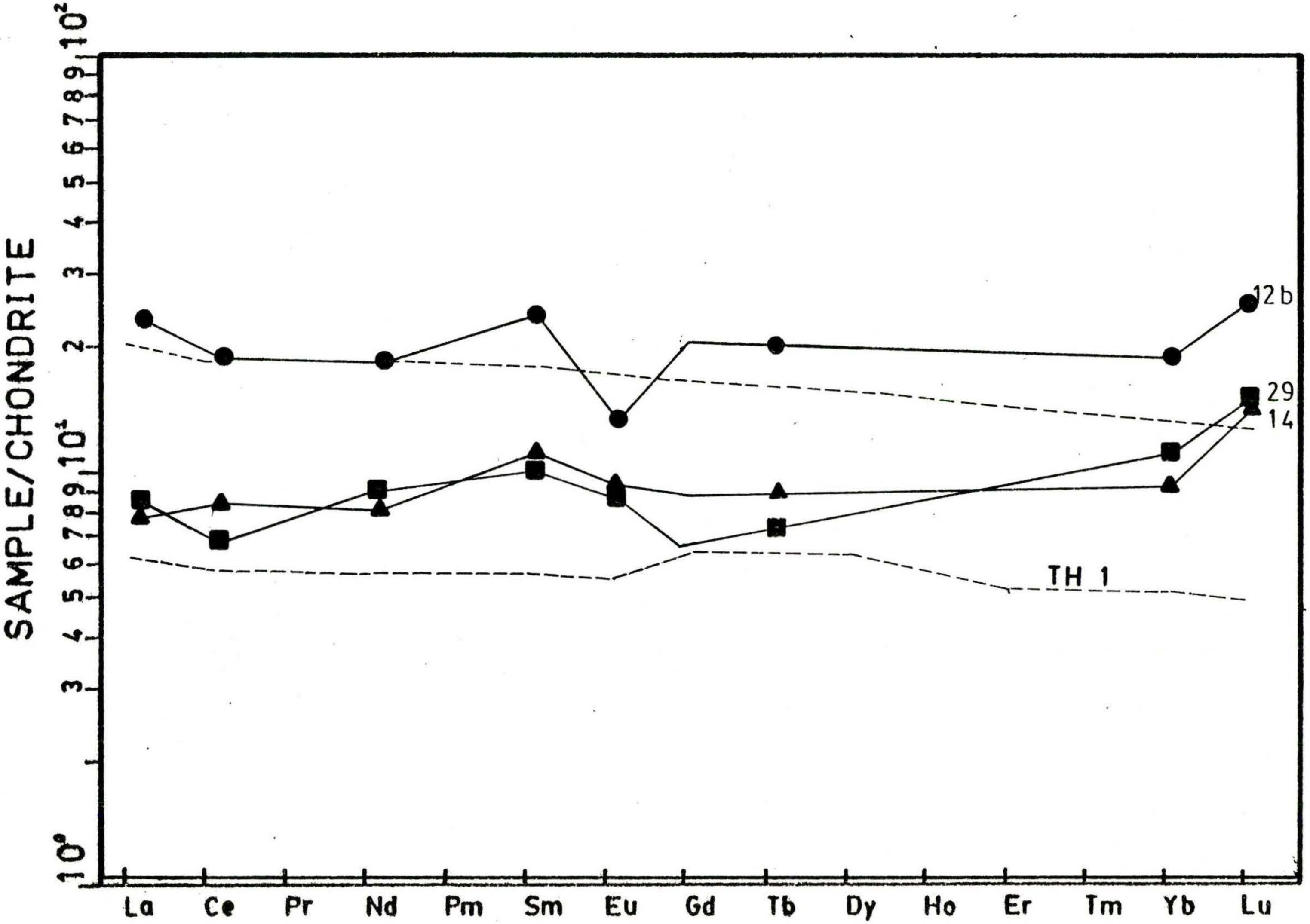

Figure 5-12.
CHONDRITE-NORMALIZED RARE EARTH ELEMENTS PATTERNS

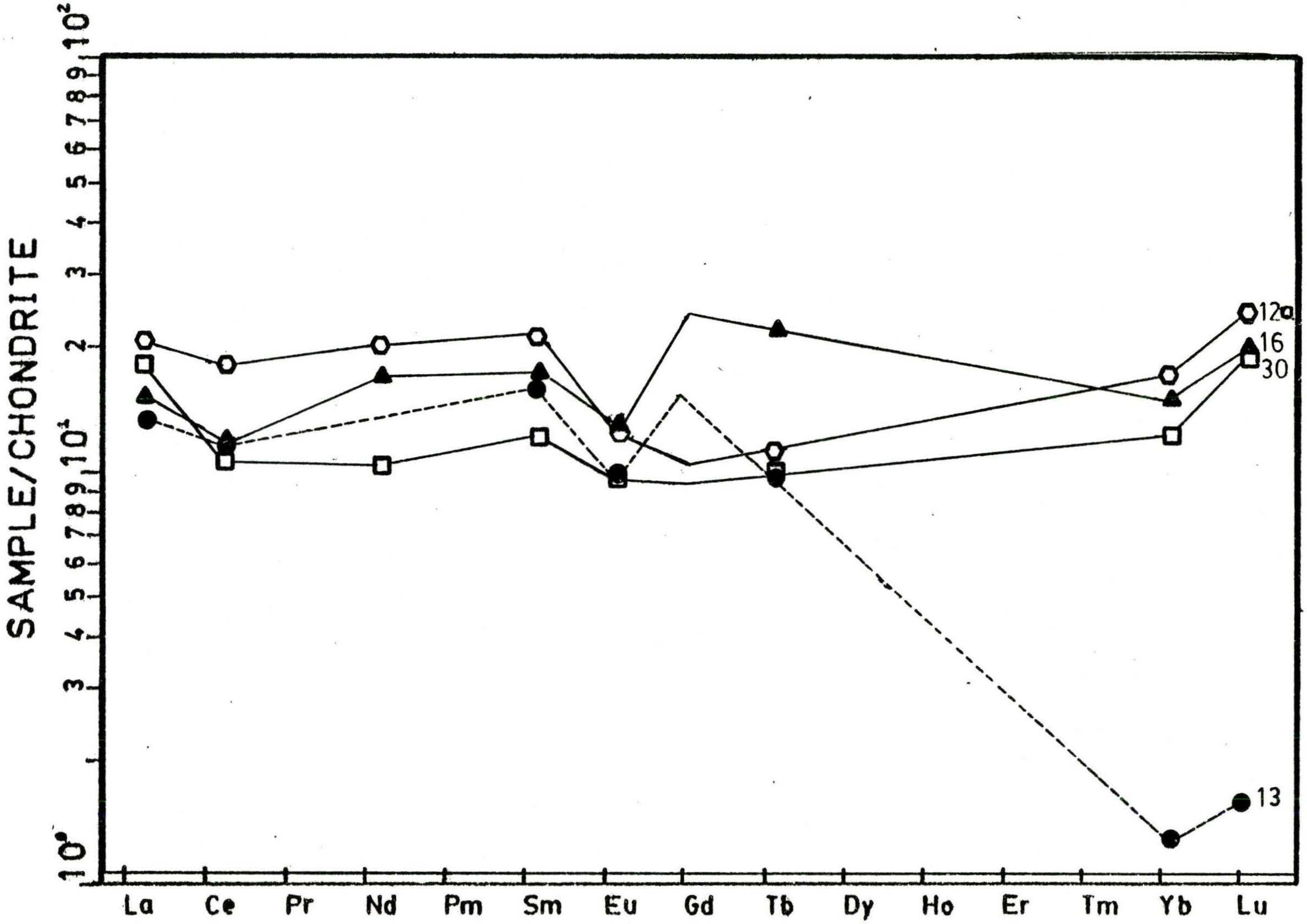

MAFIC PYROCLASTICS

Kerrich and Fryer (1979) reported similar REE patterns to each of these samples in metabasic schists from the Dome Mine, Timmins, Ontario. Also, a similar pattern to TDH 13 has been reported by Kerrich et al. (1981) for mafic tuffs from the Dickenson Mine, Red Lake, Ontario.

The mafic tuffs in the Dickenson Mine are host rocks to auriferous sediments. REE distributions in both the sediments and the mafic volcanic wall rocks are characterized by relatively flat chondrite-normalized patterns up to Sm-Gd (with or without negative Eu anomalies) followed by an abrupt continuous decrease in abundances of HREE. This pattern has been interpreted as a modification of a primary tholeiitic basalt pattern by hydrothermal solutions which selectively mobilized the HREE relative to the LREE. Such a process may involve complexing of HREE with CO3 in metamorphic fluids (Kerrich et al., 1981).

The metabasic schists of the Dome Mine are host rocks to the gold-bearing quartz-carbonate layers (Kerrich and Fryer, 1979). Both the stratiform ores and the mafic schists exhibit relatively unfractionated LREE up to Sm, followed by increasing depletion of medium to HREE. Again the pattern is explained as due to leaching of the HREE during intense hydrothermal activity. Sample TDH 13 may also have undergone a similar leaching process of the HREE.

What complicates such an interpretation is the similar chemistry and close proximity in the field of samples 12a and 13. While TDH 13 is leached of the HREE, TDH 12a is apparently slightly enriched in the HREE. A broadly similar situation was described by Kerrich and Fryer (1979) for metabasic schists from the Dome Mine. Strong HREE enrichment in one sample produced an S-shaped normalized pattern which was attributed to precipitation of the heaviest REE previously leached from the other schists in the volcanic sequence. Precipitation would have occurred when CO3 complexes broke down during waning hydrothermal activity (Kerrich and Fryer, 1979). While the metabasic schist pattern described here is comparable to that of 12a, their explanation is not necessarily subscribed to as a compelling explanation of the differing patterns of 12a and 13.

REE patterns for the auriferous veins and altered host rocks of the Dome Mine have also been reported by Roberts and Reading (1981). The patterns for the mafic volcanics (South Greenstones, Porcupine Syncline basalts) are relatively flat and exhibit neither the HREE depletion nor enrichment reported for the metabasic schists analysed by Kerrich and Fryer (1979).

5.4.2.3 Andesites, Dacites

The REE patterns for seven calc-alkaline andesites and one calc-alkaline dacite are presented in Figure 5-13. The relatively tight REE patterns support the chemical classification of these rocks based on various trace element plots. Some minor leaching of the LREE may account for the crossover of some samples (eg. TDH 10, 11 and 18).

The patterns of these samples are somewhat different than the average patterns presented by Condie (1976; 1981) for Archean andesites as shown in Figure 5-14. A steeper negative slope of the LREE, and a flatter HREE pattern distinguishes the Temagami andesites from the Type I andesites (formerly low-alkali, LAA) of Condie. Compared to the Type II andesites (formerly high-alkali, HAA) the Temagami andesites contain lower overall REE abundances and a flatter HREE pattern.

Silicification reportedly dilutes overall REE abundances (Ludden et al., 1982) and may be the cause of the lower abundances observed in the Temagami andesites. Excepting the 77 percent SiO2 value of TDH 4 (a silicified dacite), the range in SiO2 for the seven andesites is 58 to 66 percent. No correlation exists between the silica content and the LREE abundances of these samples, and the two samples with the lowest silica contents (TDH 10 and 18) appear to have been leached of the LREE.

In Figure 5-15 the Temagami andesites are compared with two andesite samples from the Marda Complex (Taylor and Hallberg, 1977). An overall similarity is apparent for the rocks except for the slightly lower overall REE abundances of the Temagami volcanics. The Marda andesites are considered Type III andesites (formerly depleted, DAA) by Condie (1981; 1982). The Marda REE pattern; however, more closely resembles that of the Type II andesite with notably enriched LREE, rather than the flat pattern with negative Eu anomalies typical of the Type III andesite. Type II andesites are most abundant in upper stratigraphic sections of volcanic piles and the modern analog is a continental

Figure 5-13.
CHONDRITE-NORMALIZED RARE EARTH ELEMENTS PATTERNS

ANDESITES

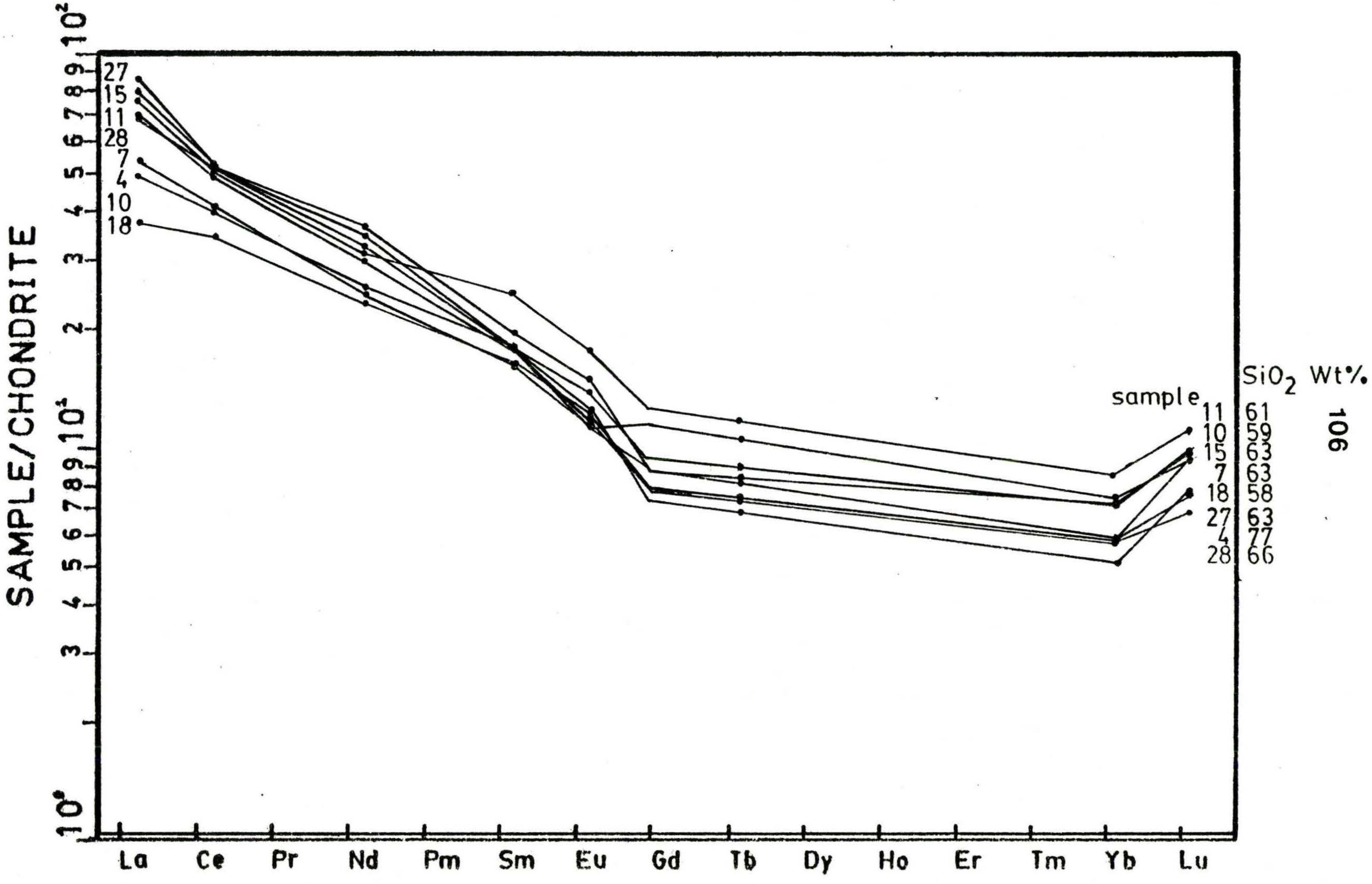

Figure 5-14.
CHONDRITE-NORMALIZED RARE EARTH ELEMENTS PATTERNS

ANDESITES

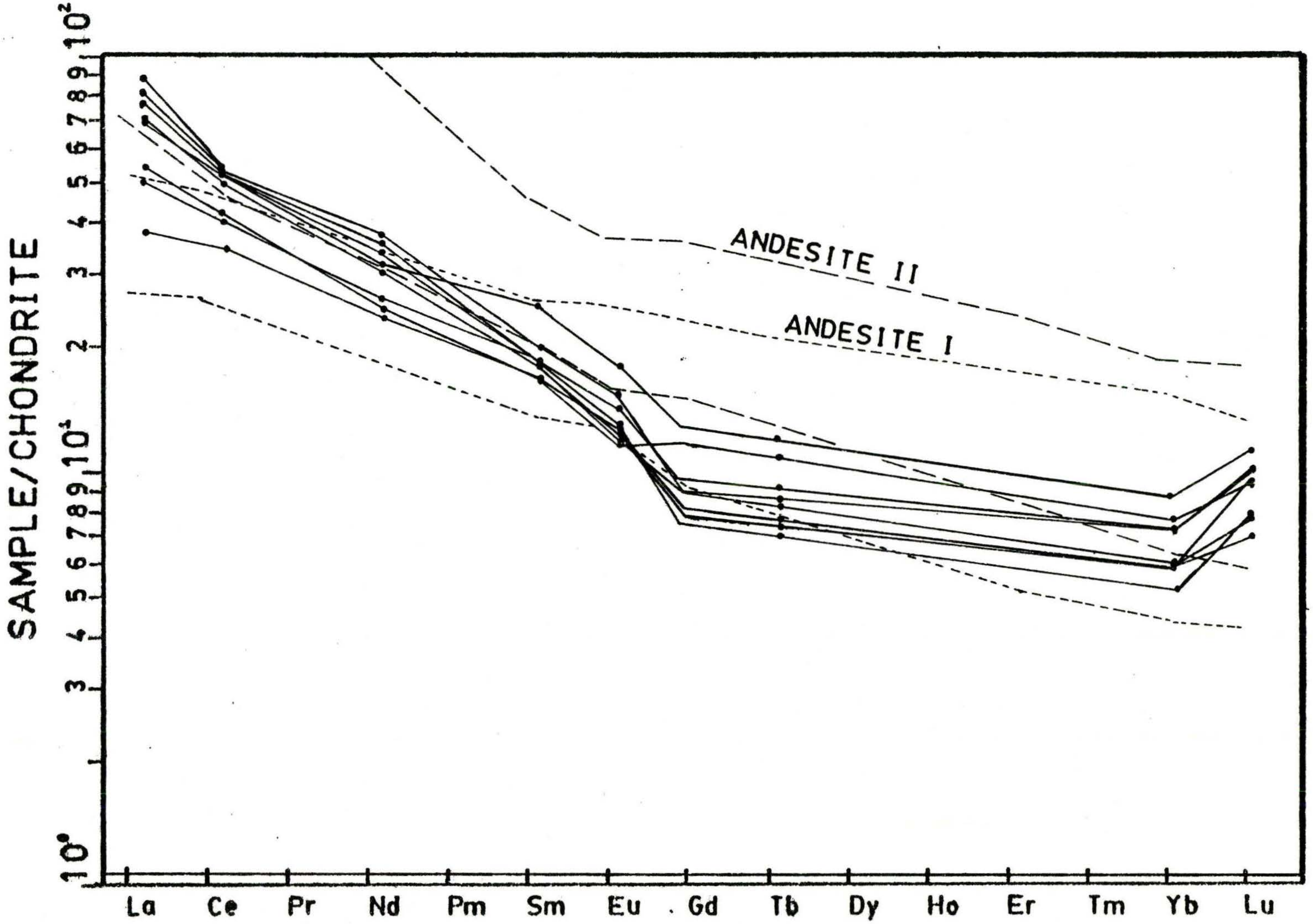

Figure 5-15.
CHONDRITE-NORMALIZED RARE EARTH ELEMENTS PATTERNS

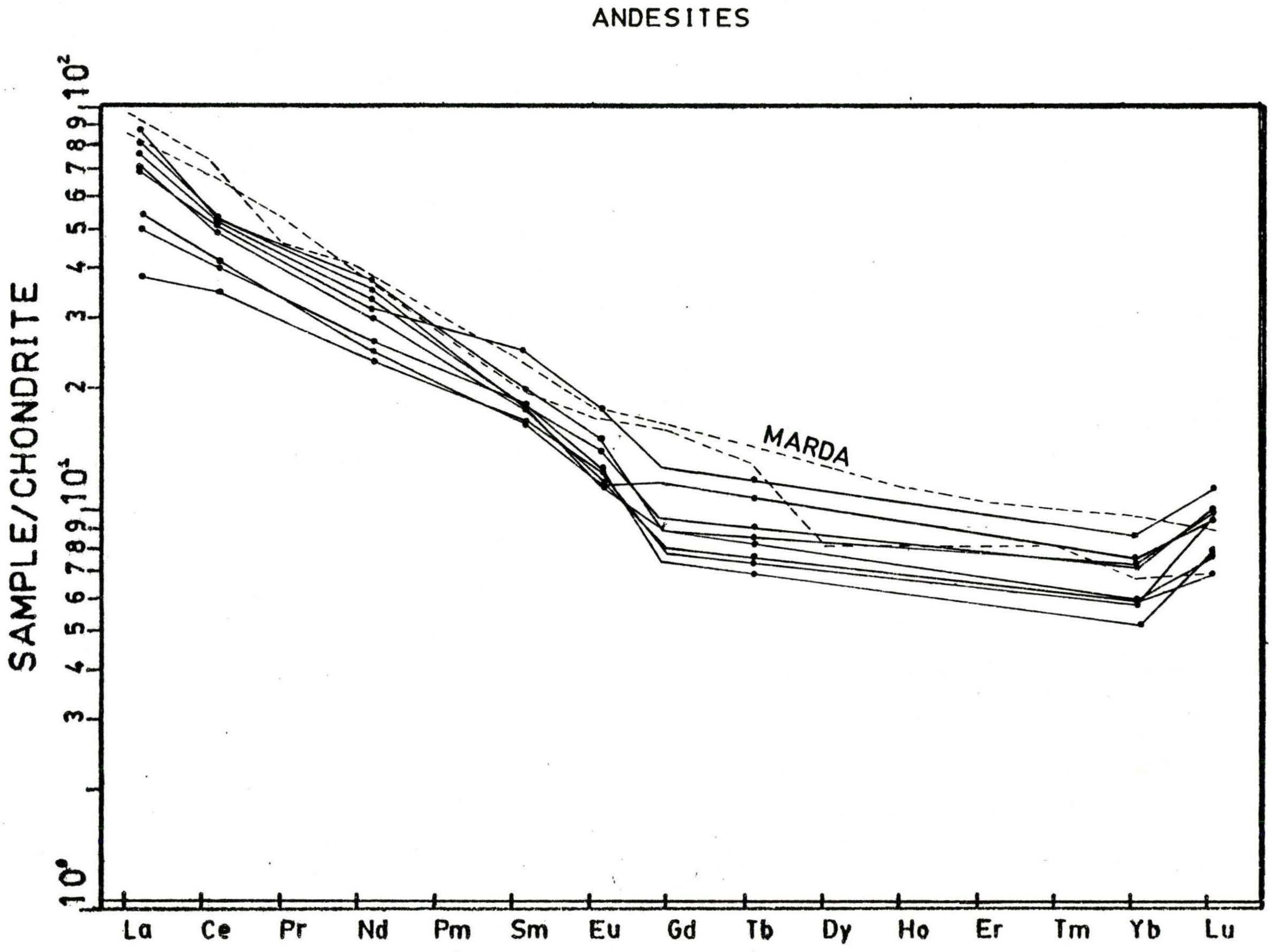

ANDESITES

margin arc system (Condie, 1981). Taylor and Hallberg (1977) consider the REE patterns of the Marda volcanics to be analogous with continental margin (Andean) calc-alkaline volcanic suites. The resemblance of the Temagami volcanics with those from the Marda Complex may imply a similar tectonic setting for the Temagami greenstone belt.

The maximum CO2 content of the andesites in Figure 5-13 is 6 percent. The affect of stronger carbonate alteration on REE patterns for two samples of altered andesite (TDH 2 and 34) is shown in Figure 5-16. Both samples contain 12 percent CO2, and are pervasively carbonatized in thin section. On trace element variation diagrams they plot in the andesite and basaltic andesite fields respectively. In comparison with the less altered andesites, these samples are notably enriched in LREE and are progressively depleted in HREE. Such nearly identical patterns for these rocks is quite significant considering that TDH 2 is a flow located nearly 2 km away from TDH 34, a mafic tuff. The stratigraphic distance between the samples is approximately 200 metres.

5.4.2.4 Rhyolites

The REE patterns for one rhyolite flow (TDH 8) and three synvolcanic felsic intrusives (TDH 22, 25 and 26), are presented in Figure 5-17. The patterns are most similar to the Type FII patterns (formerly undepleted siliceous volcanics, USV) defined by Condie (1976; 1981); however, a depletion in the overall REE

Figure 5-16.
CHONDRITE-NORMALIZED RARE EARTH ELEMENTS PATTERNS

ALTERED ANDESITES

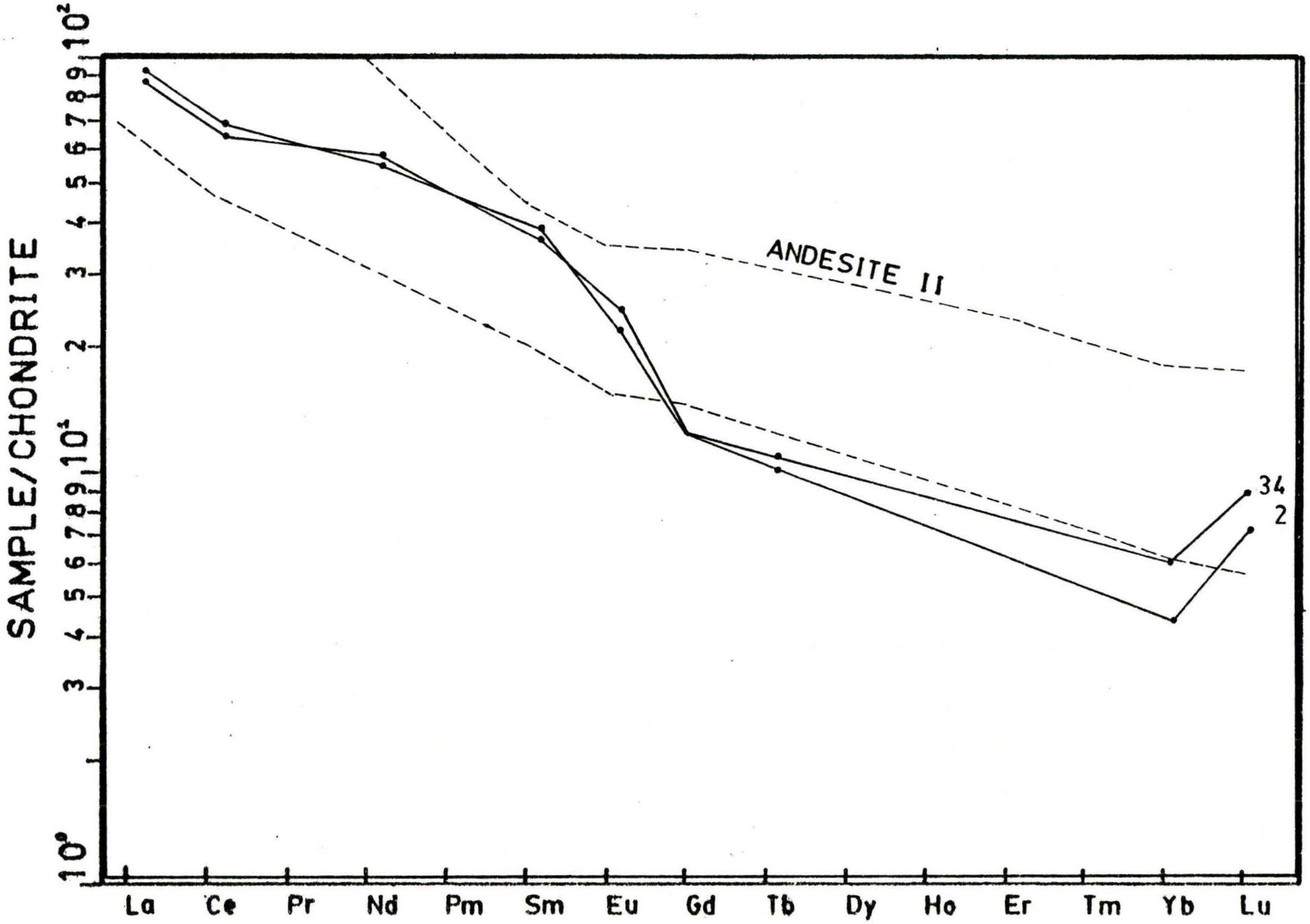

abundances is typical of the Temagami rhyolites.

Compared to the felsic flow, the intrusives are characterized by lower LREE abundances and relatively unfractionated HREE patterns. A similar change in the REE pattern for progressively differentiated felsic magmas has been reported by Miller and Mittlefehldt (1982). According to them, the LREE do not act as incompatible elements in very felsic magmas. The concentrations of the LREE decrease during differentiation of the magmas, and the degree of depletion decreases with increasing atomic number. In advanced stages of differentiation patterns change from steeply dipping to nearly flat. The change seen from TDH 8 to TDH 22, an increase in SiO2 of approximately 5 percent, is comparable to the evolution of REE patterns for progressively differentiated samples from the Granite Mountains (Miller and Mittlefehldt, 1982). As such, the felsic intrusives may represent a high level magma chamber that fed the overlying rhyolite flow.

In Figure 5-18 REE patterns of the felsic intrusives are compared with a high silica (81% SiO2) Marda rhyolite (from Taylor and Hallberg, 1977), a typical Kuroko ore-bearing felsic volcanic, and a barren felsic volcanic from the Skead area of the Abitibi greenstone belt (taken from Campbell et al., 1981). The purpose of such a comparison is to determine whether the REE patterns of the felsic rocks in the thesis area give any indication that the volcanics might host massive sulphide deposits. The Marda rhyolite has a REE pattern similar to TDH 25; however, overall REE abundances are higher. The Kuroko sample exhibits a

Figure 5-17.
CHONDRITE-NORMALIZED RARE EARTH ELEMENTS PATTERNS

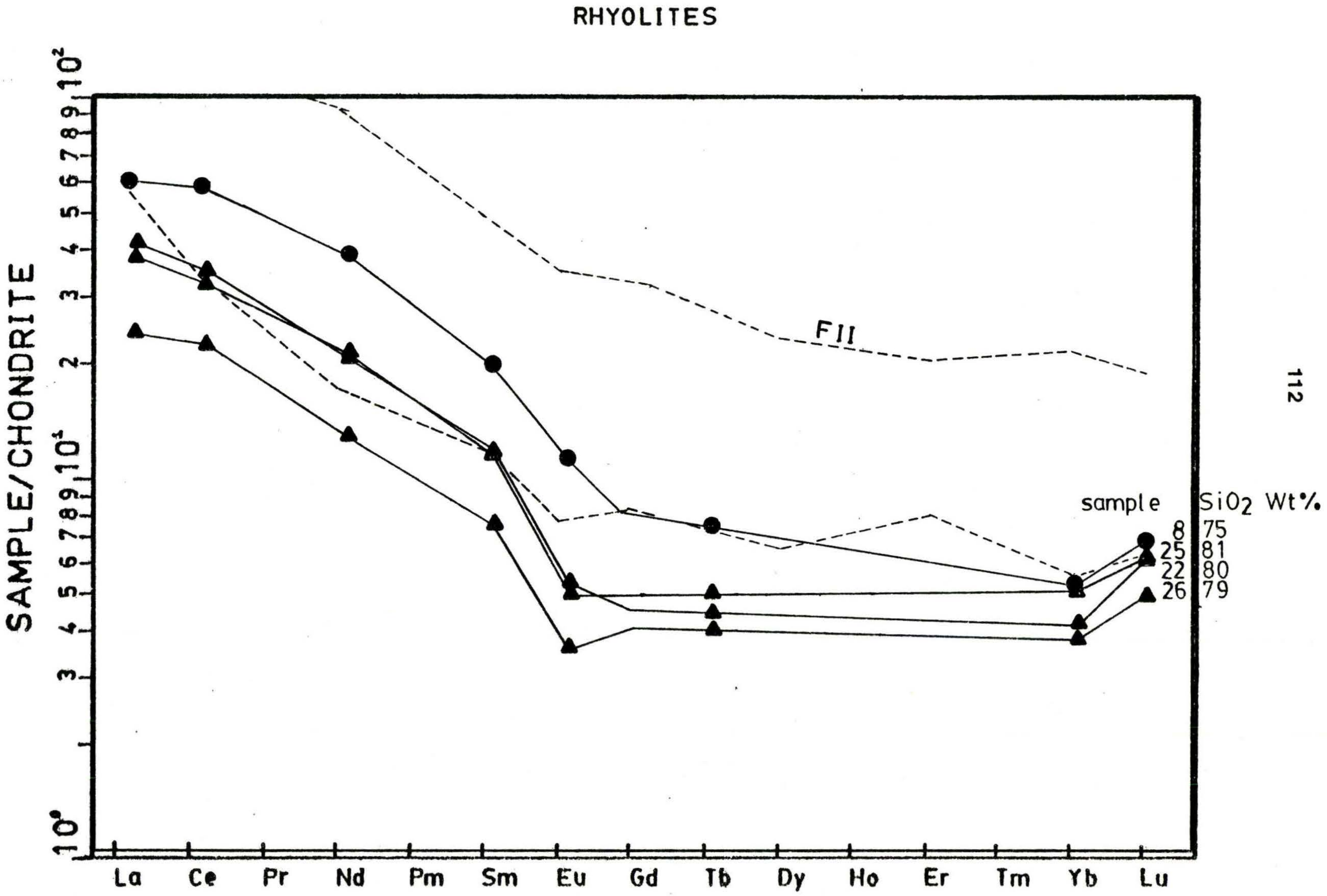

Figure 5-18.
CHONDRITE-NORMALIZED RARE EARTH ELEMENTS PATTERNS

RHYOLITES

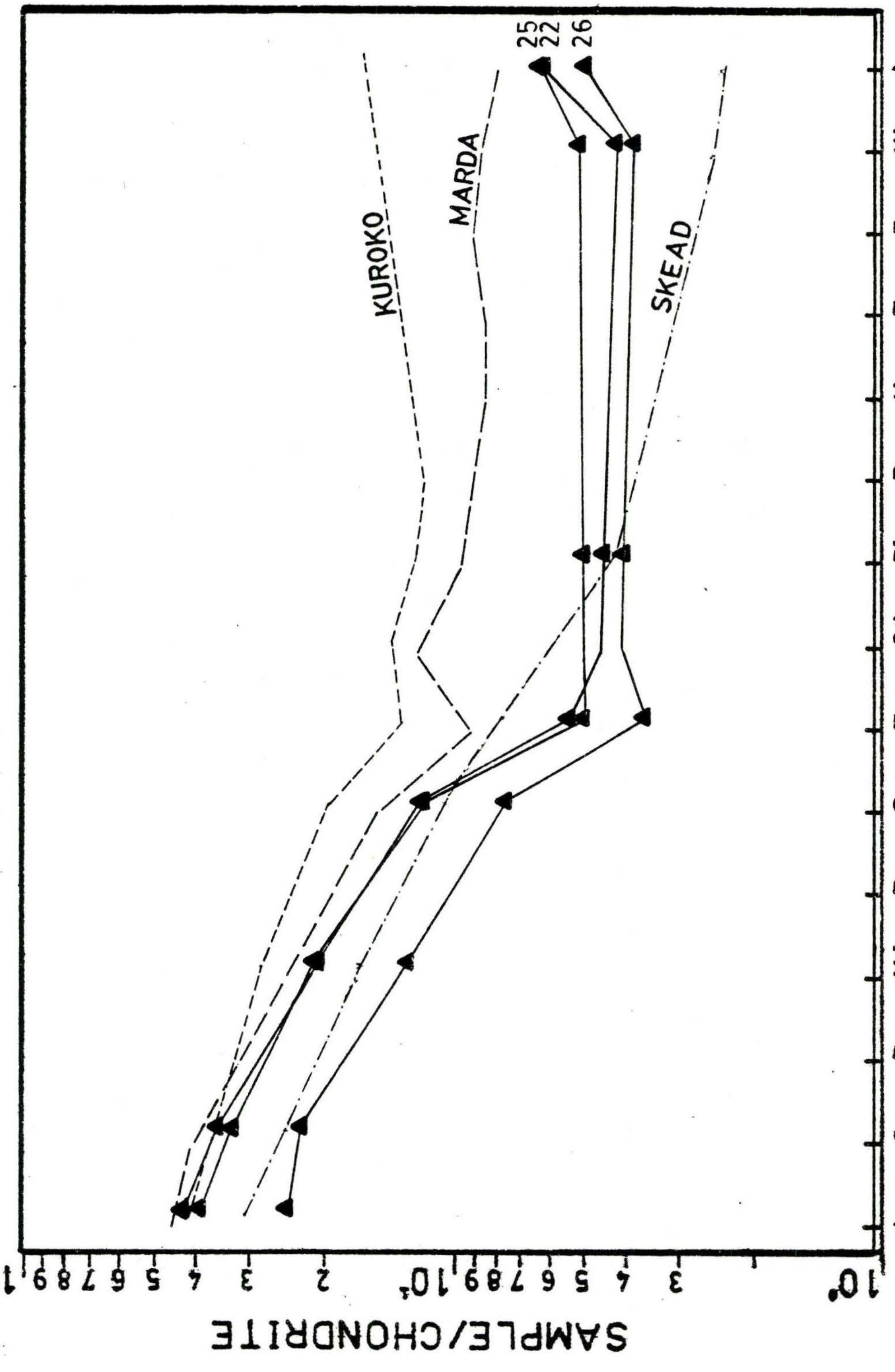

flatter LREE pattern and is also more enriched in overall REE. The Skead sample has a steeper HREE pattern compared to the rhyolites intrusives.

Archean Cu-Zn massive sulphide deposits are closely associated with felsic volcanism (Sopuck et al., 1980; Campbell et al., 1981; Franklin et al., 1981). Through the use of REE patterns it is possible to delineate most ore-bearing felsic volcanics from barren felsic volcanics (Campbell et al., 1981). According to Campbell et al., felsic volcanics associated with massive sulphides typically exhibit nearly flat REE patterns and negative Eu anomalies. Barren felsic volcanics exhibit steep REE patterns with or without weak Eu anomalies. The distinctive patterns of ore-bearing felsic volcanic rocks persist over the entire length of the ore-bearing stratigraphic unit, and are also refelected in underlying subvolcanic magma chambers which presumably feed the overlying volcanic sequence.

The felsic volcanics underlying the iron formation have not been analysed for REE. Hence it is important to study the patterns of the felsic intrusives in the event that they represent the high level magma chamber which gave rise to the felsic volcanics. Subvolcanic magma chambers are suspected to be the source rocks for the base and precious metals, and the "heat engines" that drive the ore-forming hydrothermal systems (Campbell et al., 1981). The REE patterns of the felsic intrusives of this study lie somewhere between the patterns for ore-bearing and barren felsic volcanics (Figure 5-18). The main difference from the ore-bearing patterns is the higher La/Lu ratios and fractionated LREE. Campbell et al. note that some volcanics hosting the Kidd Creek massive sulphide deposit do show LREE enrichment. Although the patterns of the Temagami felsic intrusives do not obviously indicate massive sulphide deposits, neither are they typical of barren felsic volcanics, and the possibility of sulphide mineralization occurring in the overlying felsic pyroclastics must not be disregarded.

5.4.3 Metals and Sulphur

Tables 5-2 and 5-3 are compilations of the arithmetic means ($\bar{x}$), standard deviations (s) and geometric means ($\overline{X}$) of the metal and sulphur contents in the thesis area volcanics and synvolcanic intrusives. Arithmetic means are recalculated where the population includes samples which deviate by more than 2σ from the mean. The use of 2σ as a population screen results in an arithmetic mean that compares very favourably with the geometric mean. The geometric mean is regarded as a good estimate of the population mean for data characterized by extreme skewness or exponential distribution (Moroney, 1951). Heavy metal lithogeochemical data is unfortunately prone to exhibit such strong skewness towards high values.

The samples are subdivided according to rock type (basalt to rhyolite) and irruptive mode (flows, pyroclastics and intrusives). Metal and sulphur contents of flows and pyroclastics are highly variable within each rock type. Less variation is noted between the flows and intrusives of the calc-alkaline rhyolites. The intrusives host minor disseminated sulphide which accounts for the higher As and S averages. Due to the small population of only 3 samples, low significance is placed on the geometric means of metals in the calc-alkaline basalts. While Cr, Ni, Cu and Zn are relatively constant between samples, the geometric means of S, Au, As and Sb are largely affected by sample 34, a pyritized mafic pyroclastic. The geometric means of the metal and sulphur contents in each rock type are presented in bar graphs (Figures 5-19 and 5-20).

5.4.3.1 Cr, Ni, Cu, Zn and S

A general decrease in Cr, Ni, Cu, Zn and S is noted from mafic to felsic rocks of the thesis area (Table 5-2, Figure 5-19). The decrease in Cr, Ni, Cu and Zn with increasing felsic differentiation is typical of Archean greenstone belts (Condie, 1981). Average S contents are reported to decrease with average FeO contents in Archean greenstone belts (Naldrett et al., 1978).

The Cr, Ni, Cu and Zn means are compared with average values from other Archean areas (Figure 5-19). To be consistent, comparisons are made using the same examples as in Table 5-1. A few general points can be made in this comparison.

The thesis area volcanics are notably enriched in Cr with respect to other Archean examples, and this enrichment increases in magnitude toward the felsic end members. Although the average Cr content of a tholeiitic basalt from the Eastern Goldfields region is higher than at Temagami, a lower average of 218 ppm has been reported for the tholeiitic mafic basalts from the Abitibi belt (Jolly, 1975). For comparison, Cr averages 501 ppm in the Temagami tholeiites.

Nickel contents of the intermediate to mafic volcanics at Temagami are lower than other Archean examples. The nickel contents of all the volcanics are considerably lower than the average values for equivalent rock types of the Abitibi belt presented by Jolly (1975). Mafic volcanics differ by a factor of two, and the felsic end members are lower by a factor of five.

Copper averages are notably lower in the thesis area compared to the other Archean examples. In contrast, Zn averages are all higher.

The high Cr contents at Temagami are not dependent on rock type, and are probably a characteristic of either the mantle source or the magma generation processes in the source region, rather than a product of fractionation processes in the magma chamber.

The difference in the average values of Ni, Cu and Zn at Temagami with other Archean areas may be explained in terms of secondary processes in the crustal environment. Lower Ni and Cu values could imply a selective leaching of these elements, while Zn appears to have been selectively enriched. Ellis (1968) demonstrated experimentally that at temperatures of 400 °C or more, sodium chloride solutions are capable of leaching over 80 percent of the Cu content of andesite. Bischoff and Dickson

TABLE 5-2. Cr, Ni, Cu and Zn contents in the Temagami volcanics and synvolcanic intrusives.

Rock Type	Description	N	Cr ppm		Ni ppm		Cu ppm		Zn ppm	
			$\bar{x}$ s	$\bar{X}$	$\bar{x}$ s	$\bar{X}$	$\bar{x}$ s	$\bar{X}$	$\bar{x}$ s	$\bar{X}$
THOLEIITIC		10	297±224	236	82±26	77	69±52	39	195±81	182
BASALTS		*	242±150						174±52	
	Flows	4	501±220	467	75±41	66	41±62	14	238±116	217
	Pyroclastics	6	161±75	150	87±11	86	88±39	77	166±35	163
CALC-ALKALINE BASALTS		3	307±65	303	82±25	79	76±6	76	206±168	167
	Flows	2	273±35	271	83±35	79	76±8	76	110±26	108
	Pyroclastics	1		376		80		77		399
CALC-ALKALINE ANDESITES	Flows	19	236±202	204	59±54	48	21±17	15	95±33	90
		*	192±51		48±27		18±12		90±26	
CALC-ALKALINE		11	83±25	80	17±4	17	47±97	16	83±52	75
DACITES		*			16±3		18±20		68±16	
	Flows	1		40		17		44		232
	Pyroclastics	10	88±21	85	17±4	17	47±103	14	68±16	67
		*			16±3		15±19			
CALC-ALKALINE		8	51±33	39	15±14	11		1	25±17	22
RHYOLITES		*			10±5				20±8	
	Flows	2	46±42	35	13±6	12		0	22±11	20
	Intrusives	6	53±33	41	16±17	11		2	27±19	22
		*			9±6					

$\bar{x}$ = arithmetic mean
$\bar{X}$ = geometric mean
s = standard deviation
N = number of samples
* excludes samples more than 2σ greater than the arithmetic mean

FIGURE 5-19. Geometric means of the Cr, Ni, Cu and Zn contents in the Temagami volcanics and synvolcanic intrusives, and comparison with average values from other Archean examples:-

1. Eastern Goldfields Region (Hallberg, 1972).
2. Abitibi belt (Goodwin, 1979).
3. Marda Complex (Hallberg et al., 1976).
4. Marda Complex (Hallberg et al., 1976).
5. Marda Complex (Hallberg et al., 1976).

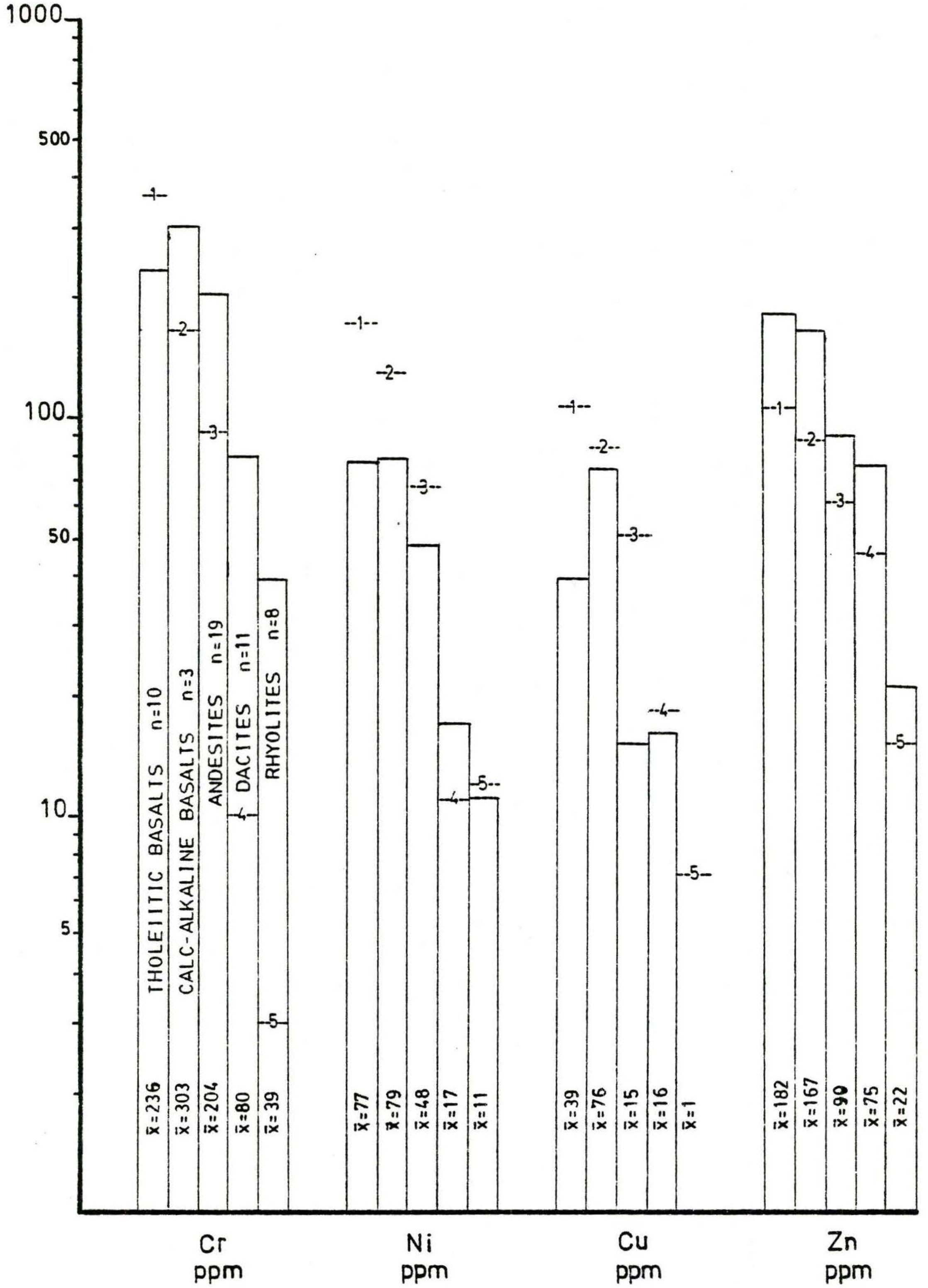
1000
500
100
50
10
5
THOLEIITIC BASALTS n=10
CALC-ALKALINE BASALTS n=3
ANDESITES n=19
DACITES n=11
RHYOLITES n=8
x̄=236
x̄=303
x̄=204
x̄=80
x̄=39
x̄=77
x̄=79
x̄=48
x̄=17
x̄=11
x̄=39
x̄=76
x̄=15
x̄=16
x̄=1
x̄=182
x̄=167
x̄=90
x̄=75
x̄=22
-1-
-2-
-3-
-4-
-5-
Cr ppm
Ni ppm
Cu ppm
Zn ppm

(1975) concluded that Cu and Ni are solubilized during basalt-seawater interaction at 200°C. The low Cu and Ni averages in the thesis area may be related to the apparent depletion of Na and Ca in the region, in that all of these elements were leached from the rocks during hydrothermal seawater circulation.

From a regional lithogeochemical study of the Abitibi belt, Sopuck et al. (1980) concluded that the local metasomatism in felsic volcanics associated with Cu-Zn deposits was also reflected on a regional scale. According to them, the dominant features on a mine scale are Fe and Mg enrichment, and Na and Ca depletion. Zinc and Mn are also depleted in the highly altered chlorite-sericite schist zones which represent points of high heat flow of hydrothermal fluids. On a regional scale, the felsic host rocks are enriched in Fe, Zn and Mn, and depleted in Na (Sopuck et al., 1980). Although a depletion in Cu and Ni on a regional scale was not reported by them, their data indicate that the mean Ni contents are less than 11 ppm in the felsic host rocks to productive ore-bearing cycles, while Ni contents of unproductive cycles are greater than 11 ppm. A similar depletion in Cu content is not evident.

5.4.3.2 Au, As, and Sb

The arithmetic and geometric means of Au, As, and Sb for each rock type are presented in Table 5-3, and geometric means for each element are shown graphically in Figure 5-20.

Arsenic contents of the thesis area volcanics are highest in the basalts (3.9 ppm) and low but variable in the intermediate to felsic rocks (andesites 1.1 ppm, dacites 0.75 ppm, rhyolites 1.6 ppm). This contrasts with the average As contents of igneous rock types based on a literature survey by Onishi (1974) that indicate an increase in As from basalts (1.5 ppm) to andesites, dacites (2.1 ppm) and rhyolites (3.5 ppm).

Antimony averages in the thesis area volcanics are generally high and decrease from the mafic (0.99 ppm) to felsic (0.21 ppm) volcanics. The average Sb contents of igneous rocks are 0.1 to 0.2 ppm for basalts, and 0.2 ppm for intermediate and felsic rocks (Onishi, 1974).

The average Au contents in the volcanics at Temagami are quite variable between rock types. The highest Au average (4.9 ppb) is found in the dacites. Crocket (1974) concluded that Au generally decreases from mafic to felsic volcanics. He noted; however, that there are examples of high quality, large volume (number of samples) surveys in specific geographic regions where no difference in the Au content of basalt, andesite, dacite and rhyolite occur. The average Au contents of volcanic rocks reported by Crocket (1974) are 3.6 ppb for the mafic to intermediate rocks and 1.5 ppb for the felsic rocks. In comparison, the dacites and rhyolites at Temagami are slightly enriched with Au averages of 4.9 ppb and 2.6 ppb respectively. Background Au abundances noted for the Kakagi Lake area in the Wabigoon greenstone belt (Kwong and Crocket, 1978) are also lower than at Temagami with Au averages of 1.75 ppb for the mafic volcanics and

TABLE 5-3. S, Au, As and Sb contents in the Temagami volcanics and synvolcanic intrusives.

			S ppm		As ppm		Sb ppm		Au ppb	
Rock Type	Description	N	$\bar{x}$ s	$\bar{X}$	$\bar{x}$ s	$\bar{X}$	$\bar{x}$ s	$\bar{X}$	$\bar{x}$ s	$\bar{X}$
THOLEIITIC		10	1295±2149	669	8.8±11.4	3.9	.69±2.6	.64	6.1±6.6	3.8
BASALTS		*	628±435		5.8±6.8				4.1±2.5	
	Flows	4	350±58	346	17.9±13.9	11.4	.69±.19	.67	2.7±2.0	2.2
	Pyroclastics	6	1925±2669	1038	2.7±2.6	1.9	.69±.31	.62	8.3±7.8	5.5
		*	850±487							
CALC-ALKALINE		3	3367±5052	1225	14.2±21.9	3.9	4.3±6.9	.99	2.4±2.0	1.9
BASALTS		*	450±71							
	Flows	2	450±71	447	1.5±1.2	1.2	.31±.18	.28	1.3±0.8	1.3
	Pyroclastics	1		9200		39.5		12.3		4.6
CALC-ALKALINE										
ANDESITES	Flows	19	404±383	241	1.2±.45	1.1	.42±.20	.38	3.5±2.5	2.6
		*	343±283				.40±.15		3.2±2.2	
CALC-ALKALINE		11	1653±4470	162	2.4±3.8	.75	.53±.24	.48	5.5±3.0	4.9
DACITES		*	247±508		1.4±1.9				4.8±1.8	
	Flows	1		14300		5.6		.48		13.0
	Pyroclastics	10	443±782	134	2.1±3.8	.61	.54±.26	.49	4.8±1.8	4.5
		*	247±508		.92±1.3					
CALC-ALKALINE		8	311±334	189	3.5±4.7	1.6	.38±.58	.21	4.0±3.2	2.6
RHYOLITES		*	213±199		2.0±1.9		.18±.09			
	Flows	2	89±16	88	.35±.19	.32	.21±.06	.21	2.6±1.8	2.8
	Intrusives	6	386±360	244	4.6±5.1	2.8	.44±.67	.22	4.5±3.6	2.8
		*					.16±.10			

$\bar{x}$ = arithmetic mean
$\bar{X}$ = geometric mean
s = standard deviation
N = number of samples
* excludes samples more than 2σ greater than the arithmetic mean

FIGURE 5-20. Geometric means of the S, Au, As and Sb contents in the Temagami volcanics and synvolcanic intrusives.

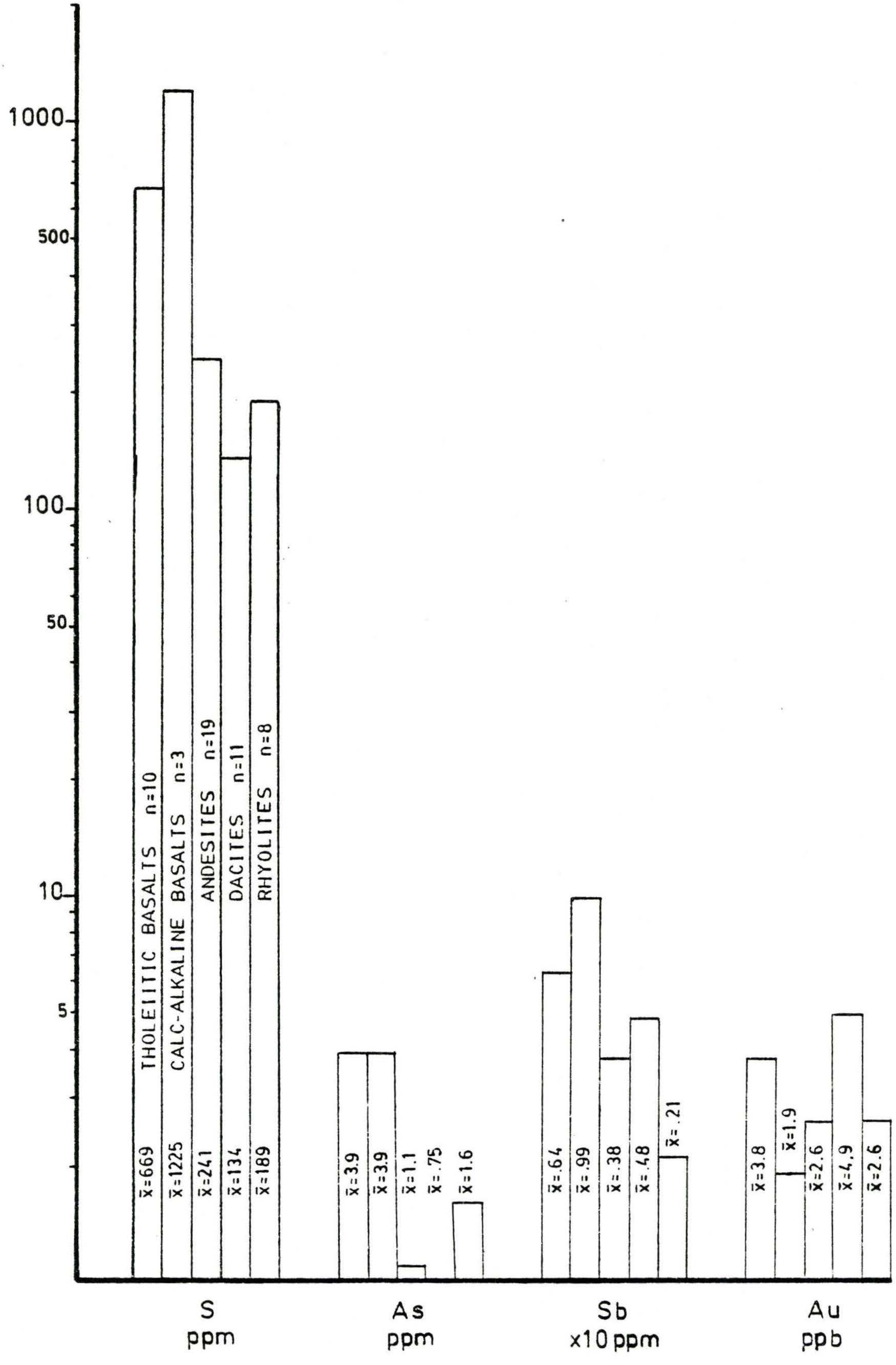
1000
500
100
50
10
5
THOLEIITIC BASALTS n=10
CALC-ALKALINE BASALTS n=3
ANDESITES n=19
DACITES n=11
RHYOLITES n=8
x̄=669
x̄=1225
x̄=241
x̄=134
x̄=189
x̄=3.9
x̄=3.9
x̄=1.1
x̄=.75
x̄=1.6
x̄=.64
x̄=.99
x̄=.38
x̄=.48
x̄=.21
x̄=3.8
x̄=1.9
x̄=2.6
x̄=4.9
x̄=2.6
S
ppm
As
ppm
Sb
x10 ppm
Au
ppb

1.47 ppb for the felsic volcanics. These averages; however, apply to populations which have been screened for any samples showing evidence of alteration, structural disturbance and mineralization.

Massive sulphide samples (TDH 178 and 182) taken from the stratigraphic base of the West Pit carry high Au (69 and 24 ppb), high As (184 and 192 ppm) and high Sb (15 and 6 ppm) contents. The host rocks to the massive sulphides are fine-grained felsic tuffs and graphitic sediments. The sulphide-poor felsic pyroclastics footwall to the West Pit (TDH 60-67) carry weakly anomalous Au (4.6 ppb), As (2.3 ppm) and Sb (4.4 ppm) contents.

CHAPTER 6

SUMMARY AND CONCLUSIONS

6.1 VOLCANOLOGICAL INTERPRETATION

A volcanological interpretation of a section only 1.5 by 5.5 km in area must be regarded with caution. However, it may be possible to classify the area as central, proximal or distal with respect to the distance from a large central vent. Criteria for the recognition of central, proximal and distal facies are taken from Williams and McBirney (1979).

Central facies rocks are located within about 0.5 to 2 km of a central vent. Central vent areas are characterized by lithologic diversity and pervasive hydrothermal alteration. Other features of the facies include the presence of:- intrusive sills and radially or randomly oriented dykes; breccia pipes and stocks; thick banded siliceous lavas; coarsely stratified but poorly sorted tephra layers; and thin lava flows volumetrically subordinate to fragmental ejecta. Although rhyolite flows do not travel far from their feeders, (1-2 km), siliceous domes are not restricted to summits of large volcanoes, but may emerge farther down on the slopes of composite cones.

Proximal facies rocks are located up to 5 to 15 km from central vents. The proximal zone is characterized by broad thick lavas, lahars containing blocks up to 10 metres in diameter, well sorted tephra layers, rewoked clastic debris and ignimbrites.

Distal facies rocks are located more than 5 to 15 km from the central vent. The distal zone is composed of finely layered ash trephra, lahars containing blocks up to 1 metre in diameter, ignimbrites, lava flows restricted to isolated vents, and interlayered shallow water sediments, soils and organic debris.

The volcanic section lying north of Vermillion Lake is characterized by very poor lateral continuity, thin discontinuous flows and flow breccias, coarsely stratified and poorly sorted pyroclastics, many randomly oriented mafic and felsic intrusives, flow laminated siliceous lava, and small pyroclastic debris flows. Of the three facies previously described, the section most closely resembles the central facies; that is, rocks located within 0.5 to 2 km of a central vent.

According to Bennett (1978) the iron formation overlying this section, (south of Vermillion Lake), is composed of small, discontinuous pyrite- and pyrrhotite-rich beds. The iron formation thickens to the west and can be traced for at least 10 km west of O'Conner Lake. In the West Pit the immediate host rocks of the iron formation are coarse felsic tuffs to fine ash tuffs, cherts and graphitic sediments. With respect to the three facies described by Williams and McBirney (1979) these rocks best represent the distal facies.

The lateral distance separating the inferred felsic intrusive center north of Vermillion Lake from the North Pit iron formation is less than 2 km. The relative proximity of the apparent central facies volcanics in the section lying north of Vermillion Lake to the more distal facies rocks which host the iron formation, may be explained in terms of a composite cone. The volcanic section lying north of Vermillion Lake may be in part derived from a small eruptive center or parasitic cone located on the flank of a much larger volcano. The presence of a rhyolite flow and a highly siliceous felsic intrusive center supports a focus of volcanism in the immediate area.

6.2 GEOCHEMICAL INTERPRETATION

The 1.5 km wide volcanic section underlying the north band of iron formation at Temagami is composed largely of calc-alkaline andesites, dacites and rhyolites, with subordinate intercalated tholeiitic and calc-alkaline basalts.

Various degrees of chloritization, carbonatization and silicification reflect hydrothermal alteration of the volcanic pile. The alteration has affected the whole rock chemistry of the volcanics and is a major contributing factor to discrepancies noted in various chemical rock classifications. The rock classification used in this study is based on several cation and trace element plots, as well as on detailed petrography.

The volcanics contain anomalously low Cu and Ni contents, and are notably depleted in Na. It is suggested that these elements were leached from the rocks during hydrothermal seawater circulation.

The REE patterns of the calc-alkaline andesites, dacites and rhyolites are unique compared to the average patterns presented for Archean rocks. A similarity in the whole rock chemistry and REE patterns exists between the Temagami volcanics and the Marda Complex volcanics of western Australia. A similar tectonic setting between the Marda Complex and the Temagami greenstone belt is inferred from this similarity. The Marda volcanics are considered by Taylor and Hallberg (1977) to be analogous with a continental margin (Andean) calc-alkaline volcanic suite. Evidence of hydrothermal seawater circulation in the Temagami volcanics suggests some separation of the volcanism from a continental margin, perhaps by a small ocean basin.

REFERENCES CITED

Abbey, S., 1977. Studies in standard samples for use in the general analysis of silicate rocks and minerals. GSC Paper 77-34, Pt. 5. Edition of usuable values, 31p.

Baker, P.E., 1968b. Petrology of Mt. Misery volcano, St. Kitts, West Indies. Lithos 1, pp.124-150.

Barlow, A.E., 1897. Report on the geology and natural resources of the area included by Nipissing and Temiskaming Map Sheets. GSC X, Pt. 1, 302p.

Bennett, G., 1978. Geology of the Northeast Temagami Area. O.G.S. Rpt. 163, 116p.

Bischoff, J.L. and Dickson, F.W., 1975. Seawater-basalt interaction at 200 C and 500 bars: Implications for origin of sea-floor heavy-metal deposits and regulation of seawater chemistry. Earth Planet. Sci. Let. 25, pp.385-397.

Blum, N., 1986. Geochemical, isotopic and petrological characterization of Archean banded iron formation and associated volcanics in the Kirkland Lake and Temagami areas. Unpub. Ph.D. thesis, McMaster University, Hamilton, Ont.

Boyum, B.H. and Hartviksen, R.C., 1970. General geology and ore grade control at the Sherman Mine, Temagami, Ontario. CIM Trans. 73, pp.267-276.

Campbell, G.J., 1978. Petrography and stratigraphy of the north band of iron formation, Sherman Mine, Temagami, Ontario. Unpub. M.Sc. thesis, Laurentian University, 75p.

Campbell, I.H., Coad, P., Franklin, J.M., Gorton, M.P., Hart, T.R., Scott, S.D., Sowa, J., and Thurston, P.C., 1981. Rare earth elements in felsic volcanic rocks associated with Cu-Zn massive sulphide mineralization. O.G.S. Misc. Paper 98, pp.45-53.

Coleman, A.P., 1900. Copper and iron regions of Ontario. OBM 9, pp.143-191.

Condie, K.C., 1976. Trace-element geochemistry of Archean greenstone belts. Earth Sci. Rev. 12, pp.393-417.

Condie, K.C., 1981. Archean Greenstone Belts. Elsevier, New York 381p.

Condie, K.C., 1982. Archean Andesites, in Andesites, ed. by R.S. Thorpe, John Wiley and Sons, Toronto, pp.575-590.

Crocket, J.H., 1974. Gold, in the Handbook of Geochemistry, vol. II/4. Springer-Verlag, New York. Section 79 B-O.

Crocket,J.H., McNutt, R.H., Schwarcz, H.P., Rees, C.E., Blum, N., Hurley, T., Bowins, R., and Kabir, A., 1983. Isotopic and geochemical characterization of Archean iron formations and associated volcanic rocks - Some preliminary results from the Temagami and Boston iron formations. O.G.S. Misc. Paper 113, pp.29-40.

Crocket, J.H., Blum, N., Hurley, T., Bowins, R., McRoberts, G., Fyon, A., McNutt, R.H., Schwarcz, H.P., and Rees, C.E., 1984. Geological and geochemical studies of the Boston and Temagami iron formations and their contiguous volcanosedimentary piles. O.G.S. Misc. Paper 121, pp.72-83.

Davies, J.F. , Grant, R.W.E., and Whitehead, R.E.S., 1978. Immobile trace elements and Archean volcanic stratigraphy in the Timmins mining area, Ontario. Can. J. Earth Sci. 16, pp.305-311.

Dimroth, E., 1977. Archean subaqueous autoclastic volcanic rocks, Rouyn-Noranda area, Quebec: Classification, diagnosis and interpretation. G.S.C. Paper 77-1A, pp.513-522.

Dimroth, E., Cousineau, P., Leduc, M., Sanschagrin, Y. and Provost, G., 1979. Flow mechanisms of Archean subaqueous basalt and rhyolite flows, in Current Research, Part A, G.S.C. Paper 79-1A, pp.207-211.

Dimroth, E. and Lichtblau, A.P., 1979. Metamorphic evolution of Archean hyaloclastites, Noranda area, Quebec, Canada. Part I: Comparison of Archean and Cenozoic sea-floor metamorphism. Can. J. Earth Sci. 16, pp.1315-1340.

Dimroth, E. and Rocheleau, M., 1979. Volcanology and sedimentology of Rouyn-Noranda area, Quebec. G.A.C., Ann. Mtg., Quebec, Guidebook, Fieldtrip A-1, 193p.

Dostal, J. and Strong, D.F., 1983. Trace-element mobility during low-grade metamorphism and silicification of basaltic rocks from Saint John, New Brunswick. Can. J. Earth Sci. 20, pp.431-435.

Downie, I.F., 1963. Report on geological mapping and exploration: Doris Lake Group, Strathy Township, Ontario for Keevil Consultants Ltd. Unpub. Rpt. 419T, Asses. Files, M.N.R. (Geol.) Cobalt, Ontario. 10p.

Ellis, A.J., 1968. Natural hydrothermal systems and experimental hot-water/rock interaction: Reactions with NaCl solutions and trace metal extraction. Geochim. Cosmochim. Acta 32, pp.1356-1363.

Fisher, R.V., 1966. Rocks composed of volcanic fragments and their classification. Earth Sci. Rev. 1, pp.287-298.

Floyd, P.A. and Winchester, J.A., 1978. Identification and discrimination of altered and metamorphosed volcanic rocks using immobile elements. Chem. Geol. 21, pp.291-306.

Franklin, J.M., Lydon, J.W., and Sangster, D.F., 1981. Volcanic-associated massive sulphide deposits. Econ. Geol. 75th Anniv. Vol., pp.485-627.

Fyon, J.A., 1980. Seawater alteration of Early Precambrian (Archean) volcanic rock and exploration criteria for stratiform gold deposits, Porcupine Camp, Abitibi Greenstone Belt, Northeastern Ontario. Unpub. M.Sc. thesis, McMaster University, Hamilton, Ont., 238p.

Gelinas, L., Mellinger, M. and Trudel, P., 1982. Archean mafic metavolcanics from the Rouyn - Noranda district, Abitibi Greenstone Belt, Quebec. 1. Mobility of the major elements. Can. J. Earth Sci. 19, pp.2258-2275.

Gibson, H.L., Watkinson, D.H. and Comba, C.D., 1983. Silicification: Hydrothermal alteration in an Archean geothermal system within the Amulet Rhyolite Formation, Noranda, Quebec. Econ. Geol. 78, pp.954-971.

Goodwin, A.M., 1977. Archean volcanism in Superior Province, Canadian Shield. In Volcanic Regimes in Canada, ed. by W.R.A. Baragar, L.C. Coleman and J.M. Hall. Geol. Assoc. Can. Special Paper 16, pp.205-242.

Goodwin, A.M., 1979. Archean volcanic studies in the Timmins - Kirkland Lake - Noranda region of Ontario and Quebec. G.S.C. Bull. 278, 51p.

Green, T.H. and Ringwood, A.E., 1968. Genesis of the calc-alkaline igneous rock suite. Contr. Mineral. Petrol. 18, pp.105-162.

Hallberg, J.A., 1972. Geochemistry of Archean volcanic belts in the Eastern Goldfields Region of Western Australia J. of Petrology 13, P.1 pp.45-56.

Hallberg, J.A., Johnston, C., and Bye, S.M., 1976. The Archean Marda Igneous Complex, Western Australia. Pre-Cambrian Research 3, pp.111-136.

Haskin,L.A., Wilderman, T.R. and Haskin, M.A., 1968. An accurate procedure for determination of the rare-earth elements by neutron-activation: J. Radioanal. Chem., v. 1, pp.337-348.

Hellman, P.L., Smith, R.E., and Henderson, P., 1979. The mobility of the rare earth elements: evidence and implications from selected terrains affected by burial metamorphism. Cont. Pet. Min. 71, pp.23-44.

Humphris & Thompson 1978.

Hutchinson, C.S., 1974. Laboratory Handbook of Petrographic Techniques. John Wiley and Sons, New York, pp.264-282.

Irvine, T.N. and Baragar, W.R.A., 1971. A guide to the chemical classification of the common volcanic rocks. Can. J. Earth Sci. 8, pp.523-548.

Jakes, P. and White, A.J.R., 1971. Composition of island arcs and continental growth. Earth Planet. Sci. Let. 12 pp.224-230.

Jensen, L.S., 1976. A new cation plot for classifying subalkalic volcanic rocks. Misc. Paper 66, 20p.

Jolly, W.T., 1975. Subdivision of the Archean lavas of the Abitibi area, Canada, from Fe-Mg-Ni-Cr relations. Earth Planet. Sci. Let. 27, pp.200-210.

Kerrich, R. and Fryer, B.J., 1979. Archean precious-metal hydrothermal systems, Dome Mine, Abitibi Greenstone Belt. II. REE and oxygen isotope relations. Can. J. Earth Sci. 16, pp.440-458.

Kerrich, R., Fryer, B.J., Milner, K.J., and Pierce, M.G., 1981. The geochemistry of gold-bearing chemical sediments, Dickenson Mine, Red Lake, Ontario: a reconnaissance study. Can. J. Earth Sci. 18, pp.624-637.

Kwong, Y.T.J. and Crocket, J.H., 1978. Background and anomalous gold in rocks of an Archean greenstone assemblage, Kakagi Lake area, northwestern Ontario. Econ. Geol. 73, pp.50-63.

Ludden, J., Gelinas, L. and Trudel, P., 1982. Archean metavolcanics from the Rouyn - Noranda district, Abitibi Greenstone Belt, Quebec. 2. Mobility of trace elements and petrogenetic constraints. Can. J. Earth Sci. 19, pp.2276-2287.

MacGeehan, P.J., 1978. The geochemistry of altered volcanic rocks at Matagami, Quebec: a geothermal model for massive sulphide genesis. Can. J. Earth Sci. 15, pp.551-570.

Marchand ,M., 1973. Determination of Rb, Sr, and Rb/Sr by XRF. Technical Memo 73-2, Dept. of Geology, McMaster University, Hamilton, Ont.

Menzies, M., Seyfried, W.E., and Blanchard, D., 1979. Experimental evidence of rare earth immobility in greenstones. Nature 282, pp.398-399.

Miller, W.G., 1901. Iron ores of Nipissing district. OBM 10, pp.160-180.

Miller, C.F. and Mittlefehldt, D.W., 1982. Depletion of light rare-earth elements in felsic magmas. Geology 10, pp.129-133.

Moroney, M.J., 1951. Facts From Figures. Penguin Books, New York, 472p.

Moorehouse, W.W., 1942. The Northeastern portion of the Timagami Lake Area. ODM 51, Pt. 6, 42p.

Naldrett, A.J., Goodwin, A.M., and Fisher, T.L., 1978. The sulphur content of Archean volcanic rocks and a comparison with ocean floor basalts. Can. J. Earth Sci. 15, pp.715-728.

Nockolds, S.R., Knox, O.W.O'B., and Chinner, G.A., 1978. Petrology For Students. Cambridge University Press London, 426p.

Onishi, H., 1974. Arsenic, in the Handbook of Geochemistry, Vol. II/3. Springer-Verlag, New York. Section 33, B-M.

Onishi, H., 1974. Antimony, in the Handbook of Geochemistry, Vol. II/4. Springer-Verlag, New York. Section 51, B-M.

Parsons, W.H., 1969. Criteria for the recognition of volcanic breccias: Review. G.S.A. Memoir 115, pp.263-300.

Pichler, H., 1965. Acid hyaloclastites. Bull. Volcanol. 28, pp. 293-310.

Roberts, R.G. and Reading, D.J., 1981. Volcanic-tectonic setting of gold deposits in the Timmins district - carbonate-bearing rocks at Dome Mine. O.G.S. Misc. Paper 98, pp.222-228.

Savage,W.S., 1935. Part of Strathy Township. ODM 44, Pt. 7, pp.48-56.

Shaw, D.M., 1968. A review of K-Rb fractionation trends by covariance analysis. Geochim. Cosmochim. Acta 32, pp.573-601.

Sopuck, V.J., Lavin, O.P., and Nichol, I., 1980. Lithogeochemistry as a guide to identifying favourable areas for the discovery of volcanogenic massive sulphide deposits. C.I.M. Bull. 73, pp.152-166.

Tasse, N. and Lajoie, J., 1978. The anatomy and interpretation of an Archean volcaniclastic sequence, Noranda region, Quebec. Can. J. Earth Sci. 15, pp.874-888.

Taylor, S.R. and Hallberg, J.A., 1977. Rare-earth elements in the Marda calc-alkaline suite: an Archean geochemical analogue of Andean-type volcanism. Geochim. Cosmochim. Acta 41, pp.1125-1130.

Tomblin, J.F., 1975. The Lesser Antilles and Aves Ridge, in The Ocean Basins and Margins, vol. 3. Ed. by A.E.M. Nairn and F.G. Stehli, Plenum Press, New York pp. 467-500.

Williams, H. and McBirney, A.R., 1979. Volcanology. Freeman, Cooper and Co., San Francisco, 397p.

Winchester, J.A. and Floyd, P.A., 1976. Geochemical magma type discrimination: Application to altered and metamorphosed basic igneous rocks. Earth Planet. Sci. Let. 28, pp.459-469.

Winchester, J.A. and Floyd, P.A., 1977. Geochemical discrimination of different magma series and their differentiation products using immobile elements. Chem. Geol. 20, pp.325-343.

Wright, A.E. and Bowes, D.R., 1963. Classification of volcanic breccia: A discussion. G.S.A. Bull. 74, pp.79-86.

APPENDIX A

MAJOR AND TRACE ELEMENT DATA FOR ALL SAMPLES

Sample Number	TDH 2	TDH 4	TDH 7	TDH 8	TDH 10	TDH 11	TDH 12A
			In weight %				
SiO2	52.58	76.64	62.89	74.78	59.32	61.06	44.72
Al2O3	10.50	10.93	15.80	11.29	14.05	15.88	12.35
Fe2O3	6.96	3.81	5.94	.95	6.24	6.30	15.84
MgO	7.33	1.75	5.45	1.23	2.67	4.71	4.98
CaO	8.58	.16	.21	1.89	6.32	1.47	10.30
Na2O	.76	.93	3.32	2.34	2.49	4.31	.99
K2O	.88	1.22	1.95	2.19	.59	.73	.06
TiO2	.55	.46	.76	.09	.67	.89	1.39
MnO	.13	.02	.06	.09	.10	.07	.21
P2O5	.22	.10	.15	.03	.14	.23	.08
CO2	11.81	.13	.07	2.78	4.69	.88	7.71
H2O**	3.04	2.58	3.51	1.35	2.88	3.05	3.38
Total	103.34	98.73	100.11	99.01	100.16	99.58	102.01
			In ppm				
S	99	110	<10	77	73	*.05	*.13
Cr	1045	106	134	76	177	335	119
Co	46	39	40	7	41	42	79
Cu	11	6	5	<3	8	45	80
Zn	119	69	83	30	98	106	135
V	96	67	130	4	112	176	308
Ni	253	26	64	17	41	49	73
Rb	12	19	41	50	9	9	5
Sr	364	122	58	85	183	158	95
Y	22	25	27	21	21	26	26
Zr	138	147	186	78	153	179	89
Nb	12	16	16	15	12	16	7
Ba	297	189	637	201	186	303	65
As	<2.0	2.4	<2.0	<2.0	<2.0	<2.0	3.3
Sb	.64	.53	.50	<.20	.37	.47	.63
K/Rb	609	533	395	364	544	673	100
Zr/TiO2	.025	.032	.025	.087	.023	.020	.006
Nb/Y	.546	.640	.593	.714	.571	.615	.269
			In ppb				
Au	4.9	5.5	8.9	3.8	4.5	5.7	6.7

Sample Number	TDH 12B	TDH 12C	TDH 13	TDH 14	TDH 15	TDH 16	TDH 18
				In weight %			
SiO2	48.14	43.37	45.58	47.66	62.83	46.90	57.64
Al2O3	14.37	15.53	12.52	13.91	14.70	13.70	14.45
Fe2O3	18.73	23.00	17.56	12.11	5.98	15.04	7.83
MgO	6.89	6.79	6.47	7.86	4.83	6.18	4.93
CaO	2.56	2.23	8.28	7.14	1.43	6.83	4.08
Na2O	<.20	<.20	<.20	1.46	2.98	.88	1.07
K2O	.56	.57	.21	.07	2.06	.25	1.22
TiO2	1.90	1.85	1.57	.84	.68	1.28	.68
MnO	.16	.15	.19	.19	.08	.20	.09
P2O5	.14	.15	.09	.04	.17	.09	.18
CO2	1.84	1.60	6.27	4.50	.97	4.94	5.53
H2O**	5.19	5.11	4.15	4.83	2.96	4.74	3.50
Total	100.48	100.35	102.89	100.61	99.67	101.03	101.20
				In ppm			
S	*.18	*.73	*.11	62	370	250	*.04
Cr	162	191	107	487	143	300	273
Co	113	144	91	77	37	88	51
Cu	60	21	73	50	20	130	33
Zn	176	205	169	115	100	127	119
V	429	460	339	247	107	313	132
Ni	85	90	75	218	28	96	117
Rb	5	7	5	5	38	5	18
Sr	32	28	65	118	99	98	166
Y	33	33	25	20	24	26	22
Zr	104	95	94	58	174	78	159
Nb	6	6	9	5	13	7	13
Ba	329	391	289	122	634	138	350
As	18.8	7.5	3.0	<2.0	<2.0	<2.0	<2.0
Sb	1.4	1.1	.56	.64	.39	.98	.51
K/Rb	930	676	349	116	450	415	562
Zr/TiO2	.010	.005	.006	.007	.026	.006	.023
Nb/Y	.182	.182	.360	.250	.542	.269	.571
				In ppb			
Au	9.2	23.6	6.2	3.0	3.9	6.2	7.0

Sample Number	TDH 22	TDH 25	TDH 26	TDH 27	TDH 28	TDH 29	TDH 30
				In weight %			
SiO_2	79.87	80.71	78.86	62.64	66.13	46.45	47.45
Al_2O_3	12.10	12.53	12.73	13.52	14.00	15.26	13.49
Fe_2O_3	.73	.32	.40	5.63	4.71	15.55	15.47
MgO	.57	.22	.15	4.50	4.70	10.61	6.24
CaO	.09	.07	.09	2.96	.95	2.88	6.42
Na_2O	1.10	1.27	1.24	2.34	.35	.39	2.32
K_2O	2.65	2.22	2.40	1.44	2.41	.05	.05
TiO_2	.07	.06	.06	.53	.53	.97	1.02
MnO	.02	.02	.01	.08	.07	.14	.20
P_2O_5	.02	.01	.01	.16	.13	.08	.07
CO_2	.19	.10	.05	4.02	1.24	2.07	4.77
H_2O**	2.07	1.85	1.95	2.89	3.49	6.95	3.77
Total	99.48	99.38	97.95	100.71	98.71	101.40	101.27
				In ppm			
S	*.10	160	53	87	240	79	*.12
Cr	99	60	80	173	177	591	137
Co	11	19	16	35	28	100	95
Cu	<3	<3	<3	15	18	14	114
Zn	20	17	20	87	83	202	148
V	<5	<5	<5	69	77	315	296
Ni	6	5	5	34	32	11	98
Rb	64	45	51	31	N.A.	5	5
Sr	85	102	91	74	N.A.	31	133
Y	21	23	16	20	N.A.	18	21
Zr	80 4:1	78 4:1	65 4:1	158	N.A.	59 3:1	76 3.6:1
Nb	18	19	14	14	N.A.	8	8
Ba	489	293	282	266	N.A.	76	73
As	5.5	2.9	2.7	<2.0	2.0	<2.0	<2.0
Sb	.33	<.20	<.20	.59	.59	.71	.67
K/Rb	344	410	391	386	--	83	83
Zr/TiO_2	.114	.130	.108	.030	--	.006	.008
Nb/Y	.857	.260	.875	.700	--	.444	.381
				In ppb			
Au	7.2	8.9	2.9	2.9	4.4	4.5	6.2

Sample Number	TDH 31	TDH 34	TDH 60	TDH 61	TDH 62	TDH 63	TDH 64
				In weight %			
SiO2	49.19	48.72	69.22	67.88	73.96	66.97	65.44
Al2O3	12.84	12.24	12.19	16.65	13.90	16.43	15.70
Fe2O3	18.11	7.03	2.05	3.36	2.25	3.82	7.72
MgO	5.37	5.21	1.71	1.79	1.41	2.65	1.38
CaO	7.86	11.91	2.21	2.55	2.70	1.64	1.55
Na2O	1.17	.20	.55	.29	.27	.55	.88
K2O	.06	2.06	.10	.60	.08	.93	.83
TiO2	1.42	.58	.23	.25	.19	.28	.73
MnO	.25	.24	.07	.15	.11	.14	.13
P2O5	.11	.25	.06	.05	.04	.07	.14
CO2	.16	12.29	.02	.07	.14	.11	.02
H2O**	N.A.	1.84	2.42	2.86	2.21	3.31	3.03
Total	96.54	102.57	90.83	96.50	97.26	96.90	97.55
				In ppm			
S	*.19	*.92	86	52	*.16	93	91
Cr	94	376	54	91	124	110	76
Co	98	23	<3	20	21	37	48
Cu	75	77	335	10	5	3	9
Zn	134	399	96	53	41	74	55
V	284	116	8	21	15	27	35
Ni	56	80	9	17	18	18	17
Rb	5	37	5	9	5	23	26
Sr	297	103	72	86	73	97	155
Y	32	26	18	16	17	19	35
Zr	103	99	131	131	107 6.3:1	134	317 10:1
Nb	4	12	15	10	12	15	23
Ba	109	515	48	90	28	128	N.A.
As	N.A.	39.5	<2.0	<2.0	3.7	<2.0	<2.0
Sb	N.A.	12.3	.58	.52	.22	.33	.47
K/Rb	100	462	166	553	133	336	265
Zr/TiO2	.007	.017	.057	.052	.056	.048	.043
Nb/Y	.125	.462	.833	.625	.706	.790	.657
				In ppb			
Au	N.A.	4.6	8.1	6.1	3.5	5.5	2.1

Sample Number	TDH 65	TDH 66	TDH 67	TDH 100	TDH 102	TDH 103	TDH 106
			In weight %				
SiO2	61.51	64.84	64.33	45.56	47.46	47.10	76.24
Al2O3	17.40	13.93	14.73	14.56	14.97	15.31	13.68
Fe2O3	10.52	10.06	11.46	11.09	19.83	9.87	.84
MgO	1.89	1.90	1.35	3.88	8.51	4.35	.06
CaO	1.47	.41	.22	10.09	2.75	12.61	5.00
Na2O	1.09	.30	<.20	.37	.20	.66	1.65
K2O	.58	2.14	.92	1.51	.05	1.47	1.81
TiO2	.84	.73	.79	.86	.74	.63	.22
MnO	.22	.18	.33	.25	.22	.21	.06
P2O5	.16	.13	.14	.15	.08	.17	.13
CO2	.00	.13	.04	7.96	3.48	9.74	3.72
H2O**	3.50	3.29	2.73	3.59	5.47	3.41	1.66
Total	99.18	98.04	97.04	99.87	103.76	105.53	105.07
			In ppm				
S	18	115	62	*.04	*.03	*.03	*.05
Cr	72	73	95	347	791	551	<10
Co	49	46	58	42	107	30	<3
Cu	12	14	12	4	133	24	<3
Zn	67	84	68	125	379	163	63
V	38	36	40	270	287	187	13
Ni	17	15	19	36	110	43	48
Rb	12	60	27	33	3	34	37
Sr	154	49	120	42	10	62	230
Y	45	32	45	19	14	14	19
Zr	353 7:1	335 10:1	358 7:1	54	44	47	194
Nb	28	28	29	9	8	10	17
Ba	75	558	129	323	41	121	457
As	<2.0	<2.0	<2.0	17.7	16.8	35.6	14.3
Sb	.51	.28	.93	.59	.85	.85	1.8
K/Rb	401	296	283	380	138	359	406
Zr/TiO2	.042	.046	.045	.006	.006	.008	.008
Nb/Y	.623	.875	.645	.474	.572	.715	.895
			In ppb				
Au	5.4	5.4	3.2	<2.0	3.4	5.3	6.7

Sample Number	TDH 110	TDH 116	TDH 120	TDH 123	TDH 124	TDH 130	TDH134
				In weight %			
SiO2	48.22	49.78	52.94	73.66	79.93	64.66	55.54
Al2O3	13.77	14.46	15.75	12.64	13.71	15.25	14.64
Fe2O3	15.33	16.60	8.68	5.34	.74	5.81	6.35
MgO	6.68	6.68	3.77	.34	.04	3.46	4.56
CaO	7.50	5.23	8.13	.49	.43	1.26	5.53
Na2O	.52	2.71	1.95	.92	1.93	3.34	2.08
K2O	.25	.03	1.00	1.56	2.67	1.53	1.17
TiO2	1.12	1.16	.97	.48	.11	.59	.71
MnO	.17	.25	.12	.05	.04	.07	.10
P2O5	.16	.16	.28	.13	.03	.16	.21
CO2	5.44	2.08	6.40	.56	.72	.88	7.42
H2O**	4.23	4.05	3.10	2.52	1.88	2.76	2.77
Total	103.39	103.19	103.09	98.69	102.23	99.77	101.08
				In ppm			
S	*.09	*.04	*.05	*.22	*.01	*.01	*.01
Cr	161	112	248	76	16	136	164
Co	83	95	42	38	4	32	39
Cu	102	112	82	65	<3	22	17
Zn	211	210	128	76	14	90	83
V	299	299	178	74	<5	102	108
Ni	106	90	58	17	9	34	116
Rb	<3	<3	20	31	68	34	30
Sr	53	129	171	126	90	58	194
Y	23	26	21	20	21	21	22
Zr	68	74	136	147	83	165	151
Nb	10	10	12	14	18	15	15
Ba	99	59	173	249	413	496	303
As	5.5	<2.0	2.4	12.4	<2.0	<2.0	<2.0
Sb	1.1	.22	<.20	1.0	.25	.24	<.20
K/Rb	692	83	415	418	326	374	324
Zr/TiO2	.006	.006	.014	.031	.076	.028	.021
Nb/Y	.435	.385	.571	.70	.857	.714	.682
				In ppb			
Au	2.6	<2.0	<2.0	3.1	<2.0	2.1	<2.0

Sample Number	TDH 137	TDH 138	TDH 139	TDH 141	TDH 145	TDH 146	TDH 150
				In weight %			
SiO2	47.48	52.26	74.34	61.82	98.31	60.01	65.21
Al2O3	13.00	14.25	12.00	15.20	.51	14.24	14.54
Fe2O3	15.44	9.19	2.89	7.72	<.20	5.80	4.64
MgO	5.77	5.46	.23	2.81	<.05	2.27	1.97
CaO	7.33	5.99	1.68	1.77	.23	6.20	4.02
Na2O	2.27	3.73	1.18	3.10	<.20	2.42	1.88
K2O	<.05	<.05	1.94	1.23	.05	2.03	2.28
TiO2	.87	.95	.09	.74	.01	.70	.74
MnO	.27	.16	.08	.08	.02	.14	.08
P2O5	.21	.19	.05	.17	<.01	.28	.24
CO2	4.58	4.23	2.43	1.28	.35	8.05	4.66
H2O**	2.98	3.09	.17	2.75	.00	1.65	1.79
Total	100.20	99.50	97.08	98.67	99.48	103.79	102.05
				In ppm			
S	*.01	*.04	*.05	*.1	*.04	*.04	*.04
Cr	276	297	39	175	10	177	231
Co	69	42	27	40	73	21	23
Cu	14	70	6	73	<3	18	45
Zn	116	91	30	155	<5	61	46
V	201	212	12	123	<5	91	112
Ni	117	107	18	43	9	37	46
Rb	<3	<3	48	31	<3	45	50
Sr	107	166	92	73	11	213	130
Y	18	20	17	23	11	21	22
Zr	89	103	80	162	20	154	148
Nb	9	11	16	15	16	14	14
Ba	57	341	276	316	20	385	393
As	<2.0	<2.0	<2.0	<2.0	<2.0	<2.0	<2.0
Sb	<.20	.44	<.20	<.20	.25	.53	.25
K/Rb	138	138	335	329	--	374	378
Zr/TiO2	.010	.011	.089	.022	--	.022	.020
Nb/Y	.500	.550	.941	.652	--	.667	.636
				In ppb			
Au	<2.0	<2.0	<2.0	<2.0	2.5	<2.0	2.8

Sample Number	TDH 151	TDH 154	TDH 155	TDH 158	TDH 159	TDH 160	TDH 161
				In weight %			
SiO2	66.34	70.19	46.69	81.69	61.17	46.90	52.37
Al2O3	12.15	14.09	14.00	13.23	14.73	15.54	13.55
Fe2O3	7.41	5.48	14.06	.65	7.01	15.96	8.81
MgO	2.02	.09	5.67	<.05	2.39	3.68	7.38
CaO	1.23	5.84	8.27	.08	3.44	7.83	6.73
Na2O	.83	3.38	.75	1.28	1.84	3.79	4.69
K2O	1.95	.88	.40	2.44	1.18	1.67	.32
TiO2	.37	.70	1.04	.03	.74	3.49	.74
MnO	.11	.13	.10	.02	.13	.23	.12
P2O5	.09	.23	.17	.02	.20	1.16	.34
CO2	1.71	7.27	6.17	.21	3.71	.28	.25
H2O**	2.71	2.06	4.69	1.90	3.17	.06	2.06
Total	96.92	110.34	102.01	101.55	99.71	100.59	97.36
				In ppm			
S	*1.3	*.01	*.04	*.01	*.07	*.23	*.22
Cr	300	194	314	31	209	<10	399
Co	32	23	76	5	30	58	45
Cu	82	4	3	<3	<3	45	7
Zn	207	80	285	9	93	153	44
V	75	105	279	<5	123	262	128
Ni	35	22	110	11	35	17	67
Rb	41	20	9	62	31	29	6
Sr	62	260	99	97	176	536	119
Y	15	22	23	19	20	49	24
Zr	78	150	72	65	153	331	124
Nb	9	14	10	16	13	26	12
Ba	344	304	89	277	305	1087	87
As	11.1	<2.0	<2.0	<2.0	<2.0	<2.0	<2.0
Sb	.49	.50	.48	<.20	.40	<.20	.47
K/Rb	395	365	369	327	316	--	443
Zr/TiO2	.021	.021	.007	.217	.021	--	.017
Nb/Y	.600	.636	.435	.842	.650	--	.500
				In ppb			
Au	11.5	7.6	<2.0	<2.0	<2.0	<2.0	<2.0

Sample Number	TDH 162	TDH 164	TDH 165	TDH 169	TDH 174	TDH 177	TDH 178	TDH 182
				In weight %				
SiO_2	59.86	63.02	58.73	60.64	72.18	62.84	35.81	N.A.
Al_2O_3	14.93	15.89	14.41	14.34	15.85	14.58	1.84	N.A.
Fe_2O_3	6.33	4.72	6.31	5.73	1.78	4.51	40.29	N.A.
MgO	2.81	1.79	2.48	3.47	.71	1.51	.67	N.A.
CaO	3.28	2.85	4.02	5.03	2.90	4.65	.10	N.A.
Na_2O	2.40	2.18	2.62	2.83	4.94	.57	<.20	N.A.
K_2O	1.12	2.43	1.60	1.37	1.08	2.74	.09	N.A.
TiO_2	.77	.75	.67	.68	.22	.49	.07	N.A.
MnO	.09	.07	.08	.08	.08	.09	.15	N.A.
P_2O_5	.20	.20	.19	.20	.14	.15	.03	N.A.
CO_2	2.62	2.01	2.97	3.97	2.13	5.49	N.A.	N.A.
H_2O**	3.50	2.45	2.58	2.43	.81	.74	N.A.	N.A.
Total	97.91	98.36	96.66	100.77	102.82	98.36	--	--
				In ppm				
S	*.07	*.07	*.02	*.15	*.06	*1.43	N.A.	N.A.
Cr	225	199	140	187	33	40	28	51
Co	39	25	28	25	3	17	299	270
Cu	11	13	18	25	40	44	314	<3
Zn	102	54	68	185	60	232	84	44
V	127	114	111	96	19	53	27	13
Ni	48	37	35	53	11	17	12	13
Rb	28	60	41	37	41	58	<3	3
Sr	141	79	64	137	314	90	3	25
Y	25	25	21	21	16	16	<5	<5
Zr	166	174	156	156	157	137	19	19
Nb	14	16	14	14	16	12	<3	<3
Ba	373	584	458	366	736	404	19	43
As	<2.0	<2.0	<2.0	<2.0	<2.0	5.6	183.9	192.2
Sb	.25	.25	.30	.96	.35	.48	14.7	5.9
K/Rb	332	336	324	307	219	392	--	--
Zr/TiO_2	.022	.023	.023	.023	.062	.028	.027	--
Nb/Y	.560	.640	.667	.667	1.00	.750	.750	--
				In ppb				
Au	<2.0	4.7	<2.0	<2.0	<2.0	13.0	68.7	24.0

Fe_2O_3	Total Iron
N.A.	Not Analysed
*	In Weight %, analysis by XRF
**	H_2O = Loss On Ignition - CO_2

RARE EARTH ELEMENTS

Element	La	Ce	Nd	Sm	Eu	Tb	Yb	Lu
			In ppm					
Sample Number								
TDH - 2	30.2	59	32.7	6.8	1.5	.46	1.2	.17
4	23.2	43.1	17.7	3.1	.77	.37	.82	.17
7	17.5	36.1	14.7	2.9	.76	.49	1.5	.22
8	19.7	50.4	22.9	3.5	.75	.33	1	.16
10	16.2	34.9	15.4	3.3	.94	.41	1.3	.23
11	25.3	44.9	18.5	4.5	1.2	.54	1.4	.25
12a	6.5	15.3	11.7	3.8	.82	.54	2.9	.57
12b	7.5	16	10.6	4.2	.88	.93	3.6	.59
13	4.3	9.6	.95	2.8	.64	.43	.29	.05
14	2.5	7.2	4.7	2	.63	.41	1.8	.32
15	26.5	46	22.3	3.5	1	.39	1.6	.23
16	4.9	9.6	9.9	3	.84	.97	2.7	.46
18	12.2	29.9	13.8	2.9	.82	.34	1.1	.22
22	13.8	30.4	12.2	2.1	.35	.21	.83	.15
25	12.5	28.2	12.4	2	.33	.23	.86	.15
26	7.9	19.6	7.4	1.3	.24	.18	.66	.12
27	28.3	44.7	20.7	3.2	.84	.31	.99	.18
28	22.3	45.3	19.6	3.2	.81	.33	1.1	.16
29a	2.7	5.8	5.3	1.8	.58	.33	2.2	.34
29b	2.2	5.8	5.8	1.9	.56	.88	1.9	.33
30	5.8	8.7	5.8	2.1	.61	.43	2.3	.42
34	28.4	56	34.1	6.6	1.7	.5	1.4	.21

APPENDIX B

PRECISION AND ACCURACY FOR MAJOR AND TRACE ELEMENTS

MAJOR ELEMENTS

Sample TDH 8

	$\bar{x}$	s	s^2	c.v.%	Detection Limit,wt%
SiO_2	74.78	.29	.08	.39	.25
Al_2O_3	11.29	.07	.01	.65	.10
Fe_2O_3	.95	.02	0	1.61	.20
MgO	1.23	.19	.03	15.13	.05
CaO	1.89	.04	0	1.86	.05
Na_2O	1.71	.21	.05	12.53	.20
K_2O	1.52	.59	.34	38.47	.05
TiO_2	.09	0	0	0	.01
MnO	.09	0	0	0	.01
P_2O_5	.03	0	0	0	.01

Sample TDH 28

	$\bar{x}$	s	s^2	c.v.%	Detection Limit,wt%
SiO_2	66.13	.24	.06	.37	.25
Al_2O_3	14.00	.01	0	.07	.10
Fe_2O_3	4.71	.02	0	.49	.20
MgO	4.70	.07	0	1.47	.05
CaO	.95	.04	0	4.27	.05
Na_2O	.02	0	0	0	.20
K_2O	2.41	.02	0	.72	.05
TiO_2	.53	.01	0	.94	.01
MnO	.07	0	0	0	.01
P_2O_5	.13	.01	0	4.33	.01

$\bar{x}$= mean of duplicate samples

s^2= standard deviation

S= variance

c.v.%= coefficient of variation

$V = \frac{S}{x} \times 100$

TRACE ELEMENTS

Sample TDH 116

	$\bar{x}$	s	s^2	c.v.%	Detection Limit,ppm
Cr	112	8.5	72	7.6	10
Co	94.5	3.5	12.5	3.7	3
Cu	111.5	3.5	12.5	3.2	3
Zn	209.5	.71	.5	.3	5
V	299	4.2	18	1.4	5
Ni	89.5	.7	.5	.8	3
Rb	3				3
Sr	128.5	.7	.5	5.4	3
Y	26	1.4	2	5.4	5
Zr	73.5	.7	.5	.9	5
Nb	10	0	0	0	3
Ba	59	1.4	2	2.4	10

Sample TDH 120

	$\bar{x}$	s	s^2	c.v.%	Detection Limit,ppm
Cr	247.5	16.3	264.5	6.6	10
Co	41.5	3.5	12.5	8.5	3
Cu	82	0	0	0	3
Zn	128	2.8	8	2.2	5
V	178	11.3	128	6.4	5
Ni	57.5	.7	.5	1.2	3
Rb	19.5	.7	.5	3.6	3
Sr	170.5	.7	.5	0.4	3
Y	21.5	.7	.5	3.3	5
Zr	136	0	0	0	5
Nb	12	0	0	0	3
Ba	172.5	19.1	364.5	11.9	10

Sample TDH 124

	$\bar{x}$	s	s^2	c.v.%	Detection Limit,ppm
Cr	15.5	13.7	4.5	13.7	10
Co	3				3
Cu	3				3
Zn	14	0	0	0	5
V	3	0	0	0	5
Ni	9	0	0	0	3
Rb	67.5	2.1	4.5	3.1	3
Sr	90	0	0	0	3
Y	20.5	2.1	10.3	10.3	5
Zr	82.5	.7	.9	.9	5
Nb	17.5	.7	4.0	4.0	3
Ba	412.5	23.3	5.7	5.7	10

ACCURACY
MAJOR AND TRACE ELEMENTS

	JB-1				NIM-N			
	ABBEY	BLUM			ABBEY	BLUM		
	$\bar{x}$	$\bar{x}'$		s	$\bar{x}$	$\bar{x}'$		s
SiO2	52.62	53.19	±	.39	52.56	52.92	±	.54
Al2O3	14.62	14.49	±	.19	16.54	16.58	±	.26
Fe2O3	9.05	9.01	±	.14	8.91	8.88	±	.25
MgO	7.76	7.88	±	.15	7.48	7.39	±	.45
CaO	9.35	9.36	±	.20	11.46	11.26	±	.32
Na2O	2.79	2.85	±	.29	2.46	2.34	±	.28
K2O	1.42	1.49	±	.11	.25	.24	±	.12
TiO2	1.34	1.28	±	.06	.20	.19	±	.06
MnO	.15	.16	±	.02	.18	.18	±	.12
P2O5	.26	.28	±	.03	.03	.03	±	.02
Cr	400	387	±	12	34	32	±	4
Co	39	41	±	7	60	57	±	6
Cu	56	53	±	10	11	10	±	7
Zn	84	82	±	8	62	61	±	9
V	210	216	±	15	210	204	±	16
Ni	135	139	±	9	120	124	±	8
Y	26	24	±	4	7	8	±	2
Zr	155	163	±	11	22	20	±	3
Nb	--	60	±	8	2	2	±	2

Major elements in weight percent
Trace elements in ppm
$\bar{x}$ = mean, from Abbey (1977).
$\bar{x}'$ = mean of five determinations of one pellet, from Blum (1986).
s = standard deviation

APPENDIX C

SAMPLE DESCRIPTIONS

Sample	Location	Description	Geochemical Classification
1	Map 1	flow breccia	
2	1	phyric flow	calc-alkaline andesite
3	1	lithic tuff breccia	
4	1	lithic tuff breccia	calc-alkaline dacite
5	1	quartz-diorite	
6	1	quartz-diorite	
7	1	feldspar porphyritic flow	calc-alkaline andesite
8	1	quartz porphyritic flow	calc-alkaline rhyolite
9	1	flow breccia	
10	1	phyric flow	calc-alkaline andesite
11	1	phyric flow	calc-alkaline andesite
12a	1	crystal tuff	Fe tholeiitic basalt
12b	1	quartz diorite	Fe tholeiitic basalt
12c	1	crystal tuff	Fe tholeiitic basalt
13	1	crystal tuff	Fe tholeiitic basalt
14	1	quartz diorite	Mg tholeiitic basalt
15	1	feldspar porphyritic flow	calc-alkaline andesite
16	1	crystal tuff	Fe tholeiitic basalt
17	1	hyaloclastite	
18	1	phyric flow	calc-alkaline andesite
19	1	lamprophyre	
20	4	quartz diorite	
21	4	flow breccia	
22	4	felsic intrusive	calc-alkaline rhyolite
23	4	quartz diorite	
24	4	flow	
25	4	felsic intrusive	calc-alkaline rhyolite
26	4	felsic intrusive	calc-alkaline rhyolite
27	2	phyric flow	calc-alkaline andesite
28	2	phyric flow	calc-alkaline andesite
29	2	quartz diorite	Mg tholeiitic basalt
30	2	crystal tuff	Fe tholeiitic basalt
31	2	quartz diorite	
32	2	quartz porphyritic flow	
33	4	felsic intrusive	
34	4	crystal tuff	calc-alkaline basalt
60	Figure 3-2	lithic tuff	calc-alkaline dacite
61	"	lithic tuff	calc-alkaline dacite
62	"	lithic tuff	calc-alkaline rhyolite
63	"	lithic tuff	calc-alkaline dacite
64	"	lithic tuff	calc-alkaline dacite
65	"	lithic tuff	calc-alkaline dacite
66	"	lithic tuff	calc-alkaline dacite
67	"	lithic tuff	calc-alkaline dacite
100	Map 5	flow	Mg tholeiitic basalt
101	5	flow breccia	
102	5	phyric flow	Fe tholeiitic basalt
103	5	phyric flow	Mg tholeiitic basalt
104	5	fuchsite vein	

Sample	Location	Description	Geochemical Classification
105	Map 5	hyaloclastite	
106	4	felsic intrusive	calc-alkaline rhyolite
107	4	quartz diorite	
108	4	quartz diorite	
109	4	quartz diorite	
110	4	quartz diorite	Fe tholeiitic basalt
111	4	flow breccia	
112	4	intrusion containing fragments of underlying strata	
113	4	flow breccia	
115	4	flow breccia	
116	2	crystal tuff	Fe tholeiitic basalt
117	2	lithic tuff breccia	
118	1	flow breccia	
119	1	lithic tuff breccia	
120	1	flow	calc-alkaline basalt
121	1	crystal tuff	
122	1	phyric flow	
123	1	lithic tuff breccia	calc-alkaline dacite
124	1	quartz porphyritic flow	calc-alkaline rhyolite
125	1	quartz diorite	
126	1	quartz diorite	
127	1	hyaloclastite	
128	1	debris flow	
129	1	quartz diorite	
130	1	feldspar porphyritic flow	calc-alkaline andesite
131	1	quartz diorite	
132	1	flow breccia	
133	1	hyaloclastite	
134	1	phyric flow	calc-alkaline andesite
135	1	crystal tuff	
136	1	lithic lapilli tuff	
137	1	lithic lapilli tuff	Fe tholeiitic basalt
138	1	phyric flow	calc-alkaline basalt
139	1	felsic intrusive	calc-alkaline rhyolite
140	1	quartz diorite	
141	1	phyric flow	calc-alkaline andesite
142	1	flow breccia	
143	1	quartz diorite	
144	1	flow	
145	1	quartz vein	
146	1	feldspar porphyritic flow	calc-alkaline andesite
147		no sample	
148	4	quartz diorite	
149	4	crystal lapilli tuff	
150	1	phyric flow	calc-alkaline andesite
151	4	intrusive breccia	calc-alkaline dacite
152	4	hyaloclastite	
153	4	quartz diorite	

Sample	Location	Description	Geochemical Classification
154	Map 2	phyric flow	calc-alkaline andesite
155	2	phyric flow	Fe tholeiitic basalt
156	2	no sample	
157	2	olivine diabase	
158	2	felsic intrusive	calc-alkaline rhyolite
159	2	phyric flow	calc-alkaline andesite
160	2	olivine diabase	Fe tholeiitic basalt
161	3	quartz diorite	Mg tholeiitic basalt
162	3	phyric flow	calc-alkaline andesite
163	3	quartz diorite	
164	3	phyric flow	calc-alkaline andesite
165	3	phyric flow	calc-alkaline andesite
166	3	quartz diorite	
167	3	flow breccia	
168	3	hyaloclastite	
169	3	phyric flow	calc-alkaline andesite
170		no sample	
171		no sample	
172	Figure 3-2	crystal tuff	
173	"	lamprophyre	
174	"	quartz-feldspar porphyry	calc-alkaline rhyolite
175	"	flow	
176	Map 4	crystal lapilli tuff	
177	4	phyric bearing dacite	calc-alkaline dacite
178	Figure 3-2	ash tuff	
179	"	cherty sediment	
180	"	ash tuff + chert	
181	"	lithic tuff	
182	"	graphitic sediment	
183	"	chert + magnetite iron formation	

MAP 1

SCALE

1 cm to 6 m

or

1 inch to 50 feet

MAP 2

SCALE

1 cm to 6m
or
1 inch to 50 feet

MAP 3

SCALE
1 cm to 6m
or
1 inch to 50 feet

MAP 4

SCALE
1 cm to 6 m
or
1 inch to 50 feet

MAP 5
LEGEND SYMBOLS
SCALE
1 cm to 6m
or
1 inch to 50 feet

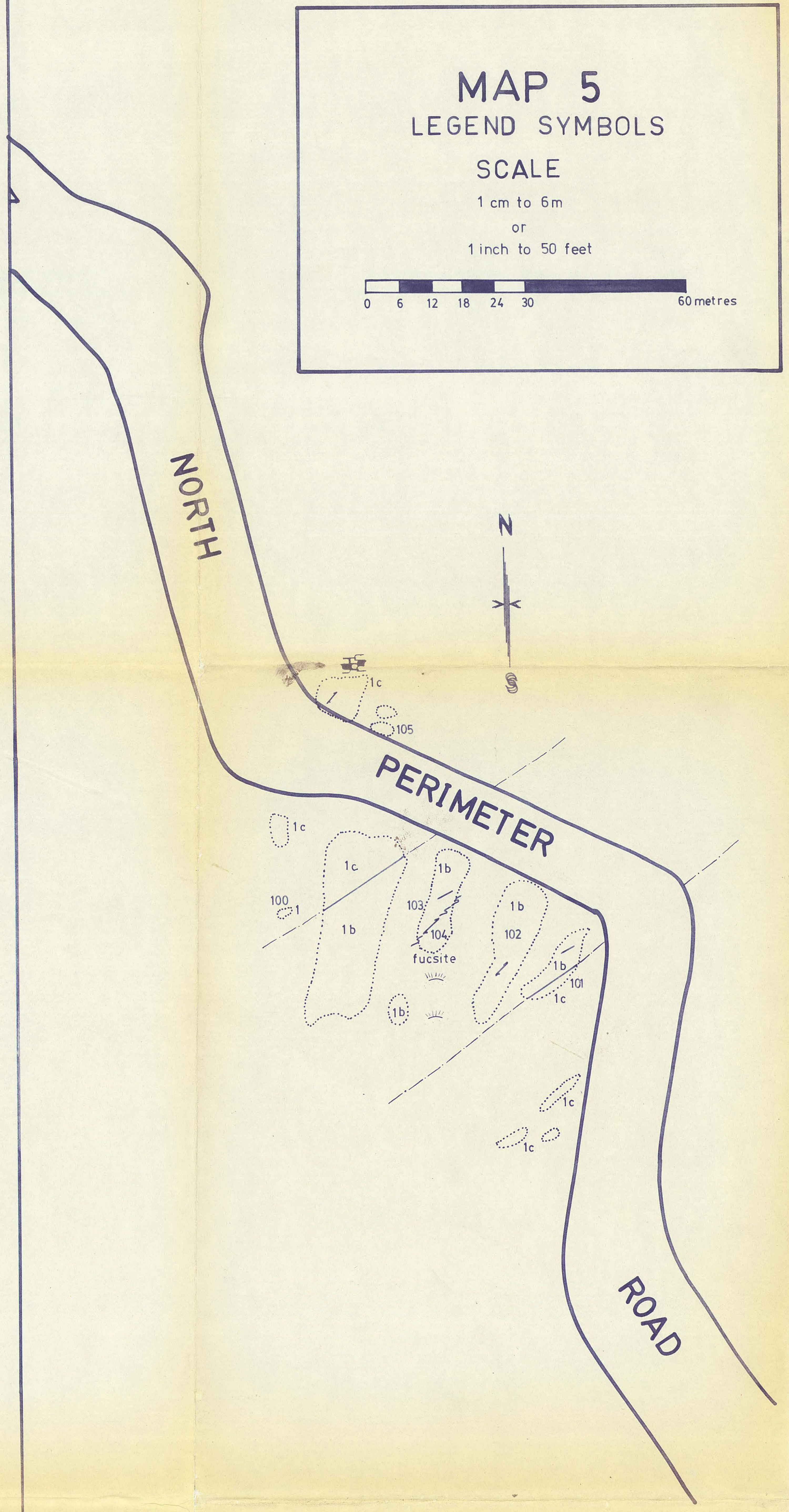

LEGEND

MAFIC INTRUSIVE ROCKS

7

7a Olivine diabase

FELSIC INTRUSIVE ROCKS

6

6a Quartz-feldspar porphyry

INTERMEDIATE TO MAFIC INTRUSIVE ROCKS

5

5a Diorite, quartz diorite
5b Lamprophyre

METASEDIMENTS

4

4a Iron formation

FELSIC TO INTERMEDIATE METAVOLCANICS

INTRUSIVES

3

3 Unsubdivided
3a Felsic intrusion - early
3b Felsic intrusion - late
3c Felsic intrusive breccia
3d Intermediate intrusion containing fragments of underlying strata

FLOWS, PYROCLASTICS

2

2 Unsubdivided dacite
2a Quartz porphyritic rhyolite
2b Phyric bearing dacite
2c Flow breccia
2d Lithic tuff (<4mm)
2e Crystal tuff (<4mm)
2f Lapilli tuff (4-32mm)
2g Tuff breccia (>32mm)

INTERMEDIATE TO MAFIC METAVOLCANICS

1

1 Unsubdivided andesite, basalt
1a Feldspar porphyritic andesite
1b Phyric bearing andesite, basalt
1c Flow breccia
1d Lithic tuff (<4mm)
1e Crystal tuff (<4mm)
1f Lapilli tuff (4-32mm)
1g Tuff breccia (>32mm)
1h Pyroclastic debris flow

<u>LEGEND</u> and <u>SYMBOLS</u> may be used for maps 1 thru 5.
Not all lithologies are represented on each map.

SYMBOLS

x	boundary of rock outcrop
	geological boundary (defined, assumed)
	lateral facies change
85	strike, dip of flows or strata
	direction of top of strata
	foliation, vertical
	minor drag folding
	shear zone
	hyaloclastite texture
·4, 123	sample number
	lowland, swamp
P	pyrite mineralization
	ring structures